Journal of Atmospheric and Solar-Terrestrial Physics 73 (2011) 2237–2271

Contents lists available at ScienceDirect

Journal of Atmospheric and Solar-Terrestrial Physics

journal homepage: www.elsevier.com/locate/jastp

Monthly mean vertical profiles of pressure, temperature and water vapour volume mixing ratio in the polar stratosphere and low mesosphere from a multi-year set of MIPAS-ENVISAT limb-scanning measurements

Claudio Tomasi [a,*], Boyan Petkov [a,b], Bianca Maria Dinelli [a], Elisa Castelli [a], Enrico Arnone [a], Enzo Papandrea [c]

[a] Institute of Atmospheric Sciences and Climate (ISAC), Consiglio Nazionale delle Ricerche (CNR), via Gobetti 101, I-40129 Bologna, Italy
[b] International Centre for Theoretical Physics (ICTP), Strada Costiera 11, I-34014 Trieste, Italy
[c] Department of Physical and Inorganic Chemistry, University of Bologna, Viale Risorgimento 4, 40136 Bologna, Italy

ARTICLE INFO

Article history:
Received 27 October 2010
Received in revised form
24 May 2011
Accepted 10 June 2011
Available online 21 July 2011

Keywords:
Pressure and temperature in the polar stratosphere
Polar stratospheric moisture parameters
Polar stratospheric water vapour content
Multi-year MIPAS limb-scanning measurements

ABSTRACT

Measurements performed at polar latitudes by the MIPAS limb-scanning Fourier Transform spectrometer aboard ENVISAT, from July 2002 to March 2004 (FR mission) and January 2005 to April 2010 (OR mission) were analysed with the 2-D tomographic Geofit Multi-Target Retrieval (GMTR) procedure (Dinelli et al., 2010. The MIPAS2D database of MIPAS/ENVISAT measurements retrieved with a multi-target 2-dimensional tomographic approachAtmos. Meas. Techn. Discuss. (AMTD) 2, 2639–2688.) to obtain the MIPAS2D database, and extract more than 386,000 vertical profiles of pressure p, temperature T and water vapour volume mixing ratio Q. They were subdivided into 12 latitudinal classes selected in steps of 5° from 65°N to 90°N and 65°S to 90°S, each vertical profile consisting of values measured at 14 altitude levels from 12 to 60 km. Each latitudinal set was subdivided into 12 monthly sets to determine the multi-year monthly mean vertical profiles of the three parameters: those of p (monthly average standard deviations (SD) 5–15%) provide evidence of marked seasonal variations above 30 km; those of T (SD values of a few percent) show large seasonal variations, with summer maxima at all stratospheric levels; and those of Q (SD lower than 20% from 20 to 50 km) present values ranging in general between 2 and 6 ppmv at the 12–25 km levels and 4 and 7 ppmv at higher altitudes. To verify the reliability of the MIPAS results, the pressure profiles are compared with those obtained from radiosounding data-sets taken at Arctic and Antarctic sites from 2000 to 2003; those of T with both radiosounding measurements and MLS/Aura satellite data from 2005 to 2010; and those of Q with the MLS/Aura satellite data, finding a substantial agreement in all cases. Comparison of MIPAS pressure and temperature profiles with pre ozone-hole CIRA models at 70° and 80° latitudes highlights the variations occurring in the polar atmosphere over the last 3 decades, with relative pressure decreases of 5–10% on average, and overall average decreases in temperature of 0.4 and 2.0 K in the Arctic and Antarctica, respectively. Using the MIPAS profiles of p, T and Q, the monthly mean vertical profiles of absolute humidity were also calculated, from which the monthly values of stratospheric water vapour content from 12 to 50 km were determined, varying between 0.0047 and 0.0070 mm at Arctic latitudes and between 0.0026 and 0.0055 mm at Antarctic latitudes.

1. Introduction

Realistic evaluations of the incoming short-wave radiation and downwelling infrared radiation flux densities at the surface can be obtained at polar sites using radiative transfer codes for known vertical profiles of atmospheric pressure, temperature and relative humidity (Town et al., 2007). In addition, measurements of the outgoing short- and long-wave radiance fluxes derived from satellite observations can be compared with radiative transfer calculations performed for well-defined thermodynamic conditions of the polar atmosphere determined by means of radiosoundings and/or in-situ infrared radiance measurements (Gettelman et al., 2006; Walden et al., 2006). Radiative transfer calculations performed for the exceptionally cold and dry atmospheric conditions at high-altitude sites in Antarctica can be also used to (i) validate in-situ radiation measurements performed using ground-based solar and infrared radiometers (Walden et al., 1997, 1998; Kenyon and Storey, 2006) and (ii) provide reliable

* Corresponding author. Tel.: +39 051 639 9594; fax: +39 051 639 9652.
E-mail address: c.tomasi@isac.cnr.it (C. Tomasi).

1364-6826/$ - see front matter © 2011 Elsevier Ltd. All rights reserved.
doi:10.1016/j.jastp.2011.06.018

atmospheric transmission data at wavelengths from the mid-infrared to the millimetric spectral range for testing the suitability of astronomic observations at high-altitude sites such as South Pole, Dome A and Dome C (Chamberlin et al., 1997; Lawrence et al., 2004; Minier et al., 2007).

A knowledge of the monthly mean vertical profiles of pressure, temperature and water vapour partial pressure at polar latitudes is also useful for obtaining spectral evaluations of the volume Rayleigh-scattering coefficient at various atmospheric altitudes, from which the Rayleigh-scattering optical depth can be realistically evaluated at all ultraviolet to near-infrared wavelengths. In order to determine the attenuation of direct solar irradiance due to air molecules in the polar atmosphere, Tomasi et al. (2010) calculated the spectral values of Rayleigh-scattering optical depth from 0.2 to 4.0 μm for the vertical profiles of pressure, temperature, water vapour partial pressure and CO_2 volume concentration, determined by examining a set of 2260 radiosonde measurements performed at six Arctic sites (Cambridge Bay, Resolute, Danmarkshavn, Eureka, Alert and Ny-Ålesund) at latitudes between 69°N and 82°N, and six Antarctic sites (Neumayer, Syowa, Mario Zucchelli, McMurdo, Dome C and South Pole) at latitudes between 70°S and 90°S.

For these calculations, radiosounding measurements taken at polar sites were used to analyse reliable data of pressure and temperature up to 25–30 km on average during the local summer, and up to 12–15 km only during the local winter, due to the frequent balloon breaks caused by the very cold stratospheric temperatures. Radiosonde measurements of RH are only valid up to 10–12 km, due to extremely low Upper Troposphere/Lower Stratosphere (UTLS) humidity conditions at polar latitudes, which are below capacitive hygrometer detection limits (Wang et al., 2002; Turner et al., 2003; Miloshevich et al., 2004, 2006). To overcome such shortcomings, Tomasi et al. (2010) calculated the vertical profiles of the volume Rayleigh scattering coefficient in the 0.25–4.00 μm wavelength range. To do so, they used the vertical profiles of the main thermodynamic parameters in the polar atmospheres up to 120 km height, as determined from

(1) the CIRA (COSPAR International Reference Atmosphere 1986, 0–120 km) monthly vertical profiles of pressure and temperature at the 70° and 80° latitudes of both hemispheres (CIRA 1986, 1988; Fleming et al., 1990), available on the website http://badc.nerc.ac.uk/data/cira/);
(2) the vertical profiles of water vapour volume mixing ratio derived from a large set of satellite observations performed at polar latitudes for different seasonal conditions of the stratosphere (Russell et al., 1984; Harries et al., 1996; Chiou et al., 1997; Randel et al., 2001);
(3) the vertical profiles of water vapour volume mixing ratio given by the Subarctic Summer (July, 60°N) and Subarctic Winter (January, 60°N) models (Anderson et al., 1986); and
(4) the CO_2 vertical profile given by the Subarctic Atmosphere seasonal models of Anderson et al. (1986), suitably normalised to the sea-level average volume concentration of 380 ppmv, as measured in 2007 at various Arctic and Antarctic stations of the WMO Global Atmospheric Watch network (World Data Centre for Greenhouse Gases).

In fact, all these vertical profiles need to be updated or substituted with more recent data, because

- The monthly mean vertical profiles of the CIRA (1986) atmospheric models are given only at the 70° and 80° latitudes of both hemispheres, and were derived from data-sets recorded more than 30 years ago, before the occurrence of the marked variations in pressure and temperature associated with the ozone hole formation in the polar stratosphere.
- The vertical profiles of moisture parameters obtained from Randel et al. (2001) and the other above-mentioned satellite-based data-sets were determined by analyzing measurements of 2–3 decades ago and need to be updated with data recorded during the last 10 years.
- The standard atmosphere models of Anderson et al. (1986) refer to 60°N latitude, and are therefore unsuitable for representing the thermodynamic conditions of the polar atmosphere at stratospheric and mesospheric altitudes.
- The vertical profiles of CO_2 concentration need to be determined at stratospheric and mesospheric levels by examining more recent data than those of Anderson et al. (1986), such as those derived by López-Puertas et al. (2000) from Thermosphere Ionosphere Mesosphere Electrodynamics-General Circulation Model (TIME-GCM) runs in the mesosphere, those obtained by Mertens et al. (2009) from SABER/TIMED limb emission measurements in the mesosphere and thermosphere, and those retrieved by Foucher et al. (2011) from space observations using the Atmospheric Chemistry Experiment Fourier Transform Spectrometer (ACE-FTS) at stratospheric levels.

Thus, the analysis of recent satellite-based data could be very useful for calculating realistic monthly mean vertical profiles of pressure, temperature and moisture parameters, which are suitable for simulating the radiative transfer processes and comparing such simulations with the remote sensing measurements taken in the Arctic and Antarctic regions. In fact, a growing number of experimental stations have been set up in the two polar regions over recent years, where field measurements of various kinds are carried out, such as (i) spectral series of aerosol optical depth from sun-photometric measurements of direct solar irradiance (Tomasi et al., 2007), (ii) short- and long-wave radiation budget terms to evaluate the role of aerosols, clouds and atmospheric gases in the surface–atmosphere climatic system (Lanconelli et al., 2009) and (iii) spectral observations of atmospheric transmittance at infrared to millimetric wavelengths, for astronomical studies and experiments (Tosti et al., 2006). For this purpose, satellite-borne measurements can provide stratospheric and mesospheric data suitable for integrating local radiosounding measurements of pressure and temperature, which are usually performed only at tropospheric and low stratospheric levels. The retrieval from satellite data of the thermodynamic parameters at various levels of the polar stratosphere is particularly difficult, due to the irregular distributions and the sharp time-variations of pressure, temperature and moisture conditions that are often observed within the strong cyclonic vortexes forming in the Arctic and Antarctic regions during the local winter season (Lahoz et al., 1996; Müller et al., 2003).

To attain an updated set of monthly mean vertical profiles of p, T and Q, the data-set obtained from Michelson Interferometer for Passive Atmospheric Sounding (MIPAS)/Environment Satellite (ENVISAT) limb-scanning measurements, performed during a multi-year period from July 2002 to April 2010, are examined in the present study, selecting the measurements in the altitude range of 12–68 km at various Arctic and Antarctic latitudes. The data-set is part of an updated version of the MIPAS2D database (Dinelli et al., 2010) and represents the atmospheric fields of the three meteorological parameters listed above, as obtained analyzing the MIPAS observations with the Geofit Multi-Target Retrieval (GMTR) system (Carlotti et al., 2006), based on the Geo-fit approach (Carlotti et al., 2001) upgraded with the Multi-Target Retrieval (MTR) functionality (Dinelli et al., 2004). The retrieval method used in Dinelli et al. (2010) differs from other analysis systems applied to MIPAS measurements, since it derives the data

with a tomographic approach, which takes the atmospheric horizontal gradients properly into account and does not assume horizontal homogeneity conditions, as in the case of the other analyses.

The GMTR algorithm was operated on (i) a fixed vertical grid of 17 altitudes selected throughout the 6–68 km altitude range, and (ii) an equispaced horizontal grid of 5° resolution in latitude, for which the vertical distributions of parameters p, T and Q and volume mixing ratios (hereinafter referred to as VMRs) of five "high priority" atmospheric constituents (O_3, HNO_3, CH_4, N_2O and NO_2) were also simultaneously determined. Limiting the present analysis to parameters p, T and Q, the MIPAS2D data-set relative to polar latitudes was examined in order to determine the mean vertical profiles of these parameters, one for each month of the year, at 6 selected latitudes of both Northern and Southern hemispheres, from 65° to 90° in steps of 5°. The obtained set of vertical profiles of p, T and Q allowed a complete characterisation of the thermodynamic conditions of the polar stratosphere and low mesosphere, describing the mean variations occurring throughout the year. They can therefore be appropriately used in radiative transfer codes to simulate short- and long-wave radiation fluxes in this atmospheric region.

2. Brief description of MIPAS data and GMTR retrieval procedure

MIPAS was developed by the European Space Agency (ESA) as part of the payload of the ENVISAT satellite launched on 1 March 2002. It is a limb-scanning Fourier Transform (FT) spectrometer recording emission spectra in the mid-infrared, over the spectral range from 680 to 2410 cm^{-1}, with an original spectral resolution of 0.035 cm^{-1} full width half maximum, unapodised. ENVISAT globally covers the Earth following 14.3 daily orbits, the descending (North to South) part crossing the equator at approximately 10:00 LT and the ascending part at approximately 22:00 LT. The majority of MIPAS measurements during the Full Resolution (FR) mission (lasting until March 2004) were taken in the nominal observation mode, with one orbit consisting of 72 limb-scans looking backward along the orbit track. Each limb-scan consisted of 17 observations with tangent altitudes ranging from 6 to 68 km, in steps of 3 km up to 42 km, and then in larger steps of 5 and 8 km. The MIPAS instantaneous field of view is approximately 3 km in height and 30 km across track at tangent point. In the FR nominal observation mode, the average distance between tangent points of successive limb-scans was about 500 km (i.e. ~4.6° in latitude), with an interferogram recording time of 4.5 s and the time for a complete elevation scan (including 17 observation geometries) of about 76 s.

Due to the deterioration of the interferometer slides, the FR mission was suspended on 26 March 2004. The technical problem was overcome in January 2005 by operating MIPAS with an Optimised Resolution (OR) at 41% of the maximum spectral resolution used in the original configuration. Because of the reduced spectral resolution, a shorter acquisition time of each limb view was adopted, and all observation modes were redefined to increase their spatial sampling. Thus, in the new OR nominal observation mode, each scan consisted of 27 limb views with tangent altitudes ranging from 3 to 70 km in variable altitude steps. In the OR mission, MIPAS measured not only in the nominal mode but also in the so-called Upper Troposphere–Lower Stratosphere (UTLS) special observation mode, with a reduced but denser vertical coverage.

The GMTR algorithm is based on (i) the Geo-fit approach (Carlotti et al., 2001), which performs a tomographic retrieval on observations collected along a whole orbit carrying out a 2-D discretization of the atmosphere, and (ii) the MTR technique (Dinelli et al., 2004), which allows a reduction of systematic errors due to the presence of interfering species in the analysed spectral intervals. In a GMTR analysis of a full orbit, each limb observation contributes for deteriming the unknown quantity at a number of different locations among those spanned by its line of sight. The GMTR system enables the tomographic retrieval of MIPAS data, taking the horizontal inhomogeneities of the atmosphere into proper account. The capability of the GMTR system to model the horizontal structures of the atmosphere makes its application to MIPAS measurements particularly suitable for the work presented here, which focuses on the polar regions, where strong horizontal gradients are present, especially during the winter months, due to the lines of sight of the instrument simultaneously crossing regions inside and outside the polar vortexes.

The GMTR analysis system was applied to MIPAS observations to generate the MIPAS2D database, consisting of 2-D fields of pressure (p), temperature (T) and VMR of six "high priority" species, namely water vapour (Q), ozone, HNO_3, CH_4, N_2O and NO_2. The database has been thoroughly described in Dinelli et al. (2010); here we briefly recall the principal features of the performed analysis. The 2-D fields were obtained on a fixed vertical grid coinciding with the nominal tangent altitudes of the FR nominal observation mode, which spans the altitude range from 6 to 42 km in steps of 3 km, and upward at altitudes of 47, 52, 60 and 68 km, and a horizontal equispaced grid of 5° spatial resolution in latitude. Because of their correlations, p, T and Q were jointly retrieved with the ozone VMR by exploiting the code's MTR functionality. Their retrieval was followed by the sequential retrieval of the VMRs of the other molecules. For each target (or group of targets in the case of MTR), the GMTR analysis was performed using sets of dedicated Micro Windows (hereinafter referred to as MWs), selected with different criteria for the FR and OR missions in order to achieve the best retrieval accuracy of the final Level 2 products. Particular attention was paid to the various systematic error sources affecting MIPAS observations, as they are known to propagate their error components over all the retrieved quantities. Such effects were minimised through the selection of the MWs and the sequence in which the target quantities were retrieved. The residual systematic errors were assumed to be common to all the analyses using the same set of MWs and, hence, are characteristic of each target and may vary considerably from the FR to OR Level 2 products. They are in general due to (i) the assumptions used in the forward model internal to the retrieval system (i.e. local thermal equilibrium, shape of the profiles outside the retrieval range and spectroscopic errors); (ii) instrumental errors (i.e. instrument line shape, radiometric and frequency calibration); and (iii) the influence of the interfering species on the retrieved targets. Besides systematic errors, the MIPAS Level 2 products are affected by random errors, due to measurement noise. The MIPAS2D database described in Dinelli et al. (2010) was obtained by analysing only MIPAS measurements obtained in the nominal observation mode. The MIPAS2D data used here are an improved version of the database published in 2010. The measurements now included in the database come from the analysis of newly delivered MIPAS observations and also include the MIPAS UTLS-1 mode in order to increase the number of observations available, particularly benefiting the time coverage for the years 2006 and 2007. The retrieval of UTLS-1 measurements was performed with the same configuration of the nominal mode and the results did not show bias effects with respect to the rest of the data-set.

It must be borne in mind that in the time interval 2002–2010 considered in this work, the polar atmosphere went through a number of dynamically variable winters not only in the Northern

Hemisphere, occasionally affected by Sudden Stratospheric Warming (SSW) events, but also in the Southern Hemisphere where a split-up of the polar vortex occurred on September 2002. Some of the latter events produced very localised anomalies in the vertical profiles of p, T and Q, resulting in an enhancement of the standard deviation in the averaging procedure, which therefore correctly characterises the dynamically variable conditions of polar region. This is the case, for example, of major stratospheric warmings in 2006 and 2009. However, the strong variations observed from January to March 2004 (when a SSW event occurred in the Northern polar region) were atypical, even with respect to other disturbed winters in this polar region: during the second half of December 2003 and early January 2004 a SSW event occurred, followed by the formation of an intense vortex in February, generating low thermal conditions comparable to those characterizing the Antarctic vortex (Liu et al., 2009). During this episode, very low temperatures were measured in February 2004 at altitudes ranging between 20 and 60 km, presenting marked differences (reaching maximum values of nearly 40 K at the 35–40 km levels) compared with the temperatures measured in February of the other years. Thus, for the present analysis, it was decided to discard all pressure, temperature and moisture data recorded at the Northern latitudes during the three months from January to March 2004, which were the last three months of the FR mission, to avoid weighting the final averages towards very unlikely conditions. The same approach was adopted for the period August–October 2002, when a vortex split-up occurred in the Southern polar region, an episode that was never recorded in other years. For this reason, also this second period was discarded from the averaging procedure.

3. Monthly mean vertical profiles at polar latitudes

The MIPAS2D database contains an overall set of more than 386,000 vertical profiles for each target evenly distributed over the Earth's globe. The profiles are the result of the GMTR analyses of the MIPAS measurements in the time period from June 2002 to April 2010. For the present work, the original vertical range of the MIPAS2D database has been restricted to the region from 12 to 60 km. The data at 68 km were discarded because they were affected by high systematic errors due to the approximation used by the GMTR analysis system to represent the atmosphere above that altitude. The data below 12 km were discarded given the reduced number of high quality data, due to the cloud coverage masking the atmosphere below this altitude at MIPAS wavelengths. Therefore, each profile consists of 14 values obtained at the altitude grid of the MIPAS2D database reported in the previous section. Of all the profiles only those relative to the two polar latitudinal bands from 65°N to 90°N and from 65°S to 90°S were selected. Since the GMTR analyses were operated on a latitude fixed grid in steps of 5°, only the data for 6 latitudes in the northern polar region and 6 in the southern polar region were examined. For each latitude, the vertical profiles extracted from the MIPAS2D database were divided into monthly sets, one for each month of operation for both the FR and OR missions, each monthly set consisting of about 250–360 vertical profiles measured at different longitudes. Subsequently, the selected profiles (acquired within a single month) were averaged for every year, generating one monthly mean profile for each selected latitude repeated for all the considered years. Such averages were performed by weighting the data with their retrieval error and discarding the data with low information content (see Dinelli et al. (2010) for details). The resulting averaged profiles were then subdivided into twelve "final sets", one for each month of the year. Therefore, each final set was composed of 1 or 2 averaged profiles for the observations performed during the FR mission (from July 2002 to December 2003 at the Arctic latitudes, where the data of January–March 2004 were discarded, and from July 2002 to March 2004 at the Antarctic latitudes), and 3–6 averaged profiles for the OR mission (from January 2005 to April 2010). Finally, the multi-year monthly mean vertical profiles at each selected latitude were calculated averaging the profiles contained in the final sets.

Together with the multi-year monthly means, their errors were obtained by combining the following error sources:

(a) the Mean Retrieval Error (MRE), mainly due to the measurement noise. In the averaging process, MRE becomes so low that it can be considered negligible;
(b) standard deviation of each monthly mean (MSD), which is related to the variability of the pressure retrieved from the considered set of orbits;
(c) systematic errors (SE), common to all the profiles obtained in the analysis of each MIPAS mission (FR and OR);
(d) total error TE calculated as the sum of MRE and SE; and
(e) standard deviation SD of the final monthly averages, which are related to the year-by-year variability of the considered target.

3.1. Pressure

The monthly mean values of $p(z)$ determined at the 14 MIPAS fixed levels are reported in Table A1 of Appendix A for the 6 Arctic latitudes from 65°N to 90°N, and in Table A2 for the 6 Antarctic latitudes from 65°S to 90°S. As can be seen in Fig. 1, the monthly mean values of $p(z)$ at all the Arctic latitudes define annual

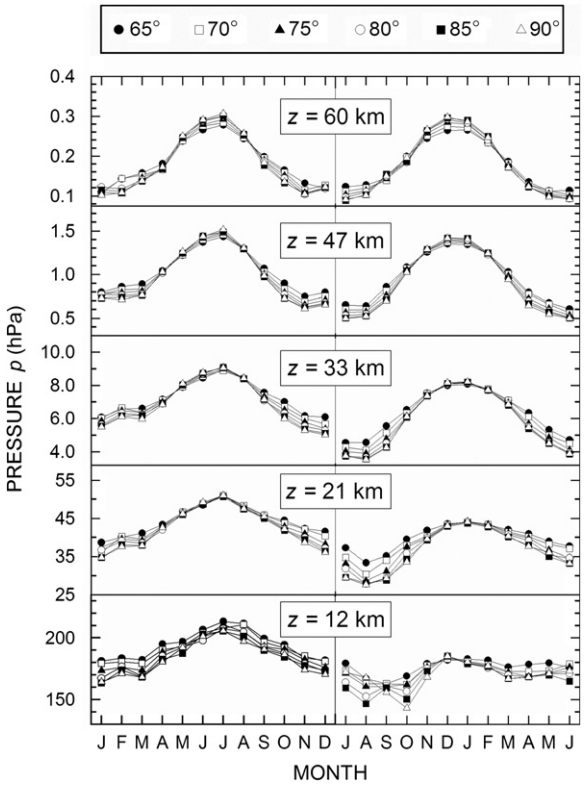

Fig. 1. Series of the monthly mean values of air pressure $p(z)$ obtained at five MIPAS fixed levels z, for the 6 selected Arctic latitudes (left) and the 6 selected Antarctic latitudes (right). The series of Antarctic months is represented over the period from July to June, taking into account that it is out of phase by 6 months with respect to that of the Arctic months, presented from January to December.

variations characterised by clear and well-defined minima in winter (January and December) at all levels, and by pronounced maxima in the summer months from June to August. The minima are more dispersed at the lower levels, presenting scattered data within $\pm 7\%$ and $\pm 9\%$ of the average values determined at the 12 and 21 km levels, respectively. All maxima occur in July and are gradually more pronounced as the altitude increases from 12 to 60 km. The series of monthly mean values of $p(z)$ calculated for the various latitudes show that the most marked winter-to-summer variations take place at levels higher than 30 km at all the six Arctic latitudes, with relative increases of $p(z)$ varying between 18% and 26% at 12 km, 32% and 47% at 21 km, 48% and 81% at 33 km, 81% and 149% at 47 km and 153% and 201% at 60 km. Conversely, the monthly mean values of $p(z)$ obtained at the selected Antarctic latitudes and given in Table A2 show that pressure is appreciably higher in December–February than in the austral summer months at all levels higher than 20 km. The minima observed in the austral winter months from June to August exhibit gradually less dispersed features as the altitude increases, showing scattered data within $\pm 9\%$, $\pm 12\%$ and $\pm 20\%$ of the average values calculated at the 12, 21 and 33 km levels, respectively. The greater variability observed in the low stratosphere compared to the Arctic is presumably due to the more variable configurations of the vertical structure of the Antarctic vortex during this seasonal period. All maxima are well pronounced, with seasonal variations similar to those observed at Arctic latitudes, although presenting more dispersed features. The austral winter-to-summer variations were estimated to vary between 12% and 29% at 12 km, 32% and 60% at 21 km, 77% and 133% at 33 km, 123% and 185% at 47 km and 135% and 232% at 60 km.

Fig. 1 clearly shows that the monthly mean values of $p(z)$ estimated at levels ranging between 12 and 21 km are more widely dispersed than those determined at the higher levels, for both Arctic and Antarctic latitudes, due to the presence of polar vortices. The wider scatter of pressure data in Fig. 1 at Antarctic latitudes, for altitudes lower than 35 km, can be reasonably explained as due to the more marked changes caused in the pressure field by the Antarctic vortex from May to September.

The large annual variations in $p(z)$ at all the 14 MIPAS fixed levels from 12 to 60 km clearly indicate, for all the selected polar latitudes, that the vertical profiles of pressure are subject to considerable changes throughout the year, with a more marked variability in Antarctica than in the Arctic region. To better illustrate these seasonal variations, Fig. 2 shows a comparison between the monthly mean vertical profiles of $p(z)$ at the 12 selected latitudes in January, April, July and October. The comparison gives a measure of the differences between the pressure fields in the Arctic and Antarctic atmospheres during the winter and summer months, and of the more limited discrepancies in April and October. The January vertical profiles of $p(z)$ at Arctic latitudes are presented together with those obtained in July at Antarctic latitudes, in order to show that appreciable discrepancies characterize the Arctic and Antarctic atmospheres, presumably due to the differently intense dynamical characteristics of the vortexes in the two polar regions. The comparison between the July vertical profiles of $p(z)$ in the Arctic and those measured in January in Antarctica shows that very similar seasonal conditions characterize the two polar atmospheres during the local summer periods. The same comparison is presented in Fig. 2 for the April (Arctic) and October (Antarctic) profiles and for the April (Antarctic) and October (Arctic) profiles. It shows, in the first case, appreciable differences at altitudes lower than 30 km and very slight differences at higher levels, while in the second case there are appreciable discrepancies

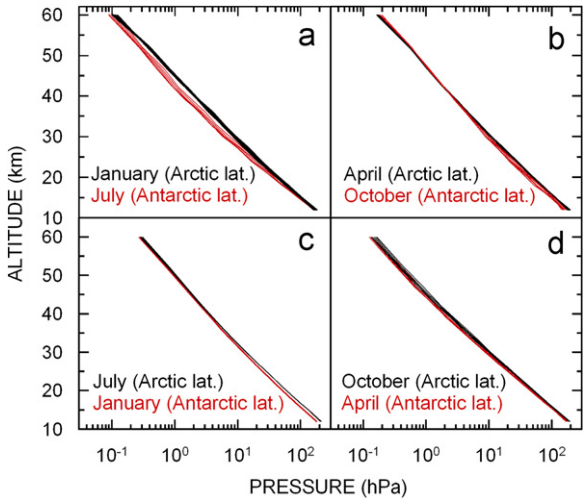

Fig. 2. Monthly mean vertical profiles of air pressure $p(z)$ obtained over the 12–60 km altitude range by averaging the MIPAS2D data at the 6 selected Arctic latitudes (black curves) and the 6 selected Antarctic latitudes (red curves) for comparison between (a) January profiles at Arctic latitudes and July profiles at Antarctic latitudes; (b) April profiles at Arctic latitudes and October profiles at Antarctic latitudes; (c) July profiles at Arctic latitudes and January profiles at Antarctic latitudes and (d) October profiles at Arctic latitudes and April profiles at Antarctic latitudes. (For interpretation of the references to color in this figure legend, the reader is referred to the web version of this article.)

between the two polar regions at all levels, reasonably explained by the not close coincidence of the periods in which the polar vortices are generated, leading to some weakly asymmetrical features between Arctic and Antarctic MIPAS profiles.

As pointed out in the previous section, the MIPAS estimates of $p(z)$ presented in Tables A1 and A2 are affected by errors of various kinds, such as (i) the Mean Retrieval Error (MRE), mainly due to the measurement noise; (ii) the monthly systematic error SE, due to the variability of pressure, which is calculated at each level as the weighted average of the FR and OR systematic errors determined by Dinelli et al. (2010); and (iii) the monthly standard deviation SD, calculated as an average over the multi-year set of data, and, hence, associated with the dispersion of data recorded using the FR or, alternatively, the OR observational modalities. The average estimates of these errors at the various MIPAS levels indicate that

(1) The MRE error is usually smaller than 1% at all levels, because of the high number of profiles used in the averaging process, presenting the highest values at levels $z < 25$ km in the summer months.
(2) As can be seen in Fig. 3, the overall SE error (obtained as weighted averages of the FR and OR systematic errors) varies on average between 3% and 7% at levels $z < 20$ km, and between 2% and 10% within the 20–60 km altitude range.
(3) The total error TE given by the sum of the MRE and SE errors is calculated to assume slightly greater values than the SE ones, due to the negligible weights of the MRE errors.
(4) The monthly standard deviation SD, giving a measure of the dispersion of the monthly data-sets at the various levels, varies mostly between 5% and 15% at all levels from 12 to 52 km and at all latitudes, followed by a sharp increase from 52 to 60 km, where values ranging between 10% and 35% are found. Such variations are partly due to the natural variability of the atmospheric pressure field with latitude, and partly to the different combinations of the experimental random errors made in analysing the data.

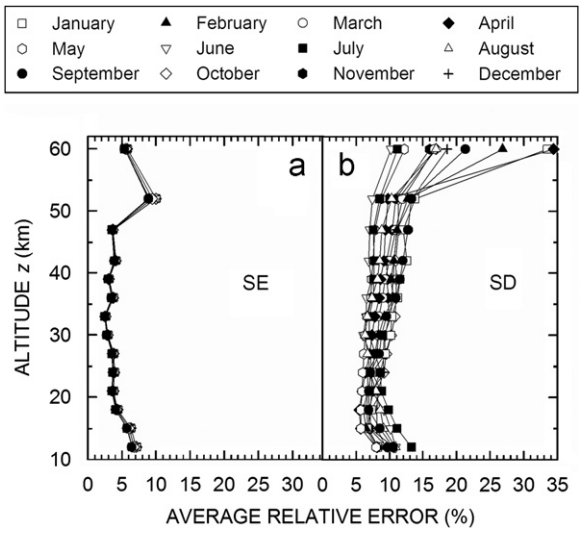

Fig. 3. Monthly vertical profiles of the average relative errors made in determining the monthly mean vertical profiles of air pressure $p(z)$ over the 12–60 km altitude range at polar latitudes: (a) weighted average systematic error SE, derived from the estimates of FR and OR systematic errors made by Dinelli et al. (2010) and (b) average standard deviation SD giving a measure of MIPAS data dispersion.

3.1.1. Comparison with radiosounding measurements

To test the reliability of the monthly mean vertical profiles of $p(z)$ given in Tables A1 and A2 for the 12 selected polar latitudes, Fig. 4 shows a comparison between the MIPAS profiles and those derived from radiosounding data-sets recorded at 4 Arctic and 3 Antarctic sites. The overall radiosounding data-set (hereinafter referred to as RDS) consists of

(a) 240 radiosoundings taken at Cambridge Bay (69° 08′N, 105° 04′W, 25 m a.m.s.l.), recorded from January 2000 to December 2003 and subdivided into 12 monthly sets, each consisting of 20 radiosoundings, analysed to determine the monthly mean vertical profiles of $p(z)$ and compare them with the 70°N latitude MIPAS profiles;
(b) 240 radiosoundings taken at Eureka (79° 59′N, 85° 56′W, 10 m a.m.s.l.), 240 radiosoundings at Alert (82° 30′N, 62° 21′W, 65 m a.m.s.l.) and 120 radiosoundings performed at Ny-Ålesund (78° 54′N, 11° 53′E, 11 m a.m.s.l.) in the summer months only: all the 600 radiosoundings were taken from January 2000 to December 2003, to obtain monthly sets of 40 radiosoundings for each of the 6 winter months from October to March and sets of 60 radiosoundings for each of the 6 summer months from April to September, for comparison with the 80°N MIPAS profiles;
(c) 120 radiosoundings performed at the German station of Neumayer (70° 39′S, 8° 15′W, 42 m a.m.s.l.) in the 6 austral summer months (October–March) from 2000 to 2003, and 240 radiosoundings taken throughout the year at the Japanese station of Syowa (69° 00′S, 39° 35′E, 29 m a.m.s.l.) from 2000 to 2003, to collect monthly sets consisting of 20 radiosoundings for each of the 6 austral winter months from April to September, and of 40 radiosoundings for each of the 6 summer months, for comparison with the 70°S MIPAS profiles; and
(d) 240 radiosoundings recorded at the U.S. McMurdo (77° 51′S, 166° 40′E, 24 m a.m.s.l.) station from January 2000 to December 2003, to collect monthly sets of 20 radiosoundings for all the months, for comparison with the 80°S MIPAS profiles.

Examining the monthly data-sets obtained from the overall RDS pressure data-set, the monthly mean vertical profiles of $p(z)$ were determined from 12 km up to the top-level reached by the

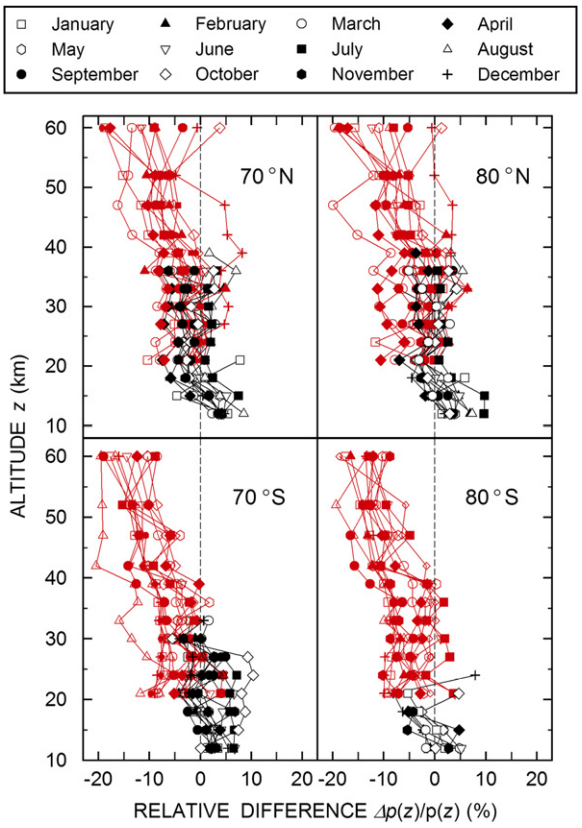

Fig. 4. Monthly vertical profiles of the relative differences $\Delta p(z)/p(z)$ calculated (i) between the present MIPAS monthly mean profiles and those obtained from radiosounding measurement sets recorded at various Arctic and Antarctic sites (black symbols), and (ii) between the present MIPAS monthly mean MIPAS profiles and those correspondingly given by the CIRA models (CIRA 1986) at the 70°N, 80° N, 70°S and 80°S latitudes (red symbols). (For interpretation of the references to color in this figure legend, the reader is referred to the web version of this article.)

radiosondes, which was found to mainly vary between 30 and 35 km during the local summer, and to not exceed 20 km during the Antarctic winter, due to the frequent radiosonde balloon breaks caused by the very cold air conditions. Fig. 4 shows the vertical profiles of the ratio $\Delta p(z)/p(z)$, where $\Delta p(z)$ is the difference between each MIPAS monthly mean value of $p(z)$ and the corresponding RDS monthly mean value, and the denominator term, $p(z)$, is the MIPAS value. The calculations give a measure of the relative differences between MIPAS and RDS data, which mainly vary between -7% and $+10\%$ at Arctic latitudes and between -6% and $+11\%$ at Antarctic latitudes. Considering that the RDS monthly mean values have been found for relative SD values ranging between $\pm 4\%$ at 12 km and $\pm 11\%$ at 30 km, and the MIPAS profiles are affected by relative SD values varying mostly between $\pm 5\%$ and $\pm 10\%$ at all stratospheric levels, as shown in Fig. 3, it can be stated that the present MIPAS results are suitable for being reliably used to represent the atmospheric pressure conditions in the Arctic and Antarctic regions, at all the selected polar latitudes and in all months.

3.1.2. Long-term variations of pressure vertical profiles

Following a similar procedure to that adopted for comparing MIPAS and RDS data, a check is also made in Fig. 4 in terms of ratio $\Delta p(z)/p(z)$ between some MIPAS monthly mean vertical profiles of $p(z)$ given in Tables A1 and A2 and the corresponding monthly vertical profiles of $p(z)$ provided by the CIRA (COSPAR International Reference Atmosphere 1986, 0–120 km) atmospheric models at the 70°N, 80°N, 70°S and 80°S latitudes

(see website http://badc.nerc.ac.uk/data/cira/). The comparison shows that the relative differences $\Delta p(z)/p(z)$ generally exhibit negative values at the 70°N, 80°N, 70°S and 80°S latitudes, indicating that the CIRA models provide on the whole appreciably higher values than those obtained from MIPAS observations at all levels. These relative differences are mainly found to vary between (i) 0% and −10% at all stratospheric levels, for the 70°N latitude; (ii) +5% and −10% at all levels, for the 80°N latitude; and (iii) 0% and −10% at 20–40 km altitudes, and −5% and −20% at 40–60 km altitudes, for both 70°S and 80°S latitudes. Therefore, it is evident that a marked decrease in pressure has taken place during the last three decades in the polar regions, equal to about 5% on average in the Arctic region and ranging between 5% and more than 10% in Antarctica.

3.2. Temperature

The monthly average values of $T(z)$ determined at the 14 MIPAS fixed levels are given with an accuracy of 0.1 K in Table A3 for the 6 selected Arctic latitudes, and in Table A4 for the 6 selected Antarctic latitudes. Fig. 5 shows the series of monthly average values of $T(z)$ obtained at 5 MIPAS levels in both polar regions. The Arctic results obtained at the 12 and 21 km levels present wide maxima during the summer, with values of 227–231 K, and slight minima at all latitudes in December and January, ranging between 211 and 217 K at 12 km and between 198 and 214 K at 21 km. More dispersed features were obtained for the minima recorded in September–November at levels higher than 30 km, while marked and wide maxima were found in the summer months, presenting values of 243–245 K at 33 km, 275–281 K at 47 km and 263–269 K at 60 km. It can be seen that the winter-to-summer temperature variations at Arctic latitudes

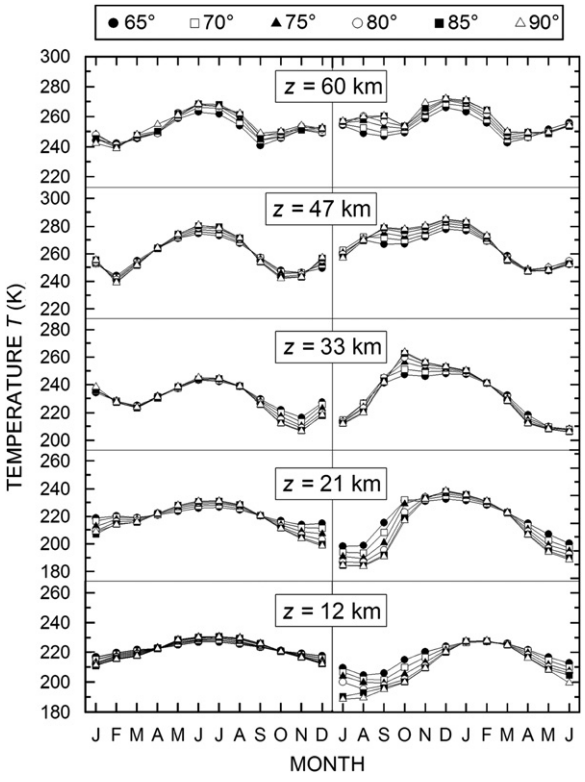

Fig. 5. Series of the monthly mean values of air temperature $T(z)$ obtained at five MIPAS fixed levels z, for the 6 selected Arctic latitudes (left) and the 6 selected Antarctic latitudes (right). The series of Antarctic months is represented over the period from July to June, taking into account that it is out of phase by 6 months with respect to that of the Arctic months, presented from January to December.

increase at all levels as the latitude varies from 70°N to 90°N: from 10 to 19 K at 12 km; from 13 to 33 K at 21 km; from 27 to 39 K at 33 km; and from 28 to 39 K at 47 km, followed by values of between 19 and 24 K at the 60 km level. These findings clearly indicate that the largest annual changes in temperature take place within the upper stratosphere.

More variable temperature conditions were found at Antarctic latitudes, especially at the 12 and 21 km levels during the period from May to November, when the low stratosphere is subject to a very strong cooling, and in the high stratosphere from October to February. More precisely, the results shown in the right part of Fig. 5 indicate that the monthly average values of $T(z)$ are characterised at all the selected latitudes by

(i) widely variable minima in the austral summer months from July to September at 12 km, ranging between 188 and 205 K, and maxima equal to 227–228 K in February at all latitudes, giving annual variations increasing with latitude from 23 to 39 K;
(ii) marked and widely variable minima in July–August at the 21 km level, ranging between 184 and 198 K, and maxima of 233–239 K in December, giving annual changes increasing with latitude from 34 to 55 K;
(iii) pronounced and stable minima of 206–208 K at 33 km in June, with maxima in December at the lower latitudes and in October at the two higher latitudes, with values of between 248 and 264 K, giving annual winter-to-summer variations ranging between 41 and 58 K;
(iv) well-defined minima of 247–252 K at 47 km, mainly found in April, and secondary minima ranging between 267 and 278 K in September–October, associated with maxima of 278–285 K in December, giving annual temperature variations increasing from 26 to 38 K as a function of altitude; and
(v) variable features at 60 km, similar to those observed in the Arctic atmosphere, which describe a pronounced minimum in March–May, ranging between 243 and 249 K, and a secondary minimum in September–October varying between 247 and 254 K, while austral summer maxima are observed in December, varying between 266 and 272 K, giving annual variations of 23–25 K.

The large temperature variations measured at the various MIPAS levels substantially depend at all polar latitudes on the warming and cooling processes occurring during the local summer and winter seasons. Such processes are closely related to the stratospheric dynamical events regulating heat exchanges between mid-latitude and polar regions, and are also due, albeit to a lesser extent, to the seasonal changes in the incoming flux of solar radiation. Fig. 6 shows a comparison between the monthly mean vertical profiles of $T(z)$ observed at the 12 selected polar latitudes in January, April, July and October. It is interesting to note that the vertical profiles of $T(z)$ obtained at the Arctic latitudes are more widely dispersed within the 12–25 km altitude range in January and the 20–40 km altitude range in October, while they are more limited in April and July. Conversely, the Antarctic vertical profiles of $T(z)$ are found to vary (i) more widely as a function of latitude within the 12–30 km and the 45–60 km altitude intervals in July, (ii) throughout the whole stratosphere in October, (iii) within the 45–60 km altitude range in January and (iv) within the 20–35 km range in April. This wide seasonal variability of the Antarctic vertical profiles of $T(z)$ as a function of latitude is particularly evident in the examples of July and October shown in Fig. 6, which are associated with the occurrence of strong variations in the thermal conditions inside the Antarctic vortex, almost totally preventing heat exchanges with the mid-latitude stratosphere, while the warming effects

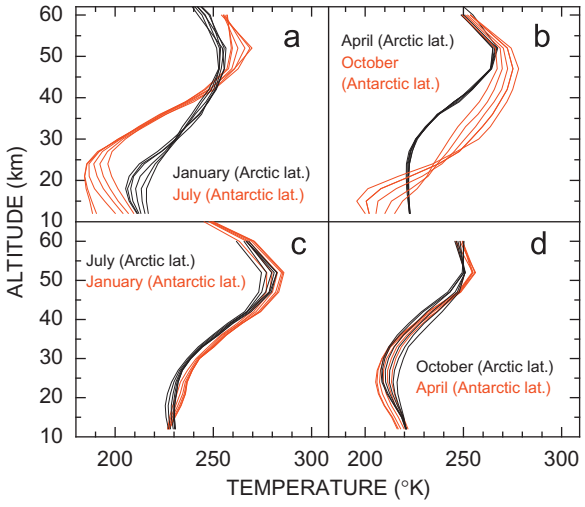

Fig. 6. Monthly mean vertical profiles of air temperature $T(z)$ obtained over the 12–68 km altitude range by averaging the MIPAS2D data at the 6 selected Arctic latitudes (black curves) and the 6 selected Antarctic latitudes (red curves) for comparison between: (a) January profiles at Arctic latitudes and July profiles at Antarctic latitudes; (b) April profiles at Arctic latitudes and October profiles at Antarctic latitudes; (c) July profiles at Arctic latitudes and January profiles at Antarctic latitudes and (d) October profiles at Arctic latitudes and April profiles at Antarctic latitudes. (For interpretation of the references to color in this figure legend, the reader is referred to the web version of this article.)

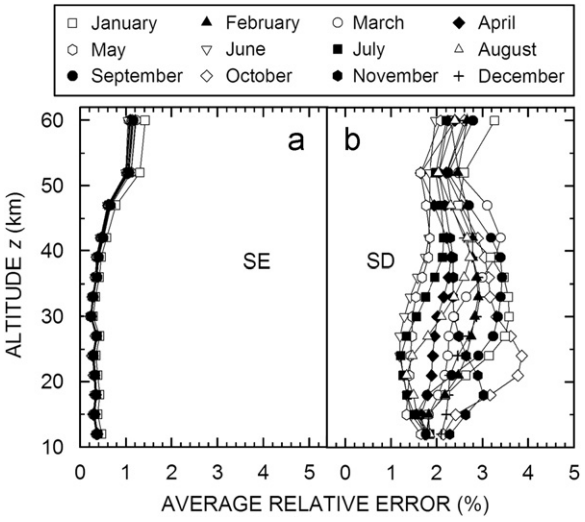

Fig. 7. Monthly vertical profiles of the average relative errors made in determining the monthly mean vertical profiles of air temperature $T(z)$ over the 12–60 km altitude range at polar latitudes: (a) weighted average systematic error SE, derived from the estimates of FR and OR systematic errors made by Dinelli et al. (2010) and (b) average standard deviation SD giving a measure of the MIPAS data dispersion.

induced by solar radiation are absent in July and very weak in October.

The large differences between the monthly mean vertical profiles of $T(z)$ obtained at Arctic and Antarctic latitudes are estimated to be only slightly due to the systematic errors made in examining the MIPAS data. In fact, the MRE errors due to measurement noise were evaluated to be all lower than 0.1% at stratospheric levels, while the multi-year values of systematic error SE, calculated as weighted averages of the FR and OR systematic errors, were estimated to decrease from 0.4% at 12 km to 0.2% at 30 km, and then to slowly increase from 30 to 50 km, up to more than 1% at the 52 and 60 km levels, as shown in Fig. 7. Consequently, due to the negligible MRE contributions, total error TE was evaluated to be only slightly higher than SE at all levels. Because of the dispersion of the single measurements of $T(z)$ derived from the MIPAS observations, the values of SD determined for the monthly mean profiles of temperature were evaluated to vary mainly between 1% and 4% over the 12–60 km range, presenting relatively higher values between 20 and 40 km. Such evaluations yield absolute values of the MIPAS multi-year average estimates of SD ranging mainly between ± 2 and ± 8 K throughout the whole altitude range.

3.2.1. Comparison with radiosounding measurements

To check the reliability of the MIPAS monthly mean vertical profiles of $T(z)$ given in Tables A3 and A4, Fig. 8 presents some comparisons made at four of the selected polar latitudes between the monthly mean vertical profiles of the MIPAS values of $T(z)$ obtained in January and July and (i) those determined from the RDS data-set recorded at various Arctic and Antarctic sites, as described in Section 3.1; (ii) those calculated from the data recorded by the Microwave Limb Sounder (MLS) on board NASA's EOS Aura satellite at the same polar latitudes, from 2005 to 2010; and (iii) those given by the CIRA models (CIRA 1986) at the 70°N, 80°N, 70°S and 80°S latitudes (see also http://badc.nerc.ac.uk/data/cira/web page).

Fig. 8 shows that the MIPAS and RDS temperature profiles defined up to 30–35 km present relatively small discrepancies, which vary mainly between -5.0 and $+4.5$ K at the two Arctic latitudes and between -4.0 and $+3.7$ K at the two Antarctic latitudes. The average (and SD) values of these differences, calculated within the 70–80°N latitude range, are equal to -0.2 (± 3.0) K in January and -0.8 (± 0.5) K in July, while those relative to the 70–80°S latitude range are equal to $+2.6$ (± 1.1) K in July (austral winter) and $+0.6$ (± 0.8) K in January (austral summer). Therefore, rather large differences were found only in Antarctica for local winter conditions. More generally, considering all the months and selected latitudes, the differences between MIPAS and RDS temperatures were estimated to range between -5.2 and $+4.6$ K in the Arctic and between -4.2 and $+3.7$ K in Antarctica. Bearing in mind that the SD estimates of the RDS monthly mean values are equal to ± 3 K at Arctic latitudes and ± 5 K at Antarctic latitudes, while those of the MIPAS

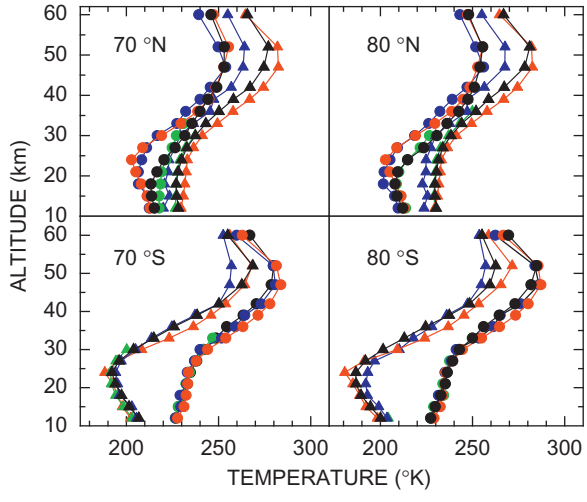

Fig. 8. Comparisons of the monthly mean vertical profiles of $T(z)$ obtained over the 12–60 km altitude range from the MIPAS2D data-sets (black symbols) at the 70°N, 80° N, 70°S and 80°S latitudes, for January (circles) and July (triangles), with (i) the corresponding vertical profiles obtained from the RDS data-set (green symbols), (ii) those derived from the MLS/Aura data-set recorded from 2005 to 2010 (blue symbols) and (iii) those given by the CIRA (1986) models (red symbols). (For interpretation of the references to color in this figure legend, the reader is referred to the web version of this article.)

monthly mean values have been estimated to be equal to ±2 K and ±10 K, respectively, the differences between MIPAS and RDS temperatures turn out to be all largely smaller than the sum of the SD values determined for the MIPAS and RDS monthly mean values. This demonstrates that the MIPAS profiles substantially agree with the RDS measurements and can be correctly used to describe the thermal conditions of the atmosphere, throughout the whole altitude range from 12 to 35 km. The discrepancies between the monthly mean vertical profiles shown in Fig. 8 can also partly be due to the fact that MIPAS data refer to the 2002–2010 period, while radiosoundings were recorded during the 2000–2003 period, MLS data in the 2005–2010 period and CIRA data mainly during the 1970–1980 period.

3.2.2. Comparison with MLS satellite-derived data

Like the MIPAS instrument, the MLS sensor measures thermal emissions at limb from a sun-synchronous polar orbiting platform, therefore ensuring global coverage during day- and nighttime conditions. Even if MLS measures the atmospheric emission at the limb like the MIPAS instrument, it operates in the microwave spectral region and adopts very different retrieval solutions, making its measurements an ideal independent data-set for comparison to our results. In fact, the MLS data-set offers the opportunity of correctly evaluating the inter-consistency of such satellite-derived data and testing the representativity of the MIPAS results obtained for the last decade's atmospheric conditions. In particular, the MLS measurements of temperature were examined, calculating the monthly mean vertical profiles of $T(z)$ on MLS pressure levels and converting the final profiles to the adopted MIPAS altitude fixed vertical grid. The comparison between MIPAS and MLS satellite-derived temperature data shown in Fig. 8 indicates that the differences recorded at levels ranging between 12 and 60 km vary mainly between −8.8 and +15.4 K at the two Arctic latitudes and between −8.7 and +11.6 K at the two Antarctic latitudes. More generally, examining the data for all months and latitudes, it was found that the MIPAS–MLS discrepancies vary between −9 and +13 K in the polar regions. Such estimates are very high and do not provide a good agreement between MIPAS and MLS evaluations. However, it can be noticed that the MLS temperatures differ from the RDS ones much more than the MIPAS data at low stratospheric levels. In fact, the differences between MLS and RDS vertical profiles of $T(z)$ shown in Fig. 8 vary between −13.8 and +4.8 K at Arctic latitudes, with predominantly negative values, and between −2.9 and +4.8 K at Antarctic latitudes, giving yearly average (and SD) values equal to +4.2 (±6.5) K in the Arctic, and −0.3 (±3.7) K in Antarctica. These findings indicate that MLS evaluations of $T(z)$ are in general considerably higher than the RDS ones in the Arctic low stratosphere, and show a closer agreement at Antarctic latitudes. Therefore, the MIPAS profiles of $T(z)$ turn out to be more reliable than those obtained from the MLS observations within the lower part of the stratosphere in both polar regions.

3.2.3. Long-term variations of temperature vertical profiles

The differences between MIPAS and CIRA vertical profiles of $T(z)$ shown in Fig. 8 for the 70°N and 80°N latitudes were found to vary between −2.2 and +17.6 K at Arctic levels from 12 to 24 km, giving average (and SD) values equal to +2.9 (±3.7) K and +2.6 (±5.8) K in January and −1.1 (±1.0) K and −1.3 (±1.1) K in July, respectively. The differences relative to the 70°S and 80°S latitudes ranged between −2.9 and +6.0 K at the 12–24 km levels, providing average (and SD) values equal to −1.0 (±1.5) K and −0.8 (±1.5) K in January (austral summer) and +3.1 (±1.3) K and +2.5 (±2.1) K in July (austral winter), respectively. More generally, the differences between MIPAS and CIRA temperatures calculated over the whole year at levels $z < 25$ km were evaluated to vary mainly between −6 and +11 K at Arctic latitudes and between −14 and +11 K at Antarctic latitudes, giving yearly average (and SD) values of 0.5 (±3.1) K over the 70–80°N latitude range, and 0.2 (±3.3) K over the 70–80°S latitude range. In particular, during the winter season (i.e. December–February in the Arctic region and June–August in Antarctica), the average (and SD) values of the seasonal variations within the low stratosphere were equal to 3.4 (±3.7) K at the 70–80°N latitudes and 1.8 (±2.2) K at the 70–80°S latitudes, while in the local summer season (i.e. June–August in the Arctic and December–February in Antarctica) they were found to be of −0.5 (±2.8) and −1.2 (±2.3) K, respectively. These evaluations provide average yearly estimates of the temperature trend within the 12–25 km altitude range that are lower than 0.2 (±1.0) K/decade in the Arctic and equal to about 0.1 (±1.5) K/decade in Antarctica, giving an average measure of the variations in the thermal conditions of the low stratosphere occurring over the last 3 decades.

The above results do not differ appreciably from the temperature variations evaluated in the low stratosphere by Randel et al. (2009), who examined both radiosonde data-sets and series of NOAA satellite data covering the period from 1979 to 2007, and found that appreciable temperature changes occurred in that period at Arctic (60°N–90°N) and Antarctic latitudes (60°S–90°S). The Arctic variations were estimated to have an average winter trend decreasing from +0.2 K/decade at 12 km to about −0.7 K/decade at 25 km, and an average summer trend decreasing from −0.3 K/decade at 12 km to about −0.6 K/decade at 25 km, while the yearly average trend varied from −0.1 K/decade at 12 km to −0.8 K/decade at 25 km. More marked variations were found for Antarctica, where the average austral winter trend was estimated to decrease from +0.2 K/decade at 12 km to a nearly null value at 25 km, and the average austral summer trend to decrease from −1.0 K/decade at 12 km to about −1.4 K/decade at 15 km, then increasing up to about −0.6 K/decade at 25 km. The yearly average trend was defined to vary from −0.3 K/decade at 12 km to −0.7 K/decade at 15 km, subsequently increasing to −0.4 K/decade at 25 km.

Therefore, the present annual average value of the MIPAS–CIRA temperature trend per decade turns out to be a little smaller than the evaluations of Randel et al. (2009), which, however, were obtained over the wider 60–90° latitude range. Thus, the MIPAS–CIRA variations are definitely smaller and, hence, more realistic than those obtained by comparing the MLS temperature profiles with the CIRA models in the low stratosphere.

In the higher part of the stratosphere, from 25 to 60 km, the differences between MIPAS and CIRA temperature data shown in Fig. 8 vary between (i) −8.2 and +17.6 K at Arctic levels, with an yearly average (and SD) value of −0.9 (±5.0) and −3.2 (±4.5) K, respectively, and (ii) −12.3 and +4.0 K at Antarctic levels, with an yearly average (and SD) value of −3.2 (±4.5) K. The seasonal average values within the 70–80°N latitudes were found to be +2.5 (±6.0) K in winter and −2.4 (±4.5) K in summer, while those for the 70–80°S latitudes were −4.5 (±4.5) K in austral winter and −3.7 (±4.3) K in austral summer. These findings suggest that large decreases in the thermal conditions of the high stratosphere could have occurred during the last 3 decades, providing yearly average estimates of this trend within the 25–60 km altitude range equal to −0.3 K/decade in the Arctic and −1.1 K/decade in Antarctica.

3.3. Water vapour volume mixing ratio

In order to minimise the presence of oscillations in the final monthly mean vertical profiles of $Q(z)$ and produce reference profiles that can be more robustly used in calculations, the

MIPAS2D original profiles were interpolated on a log-pressure scale in steps of about 1 km. The averages were then performed on this finer grid, and the averaged profiles subsequently converted to the same final altitude scale of the other quantities reported in the present paper. The vertical mean profiles were further smoothed over 5 pressure levels, i.e. over an altitude range of about 6 km. This strategy resulted in smoothed vertical profiles, which correctly reproduce the overall behaviour of the original profiles while avoiding abrupt vertical changes.

The monthly mean values of $Q(z)$ obtained at the 14 MIPAS fixed levels are reported in Table A5 for the 6 Arctic latitudes, and in Table A6 for the 6 Antarctic latitudes, with an accuracy of 0.1 ppmv. Fig. 9 presents the series of monthly average values of $Q(z)$ at the 12, 21, 33, 47 and 60 km levels for all the selected Arctic and Antarctic latitudes, ranging mainly between 3 and 7 ppmv. The series of $Q(z)$ relative to the 12 km altitude has higher monthly mean values in the warmer period of the year, varying between 5 and 9 ppmv at all the Arctic latitudes. In particular, the series of the 65°N latitude exhibits a rather high peak in July, presumably due to the fact that the tropopause height is greater than 12 km during the summer months at this latitude and, hence, parameter $Q(z)$ is due to the presence of tropospheric water vapour at this level. At higher Arctic latitudes, the values of $Q(z)$ were found to be rather stable during the year, presenting slowly increasing trends at the 47 and 60 km levels from January to September–October. In Antarctica, a marked minimum is evident at the 12 and 21 km levels for all latitudes during the austral winter months, with values ranging mainly between 2 and 4 ppmv, followed by increasing values in the austral summer. At higher levels, the monthly mean values of this parameter are more stable and vary mainly between 5 and 8 ppmv.

In Fig. 10, the monthly mean vertical profiles of $Q(z)$ for January, April, July and October at the 6 selected Arctic latitudes are compared with those obtained at the 6 Antarctic latitudes. It can be seen that $Q(z)$ varies mainly between 2 and 6 ppmv for $z < 25$ km in both the Arctic and Antarctic regions, assuming gradually higher values mainly ranging between 4 and 7 ppmv in all seasons, as the altitude increases from 25 to 50 km. The comparison also provides evidence of the similar moisture conditions observed in (a) Arctic January and Antarctic July, especially from 25 to 45 km, (b) Arctic April and Antarctic October, from less than 30 to 50 km, (c) Arctic July and Antarctic January throughout the whole altitude range and (d) Arctic October and Antarctic April from about 20 km to at least 55 km.

Estimates of the SE errors at the MIPAS fixed levels are presented in Fig. 11, showing that the MIPAS evaluations of $Q(z)$ are affected by rather high uncertainty features. The MRE errors are relatively high within the 12–30 km altitude range, varying mainly between 1% and nearly 8%, and lower than 1% at the upper levels. Calculated as weighted averages of the FR and OR errors estimated by Dinelli et al. (2010) during the two MIPAS observation phases, the SE errors decrease from 40% to 10% as the altitude increases from 12 to 20 km, remain equal to around 10% from 20 to 50 km and then increase up to 60% at 60 km. Due to the smaller contributions of MRE errors with respect to SE ones, total errors TE were estimated to be slightly higher than the SE errors shown in Fig. 11 at all levels. Therefore, the vertical profiles of SD shown in Fig. 11 assume values all greater than 90% at the 12 km level, which then decrease rapidly with altitude becoming lower than 40% at 20 km, vary between 5% and 20% from 25 to 50 km and then mainly range between 10% and 40% from 52 to 60 km.

The vertical VMR profiles shown in Fig. 12 for comparison with the MIPAS results were determined from the water vapour MLS/Aura data recorded at polar latitudes over the period from 2005 to 2010. They were averaged on the MLS original pressure levels and then smoothed by following a procedure similar to that used for the MIPAS data. The smoothing was performed on 4 MLS pressure

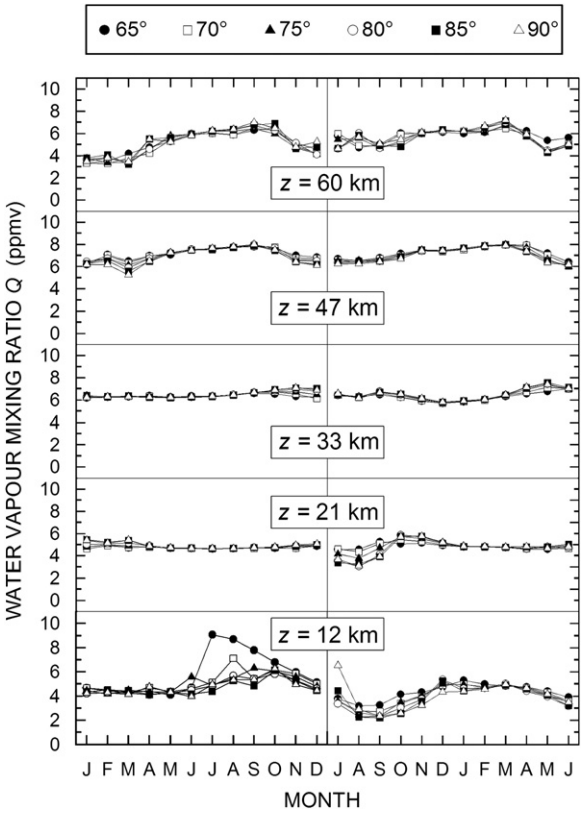

Fig. 9. Series of the monthly mean values of water vapour volume mixing ratio $Q(z)$ obtained at five MIPAS fixed levels z, for the 6 selected Arctic latitudes (left) and the 6 selected Antarctic latitudes (right). The series of Antarctic months is represented over the period from July to June, taking into account that it is out of phase by 6 months with respect to that of the Arctic months, presented from January to December.

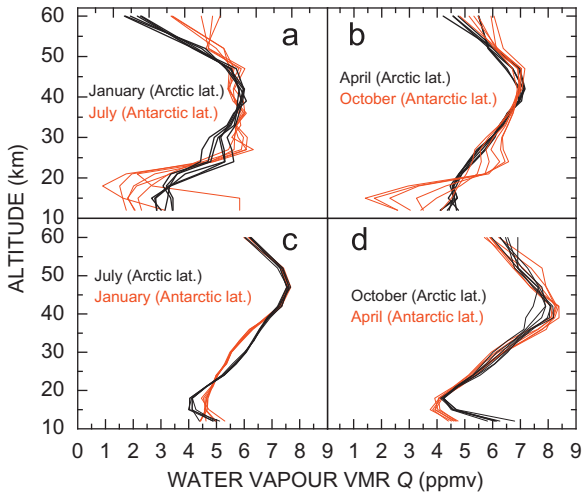

Fig. 10. Monthly mean vertical profiles of water vapour volume mixing ratio $Q(z)$ obtained over the 12–68 km altitude range by analyzing the MIPAS2D data-set at the 6 selected Arctic latitudes (black curves) and the 6 selected Antarctic latitudes (red curves) for comparison between (a) January profiles at Arctic latitudes and July profiles at Antarctic latitudes; (b) April profiles at Arctic latitudes and October profiles at Antarctic latitudes; (c) July profiles at Arctic latitudes and January profiles at Antarctic latitudes and (d) October profiles at Arctic latitudes and April profiles at Antarctic latitudes. (For interpretation of the references to color in this figure legend, the reader is referred to the web version of this article.)

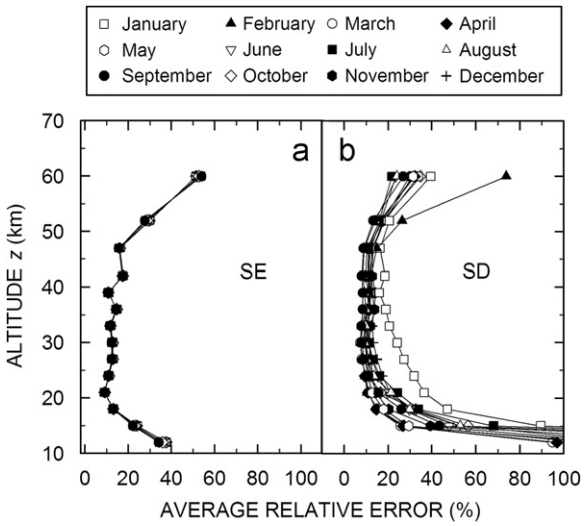

Fig. 11. Monthly vertical profiles of the average relative errors made in determining the monthly mean vertical profiles of water vapour volume mixing ratio $Q(z)$ over the 12–60 km altitude range at polar latitudes: (a) weighted average systematic error SE, derived from the estimates of FR and OR systematic errors made by Dinelli et al. (2010) and (b) average standard deviation SD giving a measure of the MIPAS data dispersion.

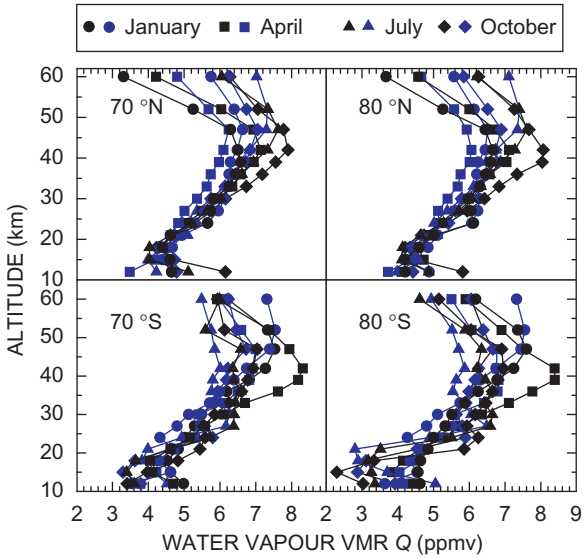

Fig. 12. Comparisons of the monthly mean vertical profiles of $Q(z)$ obtained over the 12–60 km altitude range from the MIPAS2D data-sets (black symbols) at the 70°N, 80°N, 70°S and 80°S latitudes, for January (circles), April (squares), July (triangles) and October (diamonds), with the corresponding vertical profiles obtained from the MLS/Aura data-set recorded from 2005 to 2010 (blue symbols). (For interpretation of the references to color in this figure legend, the reader is referred to the web version of this article.)

levels, i.e. over a range of about 5 km below 30 km and 10 km at higher levels. The final smoothed profiles were then converted to the adopted MIPAS fixed altitude grid.

3.3.1. Comparison with MLS satellite-derived data

Fig. 12 presents the comparison between the monthly mean vertical profiles of $Q(z)$ derived from the MIPAS data relative to the 70°N, 80°N, 70°S and 80°S latitudes, for January, April, July and October, and those correspondingly obtained from the above analysis of the MLS data. It is evident that the differences between the MIPAS and MLS evaluations of $Q(z)$ do not generally exceed ± 0.7 ppmv at altitudes $z < 20$ km, ± 1.2 ppmv from 20 to 50 km and ± 1.8 ppmv at the low mesospheric levels from 50 to 60 km. Thus, they are on average lower than 20%, i.e. comparable with the values of SD obtained in the present analysis for the MIPAS data over the whole altitude range.

Appendix B shows the comparison between the monthly vertical profiles of $Q(z)$ obtained from the MIPAS2D data-set and those derived analyzing the data extracted from sets of satellite-borne, air-borne and ground-based lidar measurements taken over the last 30 years, separately for each latitude class and for some months. These results indicate that the MIPAS vertical profiles give values of $Q(z)$ that are higher only in some cases by 1–2 ppmv than those derived in Appendix B. This suggests that appreciable changes in the volume concentration of stratospheric water vapour have been induced in the Arctic and Antarctic stratosphere over the last two decades by the pressure and temperature variations linked to climate changes and ozone depletion. They have induced an average increase of 10% at both Arctic and Antarctic latitudes from the 1991–2001 period to the 2002–2010 MIPAS observations, i.e. of about 0.5 ppmv, such increase being in good agreement with the Hurst et al. (2011) estimates obtained at mid-latitudes of the Northern hemisphere.

4. Use of the MIPAS vertical profiles in radiative transfer calculations

The monthly mean vertical profiles of $p(z)$, $T(z)$ and $Q(z)$ determined in the present analysis of the MIPAS data-set are suitable for use in radiative transfer calculations for numerous applications to remote sensing studies, measurements of atmospheric transmission of short-wave and long-wave radiation and evaluations of water vapour absorption and infrared radiation atmospheric emission. An application is here proposed to present the calculations of the vertical profiles of Rayleigh-scattering coefficient $\beta_R(\lambda)$ at visible and near-infrared wavelengths, as obtained for the 12 months at the 70° and 80° latitudes of both hemispheres. For these calculations the monthly mean vertical profiles of $p(z)$, $T(z)$ and $Q(z)$ are used together with the annual mean vertical profiles of CO_2 volume concentration defined by Tomasi et al. (2010), to determine the monthly mean vertical profiles of $\beta_R(\lambda)$ using the Tomasi et al. (2005) algorithm. Fig. 13 presents the monthly mean vertical profiles of $\beta_R(\lambda)$ calculated at the 440, 550 and 870 nm wavelengths, for a triplet of spring–summer months (May, July and September) at the 70°N and 80°N altitudes and the triplet of austral summer months (December, January and February) at the 70°S and 80°S latitudes.

The results clearly indicate that the spectral values of $\beta_R(\lambda)$ decrease exponentially with altitude, closely depending on air density, with slope coefficients slightly differing from one month to another at high stratospheric levels. It is interesting to note that the seasonal variations in the vertical profiles of pressure and temperature produce considerable changes in $\beta_R(\lambda)$ throughout the year. For instance, the winter-to-summer variations in $\beta_R(550\text{ nm})$ at 30 km altitude are equal to +48% (at 70°N latitude), +54% (at 80°N), +67% (at 70°S) and +55% (at 80°S). This means that such seasonal variations cause annual changes in parameter $\beta_R(\lambda)$ at visible wavelengths that are comparable to the ones due to spectral shifts of about – 50 nm at Arctic latitudes and of about – 60 nm at Antarctic latitudes. The example underscores how a knowledge of the present MIPAS set of stratospheric parameters is useful not only for the analysis of limb observations but also for calculating with great accuracy the stratospheric contributions of Rayleigh-scattering optical depth at various wavelengths, and obtaining more precise spectral evaluations of the overall atmospheric Rayleigh-scattering optical depth.

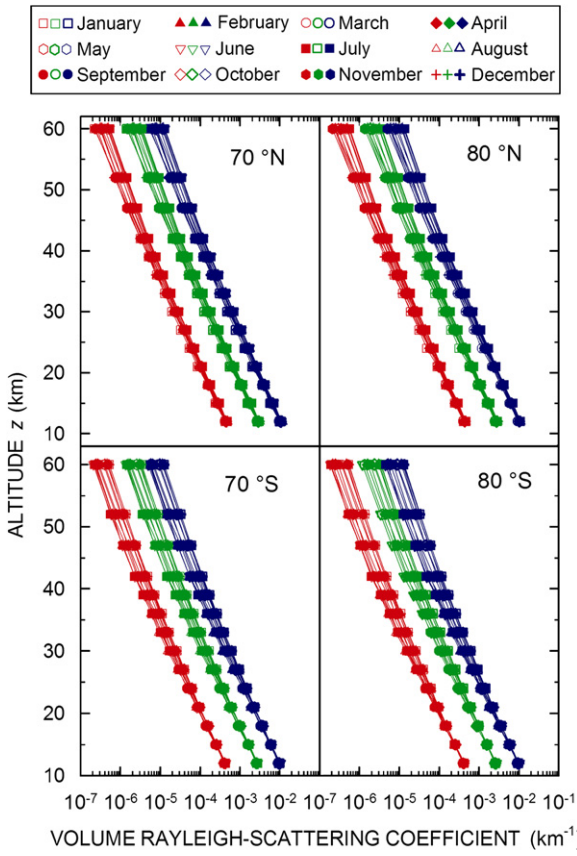

Fig. 13. Vertical profiles of volume Rayleigh-scattering coefficient calculated using the algorithm of Tomasi et al. (2005) for the MIPAS monthly mean vertical profiles of pressure, temperature and water vapour volume mixing ratio, and for the CO_2 concentration vertical profiles defined by Tomasi et al. (2010). The profiles refer to the 870 nm (red symbols), 550 nm (green symbols) and 400 nm (blue symbols) wavelengths, and are presented for all months, separately for the 70°N, 80°N, 70°S and 80°S latitudes. (For interpretation of the references to color in this figure legend, the reader is referred to the web version of this article.)

This value needs to be calculated with high precision when sun-photometer measurements are analysed at Arctic stations (Barrow, Alert, Eureka, Summit and Ny Ålesund) and Antarctic sites (Neumayer, Syowa, Maitri, Troll, Aboa, Mario Zucchelli, Halley, McMurdo, Dome C and South Pole), allowing a more accurate evaluations of aerosol optical depth at the sun-photometer wavelengths from the ultra-violet to near-infrared (Tomasi et al., 2010).

5. Monthly mean vertical profiles of absolute humidity at polar latitudes

Water vapour VMR $Q(z)$ at each level is given by the ratio between water vapour partial pressure $e(z)$ and total air pressure $p(z)$. Therefore, the monthly mean vertical profiles of $e(z)$ were calculated at all the MIPAS levels and for each of the 12 selected polar latitudes by multiplying the values of $Q(z)$ given in Tables A5 and A6 by the corresponding values of $p(z)$ given in Tables A1 and A2. The monthly mean vertical profiles of absolute humidity $\rho_w(z)$ were then calculated by assuming that $\rho_w(z)$ is given at each level as the ratio between the partial pressure $e(z)$ (measured in hPa) and the product $4.615 \times 10^{-3} T(z)$ (with $T(z)$ measured in K), according to the well-known equation of state of water vapour, in which the gas constant for water vapour $R_w = 0.4615\ \mathrm{J\,g^{-1}\,K^{-1}}$ is used.

The monthly mean values of $\rho_w(z)$ determined at the MIPAS levels for all months and the 6 selected Arctic latitudes are given in Table A7, those relative to the 6 Antarctic latitudes in Table A8. They are presented in Fig. 14 for four of the selected polar latitudes, showing that this moisture parameter decreases with altitude in an approximately exponential fashion in all cases. Examining the data in Table A7, $\rho_w(z)$ is seen to decrease at Arctic latitudes from values ranging between $7 \times 10^{-4}\ \mathrm{g\,m^{-3}}$ (in March) and $1.8 \times 10^{-3}\ \mathrm{g\,m^{-3}}$ (in July and August) at the 12 km level, to values between $3.1 \times 10^{-7}\ \mathrm{g\,m^{-3}}$ (in January) and $1.6 \times 10^{-6}\ \mathrm{g\,m^{-3}}$ (in July) at the 60 km level. In Table A8, relative to the Antarctic latitudes, $\rho_w(z)$ assumes values generally ranging between $3.7 \times 10^{-4}\ \mathrm{g\,m^{-3}}$ (in August) and nearly $1 \times 10^{-3}\ \mathrm{g\,m^{-3}}$ (in December) at the 12 km level, and then decreases sharply with altitude until varying between $3.5 \times 10^{-7}\ \mathrm{g\,m^{-3}}$ (in July) and $1.5 \times 10^{-6}\ \mathrm{g\,m^{-3}}$ (in December) at the 60 km level.

Such seasonal variations are considerably larger than the errors made in deriving $\rho_w(z)$, as indicated by the calculations of the SD of $\rho_w(z)$ performed at all levels and for all months and latitudes, using the average values of SD estimated in Fig. 3 for $p(z)$, in Fig. 7 for $T(z)$ and in Fig. 11 for $Q(z)$. The SD values were estimated to exceed 100% in the most cases at the 12 km level, to vary mainly between 30% and 40% throughout the altitude range from 21 to 52 km, and to assume in general values greater than 60% at the 60 km level.

In the Arctic, the values of $\rho_w(z)$ for the summer months (June–October) are greater than those obtained in late winter and early spring by 20% on average. In the Antarctic atmosphere, the values of $\rho_w(z)$ for the austral summer months are on average higher by 30% than those measured in the austral winter. These

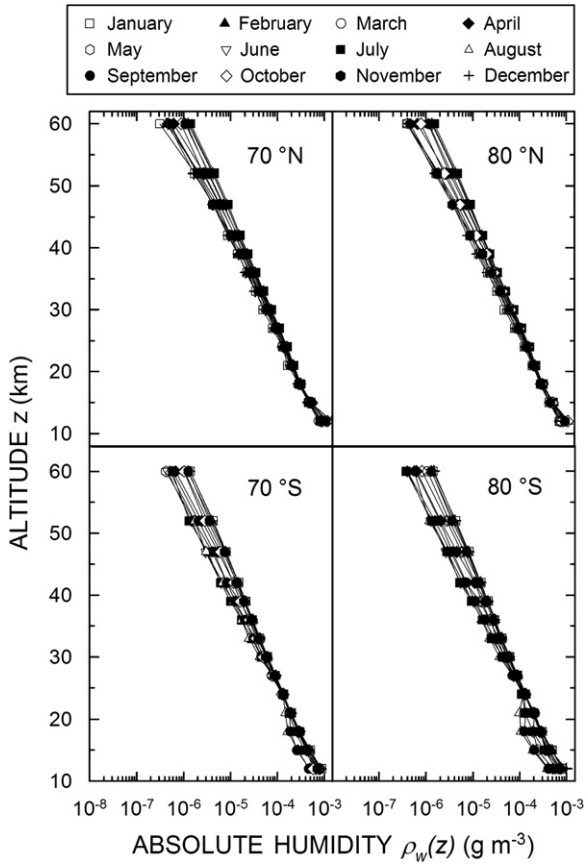

Fig. 14. Monthly mean vertical profiles of absolute humidity $\rho_w(z)$ determined at the 70°N, 80°N, 70°S and 80°S latitudes over the 12–60 km altitude range from the monthly mean vertical profiles of $p(z)$, $T(z)$ and $Q(z)$ obtained by examining the present MIPAS2D data-set and reported in Tables A1–A6.

seasonal variations of $\rho_w(z)$ imply that stratospheric water vapour content W, defined over the 12–50 km altitude range, assumes higher monthly mean values during the local summer in both polar regions. Such issues are the subject of more detailed discussion in the next section.

6. Evaluations of the monthly mean stratospheric water vapour content

The MIPAS values of stratospheric water vapour content W were calculated at each selected latitude and for each month by integrating over the 12–50 km altitude range the MIPAS monthly mean vertical profiles of $\rho_w(z)$, as given in Tables A7 and A8. In doing so, it was assumed that $\rho_w(z)$ decreases from each level to the subsequent one following an exponential trend with altitude, as shown in Fig. 14. These monthly average values of W are shown in Table 1, together with their standard deviations, while their time-patterns are shown in Fig. 15, separately for the Arctic and Antarctic latitudes. These values of W were obtained with high relative standard deviations, varying (i) in the Arctic, between $\pm 26\%$ in September at the 80°N latitude and about $\pm 160\%$ in July at the 90°N latitude, and (ii) in Antarctica, between $\pm 22\%$ in March and $\pm 167\%$ in December, in both cases at the 90°S latitude.

The monthly mean values of W determined at the 6 Arctic latitudes vary between 0.0047 mm (January, 80°N and 90°N) and 0.0070 mm (July, 65°N), presenting large minima at all latitudes from December to February, and wide maxima from July to September. The monthly mean values of W determined at the 70–90°N latitudes are quite stable throughout the year, except those measured at the 65°N latitude from July to September, which describe an abrupt and pronounced peak in August, which is higher by about 15–20% than the values measured in June and October, presumably because these estimates contain a contribution due to tropospheric water vapour. In Antarctica, relatively high values of W exceeding 0.005 mm were found at all latitudes during the austral summer (mainly from December to February) and values < 0.003 mm in August–September, at the 75–90°S latitudes. The values of W determined from June to November vary considerably, from 0.0026 to 0.0055 mm, as a result of the cooling effects produced by the Antarctic vortex, which persists also in the austral spring.

To give an idea of the importance of such low water vapour content in radiative transfer calculations, it is useful to bear in mind that measurements of total water vapour content W_1 performed with sun-photometers at the OASI site near the Italian Mario Zucchelli station (Terra Nova Bay) (74° 42′S, 164° 06′E, 92 m a.m.s.l.) in Antarctica provided values of W_1 ranging mainly between 1 and 4 mm during the austral summer periods of 1993, 1994 and 1996 (Tomasi et al., 2008). Thus, the relative contribution of stratospheric water vapour content to the total content of atmospheric water vapour is evaluated to be smaller than 0.6% at sea-level Antarctic sites. Instead, at Dome C (74° 42′S, 164° 06′E, 92 m a.m.s.l.) on the Antarctic Plateau (75° 06′S, 123° 21′E, 3233 m a.m.s.l.), parameter W_1 was evaluated to assume values ranging mainly between 0.3 and 0.6 mm (Tomasi et al., 2006). This indicates that W can contribute to W_1 by more than 1% throughout the year. For these estimates of stratospheric content W, important absorption effects on the downwelling submillimetric

Table 1
Monthly mean values of $10^3 W$ (mm) calculated within the atmospheric region from 12 to 50 km altitude, as determined for the above-chosen 12 latitudes by integrating the monthly mean vertical profiles of absolute humidity $\rho_w(z)$ shown in Tables A7 and A8 for the Arctic and Antarctic latitudes, respectively.

Month	Latitude											
	65°N	70°N	75°N	80°N	85°N	90°N	65°S	70°S	75°S	80°S	85°S	90°S
Jan.	5.1 ± 3.2	5.0 ± 2.7	4.9 ± 2.1	4.7 ± 2.2	4.8 ± 2.1	4.7 ± 2.3	5.5 ± 6.3	5.4 ± 8.9	5.4 ± 2.9	5.3 ± 2.7	5.3 ± 2.1	5.3 ± 2.0
Feb.	5.1 ± 2.5	5.1 ± 2.6	5.0 ± 2.2	5.0 ± 2.0	5.1 ± 2.0	4.9 ± 1.9	5.4 ± 4.1	5.3 ± 2.1	5.3 ± 1.9	5.2 ± 1.3	5.3 ± 1.3	5.3 ± 1.9
Mar.	4.9 ± 2.8	5.0 ± 2.3	5.1 ± 1.8	5.0 ± 1.9	5.1 ± 1.7	4.9 ± 1.9	5.1 ± 2.7	5.2 ± 3.0	5.2 ± 1.8	5.2 ± 1.3	5.1 ± 1.2	5.1 ± 1.1
Apr.	5.5 ± 2.7	5.5 ± 2.5	5.4 ± 2.1	5.3 ± 1.8	5.3 ± 1.7	5.4 ± 2.6	5.1 ± 2.5	5.0 ± 2.0	4.8 ± 1.7	4.8 ± 1.3	4.9 ± 1.4	4.9 ± 1.3
May	5.3 ± 2.4	5.4 ± 2.0	5.4 ± 1.8	5.4 ± 1.8	5.4 ± 1.8	5.4 ± 1.8	4.8 ± 2.8	4.8 ± 2.4	4.6 ± 1.7	4.6 ± 2.8	4.6 ± 1.7	4.6 ± 1.6
June	5.7 ± 4.5	5.7 ± 2.7	5.9 ± 3.8	5.8 ± 1.9	5.7 ± 4.3	5.8 ± 8.3	4.6 ± 2.4	4.6 ± 2.2	4.4 ± 2.5	4.2 ± 3.0	4.1 ± 2.5	4.1 ± 2.5
July	7.0 ± 7.7	6.1 ± 6.1	6.0 ± 3.5	6.0 ± 4.2	5.8 ± 4.6	6.1 ± 9.8	4.6 ± 3.4	4.3 ± 3.9	4.1 ± 3.6	3.7 ± 2.0	3.9 ± 2.4	5.0 ± 2.3
Aug.	7.0 ± 7.3	6.5 ± 4.8	6.0 ± 4.7	6.1 ± 2.9	6.0 ± 2.7	5.9 ± 3.2	3.9 ± 2.5	3.4 ± 2.4	3.0 ± 2.9	2.6 ± 1.6	2.6 ± 1.2	2.7 ± 1.4
Sep.	6.5 ± 4.6	5.9 ± 2.6	6.1 ± 1.9	5.8 ± 1.5	5.6 ± 2.0	5.7 ± 2.0	4.2 ± 3.5	3.6 ± 2.7	3.1 ± 2.5	2.9 ± 1.8	2.8 ± 2.6	2.7 ± 1.5
Oct.	6.2 ± 9.9	6.0 ± 2.0	5.9 ± 2.1	5.8 ± 1.8	5.8 ± 1.7	5.9 ± 1.8	5.0 ± 6.9	4.6 ± 3.0	4.2 ± 2.1	3.6 ± 2.2	3.3 ± 1.9	3.1 ± 1.4
Nov.	5.7 ± 3.9	5.7 ± 3.0	5.5 ± 2.4	5.4 ± 2.0	5.3 ± 1.7	5.2 ± 1.8	5.2 ± 2.8	5.0 ± 3.3	4.9 ± 2.5	4.6 ± 2.6	4.5 ± 2.9	4.3 ± 2.5
Dec.	5.3 ± 2.8	5.2 ± 2.4	5.0 ± 2.2	4.9 ± 2.0	4.9 ± 1.8	4.8 ± 1.8	5.3 ± 4.9	5.3 ± 4.2	5.3 ± 8.8	5.3 ± 4.3	5.2 ± 3.4	5.0 ± 5.6

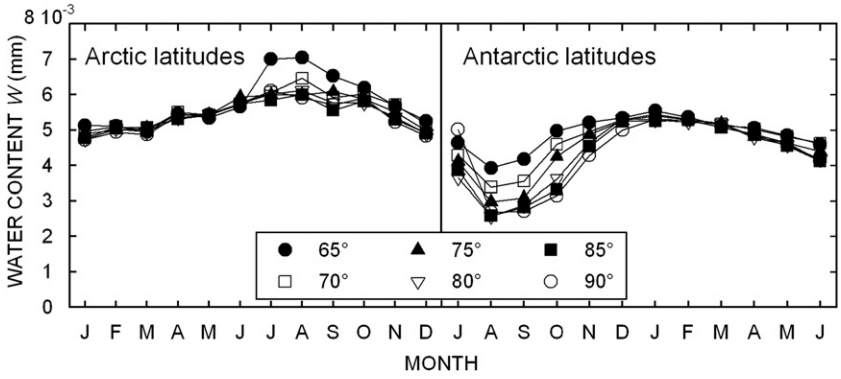

Fig. 15. Series of the monthly mean values of stratospheric water vapour content W obtained for the 6 selected Arctic latitudes (left) and the 6 selected Antarctic latitudes (right) through integration over the 12–50 km altitude range of the monthly mean vertical profiles of absolute humidity $\rho_w(z)$ reported in Tables A7 and A8, respectively.

Table A1
Monthly mean values of total air pressure p (hPa) obtained from the MIPAS data-set at 14 fixed levels from 12 to 60 km, for the 65°N, 70°N, 75°N, 80°N, 85°N and 90°N latitudes.

Latitude	Altitude (km)	Month											
		Jan.	Feb.	Mar.	Apr.	May	June	July	Aug.	Sep.	Oct.	Nov.	Dec.
65°N	12	$1.81\times10^{+2}$	$1.84\times10^{+2}$	$1.82\times10^{+2}$	$1.95\times10^{+2}$	$1.97\times10^{+2}$	$2.07\times10^{+2}$	$2.13\times10^{+2}$	$2.12\times10^{+2}$	$1.99\times10^{+2}$	$1.94\times10^{+2}$	$1.84\times10^{+2}$	$1.82\times10^{+2}$
	15	$1.06\times10^{+2}$	$1.10\times10^{+2}$	$1.11\times10^{+2}$	$1.13\times10^{+2}$	$1.24\times10^{+2}$	$1.29\times10^{+2}$	$1.35\times10^{+2}$	$1.28\times10^{+2}$	$1.22\times10^{+2}$	$1.19\times10^{+2}$	$1.12\times10^{+2}$	$1.08\times10^{+2}$
	18	$6.39\times10^{+1}$	$6.51\times10^{+1}$	$6.61\times10^{+1}$	$6.98\times10^{+1}$	$7.39\times10^{+1}$	$7.80\times10^{+1}$	$8.18\times10^{+1}$	$7.83\times10^{+1}$	$7.44\times10^{+1}$	$7.16\times10^{+1}$	$6.83\times10^{+1}$	$6.44\times10^{+1}$
	21	$3.86\times10^{+1}$	$4.01\times10^{+1}$	$4.11\times10^{+1}$	$4.34\times10^{+1}$	$4.66\times10^{+1}$	$4.84\times10^{+1}$	$5.09\times10^{+1}$	$4.82\times10^{+1}$	$4.58\times10^{+1}$	$4.44\times10^{+1}$	$4.23\times10^{+1}$	$4.16\times10^{+1}$
	24	$2.38\times10^{+1}$	$2.64\times10^{+1}$	$2.51\times10^{+1}$	$2.76\times10^{+1}$	$2.98\times10^{+1}$	$3.15\times10^{+1}$	$3.31\times10^{+1}$	$3.15\times10^{+1}$	$2.99\times10^{+1}$	$2.76\times10^{+1}$	$2.58\times10^{+1}$	$2.41\times10^{+1}$
	27	$1.54\times10^{+1}$	$1.56\times10^{+1}$	$1.64\times10^{+1}$	$1.76\times10^{+1}$	$1.88\times10^{+1}$	$2.01\times10^{+1}$	$2.12\times10^{+1}$	$2.00\times10^{+1}$	$1.85\times10^{+1}$	$1.73\times10^{+1}$	$1.63\times10^{+1}$	$1.59\times10^{+1}$
	30	9.46×10^{0}	$1.04\times10^{+1}$	$1.01\times10^{+1}$	$1.10\times10^{+1}$	$1.20\times10^{+1}$	$1.29\times10^{+1}$	$1.36\times10^{+1}$	$1.28\times10^{+1}$	$1.16\times10^{+1}$	$1.07\times10^{+1}$	9.90×10^{0}	9.62×10^{0}
	33	6.06×10^{0}	6.59×10^{0}	6.60×10^{0}	7.15×10^{0}	7.89×10^{0}	8.44×10^{0}	8.94×10^{0}	8.43×10^{0}	7.57×10^{0}	7.02×10^{0}	6.15×10^{0}	6.09×10^{0}
	36	4.06×10^{0}	3.71×10^{0}	4.07×10^{0}	4.57×10^{0}	5.09×10^{0}	5.63×10^{0}	5.90×10^{0}	5.49×10^{0}	4.91×10^{0}	4.47×10^{0}	3.91×10^{0}	3.82×10^{0}
	39	2.44×10^{0}	2.55×10^{0}	2.68×10^{0}	3.01×10^{0}	3.46×10^{0}	3.79×10^{0}	3.99×10^{0}	3.67×10^{0}	3.20×10^{0}	2.79×10^{0}	2.44×10^{0}	2.43×10^{0}
	42	1.62×10^{0}	1.70×10^{0}	1.71×10^{0}	1.99×10^{0}	2.29×10^{0}	2.52×10^{0}	2.66×10^{0}	2.43×10^{0}	2.10×10^{0}	1.77×10^{0}	1.52×10^{0}	1.56×10^{0}
	47	7.94×10^{-1}	8.60×10^{-1}	8.90×10^{-1}	1.04×10^{0}	1.22×10^{0}	1.37×10^{0}	1.44×10^{0}	1.29×10^{0}	1.07×10^{0}	8.98×10^{-1}	7.50×10^{-1}	7.96×10^{-1}
	52	4.02×10^{-1}	4.03×10^{-1}	4.51×10^{-1}	5.57×10^{-1}	6.63×10^{-1}	7.47×10^{-1}	7.78×10^{-1}	7.00×10^{-1}	5.60×10^{-1}	4.55×10^{-1}	3.74×10^{-1}	3.73×10^{-1}
	60	1.10×10^{-1}	1.43×10^{-1}	1.57×10^{-1}	1.81×10^{-1}	2.38×10^{-1}	2.66×10^{-1}	2.78×10^{-1}	2.44×10^{-1}	1.99×10^{-1}	1.64×10^{-1}	1.32×10^{-1}	1.20×10^{-1}
70°N	12	$1.79\times10^{+2}$	$1.81\times10^{+2}$	$1.79\times10^{+2}$	$1.90\times10^{+2}$	$1.93\times10^{+2}$	$2.04\times10^{+2}$	$2.08\times10^{+2}$	$2.11\times10^{+2}$	$1.96\times10^{+2}$	$1.92\times10^{+2}$	$1.85\times10^{+2}$	$1.81\times10^{+2}$
	15	$1.00\times10^{+2}$	$1.09\times10^{+2}$	$1.07\times10^{+2}$	$1.14\times10^{+2}$	$1.23\times10^{+2}$	$1.30\times10^{+2}$	$1.36\times10^{+2}$	$1.27\times10^{+2}$	$1.22\times10^{+2}$	$1.18\times10^{+2}$	$1.13\times10^{+2}$	$1.07\times10^{+2}$
	18	$6.46\times10^{+1}$	$6.35\times10^{+1}$	$6.62\times10^{+1}$	$6.94\times10^{+1}$	$7.40\times10^{+1}$	$7.83\times10^{+1}$	$8.14\times10^{+1}$	$7.80\times10^{+1}$	$7.37\times10^{+1}$	$7.10\times10^{+1}$	$6.73\times10^{+1}$	$6.41\times10^{+1}$
	21	$3.61\times10^{+1}$	$4.03\times10^{+1}$	$3.96\times10^{+1}$	$4.31\times10^{+1}$	$4.67\times10^{+1}$	$4.89\times10^{+1}$	$5.10\times10^{+1}$	$4.84\times10^{+1}$	$4.58\times10^{+1}$	$4.38\times10^{+1}$	$4.21\times10^{+1}$	$4.04\times10^{+1}$
	24	$2.32\times10^{+1}$	$2.55\times10^{+1}$	$2.46\times10^{+1}$	$2.80\times10^{+1}$	$2.98\times10^{+1}$	$3.19\times10^{+1}$	$3.30\times10^{+1}$	$3.16\times10^{+1}$	$2.97\times10^{+1}$	$2.72\times10^{+1}$	$2.54\times10^{+1}$	$2.39\times10^{+1}$
	27	$1.44\times10^{+1}$	$1.58\times10^{+1}$	$1.62\times10^{+1}$	$1.72\times10^{+1}$	$1.90\times10^{+1}$	$2.04\times10^{+1}$	$2.12\times10^{+1}$	$2.00\times10^{+1}$	$1.83\times10^{+1}$	$1.70\times10^{+1}$	$1.60\times10^{+1}$	$1.55\times10^{+1}$
	30	8.96×10^{0}	9.66×10^{0}	9.77×10^{0}	$1.10\times10^{+1}$	$1.20\times10^{+1}$	$1.32\times10^{+1}$	$1.36\times10^{+1}$	$1.27\times10^{+1}$	$1.16\times10^{+1}$	$1.03\times10^{+1}$	9.56×10^{0}	9.39×10^{0}
	33	6.03×10^{0}	6.66×10^{0}	6.35×10^{0}	7.13×10^{0}	7.92×10^{0}	8.55×10^{0}	8.88×10^{0}	8.41×10^{0}	7.40×10^{0}	6.70×10^{0}	6.00×10^{0}	5.68×10^{0}
	36	3.86×10^{0}	3.67×10^{0}	4.01×10^{0}	4.54×10^{0}	5.14×10^{0}	5.76×10^{0}	5.99×10^{0}	5.50×10^{0}	4.85×10^{0}	4.23×10^{0}	3.76×10^{0}	3.56×10^{0}
	39	2.41×10^{0}	2.47×10^{0}	2.63×10^{0}	3.02×10^{0}	3.48×10^{0}	3.87×10^{0}	4.01×10^{0}	3.67×10^{0}	3.14×10^{0}	2.67×10^{0}	2.31×10^{0}	2.37×10^{0}
	42	1.54×10^{0}	1.68×10^{0}	1.66×10^{0}	1.99×10^{0}	2.32×10^{0}	2.58×10^{0}	2.66×10^{0}	2.43×10^{0}	2.06×10^{0}	1.72×10^{0}	1.44×10^{0}	1.49×10^{0}
	47	7.76×10^{-1}	8.25×10^{-1}	8.32×10^{-1}	1.04×10^{0}	1.23×10^{0}	1.40×10^{0}	1.46×10^{0}	1.29×10^{0}	1.03×10^{0}	8.34×10^{-1}	6.90×10^{-1}	7.49×10^{-1}
	52	3.87×10^{-1}	4.07×10^{-1}	4.42×10^{-1}	5.58×10^{-1}	6.69×10^{-1}	7.67×10^{-1}	7.91×10^{-1}	7.04×10^{-1}	5.45×10^{-1}	4.25×10^{-1}	3.66×10^{-1}	3.52×10^{-1}
	60	1.07×10^{-1}	1.44×10^{-1}	1.52×10^{-1}	1.67×10^{-1}	2.39×10^{-1}	2.76×10^{-1}	2.83×10^{-1}	2.47×10^{-1}	1.95×10^{-1}	1.59×10^{-1}	1.15×10^{-1}	1.28×10^{-1}
75°N	12	$1.74\times10^{+2}$	$1.76\times10^{+2}$	$1.74\times10^{+2}$	$1.89\times10^{+2}$	$1.94\times10^{+2}$	$2.01\times10^{+2}$	$2.11\times10^{+2}$	$2.05\times10^{+2}$	$1.93\times10^{+2}$	$1.91\times10^{+2}$	$1.82\times10^{+2}$	$1.76\times10^{+2}$
	15	$9.94\times10^{+1}$	$1.07\times10^{+2}$	$1.09\times10^{+2}$	$1.13\times10^{+2}$	$1.23\times10^{+2}$	$1.30\times10^{+2}$	$1.35\times10^{+2}$	$1.26\times10^{+2}$	$1.20\times10^{+2}$	$1.16\times10^{+2}$	$1.11\times10^{+2}$	$1.06\times10^{+2}$
	18	$6.23\times10^{+1}$	$6.23\times10^{+1}$	$6.28\times10^{+1}$	$6.92\times10^{+1}$	$7.38\times10^{+1}$	$7.81\times10^{+1}$	$8.07\times10^{+1}$	$7.79\times10^{+1}$	$7.27\times10^{+1}$	$7.07\times10^{+1}$	$6.63\times10^{+1}$	$6.17\times10^{+1}$
	21	$3.74\times10^{+1}$	$3.96\times10^{+1}$	$3.92\times10^{+1}$	$4.25\times10^{+1}$	$4.64\times10^{+1}$	$4.86\times10^{+1}$	$5.10\times10^{+1}$	$4.79\times10^{+1}$	$4.53\times10^{+1}$	$4.28\times10^{+1}$	$4.10\times10^{+1}$	$3.82\times10^{+1}$
	24	$2.10\times10^{+1}$	$2.49\times10^{+1}$	$2.52\times10^{+1}$	$2.79\times10^{+1}$	$3.03\times10^{+1}$	$3.18\times10^{+1}$	$3.31\times10^{+1}$	$3.15\times10^{+1}$	$2.94\times10^{+1}$	$2.69\times10^{+1}$	$2.46\times10^{+1}$	$2.33\times10^{+1}$
	27	$1.42\times10^{+1}$	$1.54\times10^{+1}$	$1.56\times10^{+1}$	$1.72\times10^{+1}$	$1.89\times10^{+1}$	$2.03\times10^{+1}$	$2.13\times10^{+1}$	$1.98\times10^{+1}$	$1.79\times10^{+1}$	$1.65\times10^{+1}$	$1.54\times10^{+1}$	$1.42\times10^{+1}$
	30	8.78×10^{0}	9.41×10^{0}	9.55×10^{0}	$1.09\times10^{+1}$	$1.22\times10^{+1}$	$1.32\times10^{+1}$	$1.37\times10^{+1}$	$1.27\times10^{+1}$	$1.14\times10^{+1}$	$1.02\times10^{+1}$	9.20×10^{0}	8.80×10^{0}
	33	5.86×10^{0}	6.48×10^{0}	6.35×10^{0}	7.00×10^{0}	8.01×10^{0}	8.60×10^{0}	9.00×10^{0}	8.44×10^{0}	7.32×10^{0}	6.51×10^{0}	5.79×10^{0}	5.39×10^{0}
	36	3.67×10^{0}	3.73×10^{0}	3.94×10^{0}	4.55×10^{0}	5.18×10^{0}	5.76×10^{0}	6.05×10^{0}	5.47×10^{0}	4.76×10^{0}	4.05×10^{0}	3.65×10^{0}	3.23×10^{0}
	39	2.34×10^{0}	2.42×10^{0}	2.57×10^{0}	3.03×10^{0}	3.51×10^{0}	3.86×10^{0}	4.05×10^{0}	3.68×10^{0}	3.07×10^{0}	2.61×10^{0}	2.19×10^{0}	2.20×10^{0}
	42	1.51×10^{0}	1.65×10^{0}	1.62×10^{0}	1.98×10^{0}	2.36×10^{0}	2.61×10^{0}	2.71×10^{0}	2.43×10^{0}	2.03×10^{0}	1.64×10^{0}	1.37×10^{0}	1.41×10^{0}
	47	7.81×10^{-1}	7.91×10^{-1}	8.10×10^{-1}	1.03×10^{0}	1.25×10^{0}	1.42×10^{0}	1.48×10^{0}	1.29×10^{0}	1.01×10^{0}	7.93×10^{-1}	6.56×10^{-1}	7.09×10^{-1}

	52	3.81×10^{-1}	3.98×10^{-1}	4.36×10^{-1}	5.53×10^{-1}	6.68×10^{-1}	7.79×10^{-1}	8.03×10^{-1}	7.06×10^{-1}	5.28×10^{-1}	4.02×10^{-1}	3.56×10^{-1}	3.51×10^{-1}
	60	1.10×10^{-1}	1.05×10^{-1}	1.46×10^{-1}	1.67×10^{-1}	2.45×10^{-1}	2.79×10^{-1}	2.92×10^{-1}	2.50×10^{-1}	1.89×10^{-1}	1.51×10^{-1}	1.08×10^{-1}	1.18×10^{-1}
80°N	12	$1.67\times10^{+2}$	$1.77\times10^{+2}$	$1.69\times10^{+2}$	$1.85\times10^{+2}$	$1.93\times10^{+2}$	$1.98\times10^{+2}$	$2.08\times10^{+2}$	$2.05\times10^{+2}$	$1.93\times10^{+2}$	$1.88\times10^{+2}$	$1.79\times10^{+2}$	$1.73\times10^{+2}$
	15	$9.99\times10^{+1}$	$1.05\times10^{+2}$	$1.07\times10^{+2}$	$1.11\times10^{+2}$	$1.23\times10^{+2}$	$1.28\times10^{+2}$	$1.34\times10^{+2}$	$1.25\times10^{+2}$	$1.20\times10^{+2}$	$1.13\times10^{+2}$	$1.09\times10^{+2}$	$1.03\times10^{+2}$
	18	$5.92\times10^{+1}$	$6.26\times10^{+1}$	$6.18\times10^{+1}$	$6.98\times10^{+1}$	$7.41\times10^{+1}$	$7.79\times10^{+1}$	$8.08\times10^{+1}$	$7.82\times10^{+1}$	$7.25\times10^{+1}$	$6.98\times10^{+1}$	$6.51\times10^{+1}$	$6.07\times10^{+1}$
	21	$3.67\times10^{+1}$	$3.90\times10^{+1}$	$3.85\times10^{+1}$	$4.19\times10^{+1}$	$4.62\times10^{+1}$	$4.87\times10^{+1}$	$5.08\times10^{+1}$	$4.79\times10^{+1}$	$4.50\times10^{+1}$	$4.21\times10^{+1}$	$3.99\times10^{+1}$	$3.72\times10^{+1}$
	24	$2.05\times10^{+1}$	$2.45\times10^{+1}$	$2.48\times10^{+1}$	$2.79\times10^{+1}$	$3.04\times10^{+1}$	$3.21\times10^{+1}$	$3.34\times10^{+1}$	$3.17\times10^{+1}$	$2.96\times10^{+1}$	$2.66\times10^{+1}$	$2.41\times10^{+1}$	$2.25\times10^{+1}$
	27	$1.35\times10^{+1}$	$1.51\times10^{+1}$	$1.51\times10^{+1}$	$1.72\times10^{+1}$	$1.89\times10^{+1}$	$2.04\times10^{+1}$	$2.13\times10^{+1}$	$1.98\times10^{+1}$	$1.75\times10^{+1}$	$1.63\times10^{+1}$	$1.48\times10^{+1}$	$1.35\times10^{+1}$
	30	8.64×10^{0}	9.51×10^{0}	9.31×10^{0}	$1.08\times10^{+1}$	$1.23\times10^{+1}$	$1.33\times10^{+1}$	$1.37\times10^{+1}$	$1.28\times10^{+1}$	$1.13\times10^{+1}$	9.90×10^{0}	8.89×10^{0}	8.30×10^{0}
	33	5.61×10^{0}	6.32×10^{0}	6.22×10^{0}	6.89×10^{0}	8.03×10^{0}	8.70×10^{0}	9.10×10^{0}	8.43×10^{0}	7.08×10^{0}	6.30×10^{0}	5.54×10^{0}	5.28×10^{0}
	36	3.58×10^{0}	3.76×10^{0}	3.80×10^{0}	4.56×10^{0}	5.18×10^{0}	5.80×10^{0}	5.99×10^{0}	5.50×10^{0}	4.64×10^{0}	4.01×10^{0}	3.43×10^{0}	3.19×10^{0}
	39	2.31×10^{0}	2.43×10^{0}	2.55×10^{0}	3.07×10^{0}	3.54×10^{0}	3.93×10^{0}	4.09×10^{0}	3.72×10^{0}	3.05×10^{0}	2.52×10^{0}	2.14×10^{0}	2.04×10^{0}
	42	1.50×10^{0}	1.65×10^{0}	1.58×10^{0}	1.95×10^{0}	2.37×10^{0}	2.63×10^{0}	2.74×10^{0}	2.46×10^{0}	1.99×10^{0}	1.56×10^{0}	1.29×10^{0}	1.33×10^{0}
	47	7.70×10^{-1}	7.62×10^{-1}	7.77×10^{-1}	1.02×10^{0}	1.24×10^{0}	1.44×10^{0}	1.49×10^{0}	1.30×10^{0}	9.94×10^{-1}	7.69×10^{-1}	6.29×10^{-1}	6.77×10^{-1}
	52	3.68×10^{-1}	3.91×10^{-1}	4.34×10^{-1}	5.51×10^{-1}	6.82×10^{-1}	7.97×10^{-1}	8.19×10^{-1}	7.14×10^{-1}	5.16×10^{-1}	3.91×10^{-1}	3.39×10^{-1}	3.39×10^{-1}
	60	1.22×10^{-1}	1.18×10^{-1}	1.40×10^{-1}	1.66×10^{-1}	2.48×10^{-1}	2.88×10^{-1}	3.00×10^{-1}	2.55×10^{-1}	1.87×10^{-1}	1.44×10^{-1}	1.04×10^{-1}	1.18×10^{-1}
85°N	12	$1.63\times10^{+2}$	$1.74\times10^{+2}$	$1.68\times10^{+2}$	$1.83\times10^{+2}$	$1.87\times10^{+2}$	$2.03\times10^{+2}$	$2.06\times10^{+2}$	$2.01\times10^{+2}$	$1.90\times10^{+2}$	$1.84\times10^{+2}$	$1.78\times10^{+2}$	$1.73\times10^{+2}$
	15	$1.00\times10^{+2}$	$1.04\times10^{+2}$	$1.04\times10^{+2}$	$1.14\times10^{+2}$	$1.23\times10^{+2}$	$1.26\times10^{+2}$	$1.33\times10^{+2}$	$1.25\times10^{+2}$	$1.20\times10^{+2}$	$1.13\times10^{+2}$	$1.08\times10^{+2}$	$1.02\times10^{+2}$
	18	$5.73\times10^{+1}$	$6.24\times10^{+1}$	$6.33\times10^{+1}$	$6.76\times10^{+1}$	$7.36\times10^{+1}$	$7.88\times10^{+1}$	$8.08\times10^{+1}$	$7.83\times10^{+1}$	$7.19\times10^{+1}$	$6.93\times10^{+1}$	$6.47\times10^{+1}$	$6.08\times10^{+1}$
	21	$3.48\times10^{+1}$	$3.81\times10^{+1}$	$3.80\times10^{+1}$	$4.31\times10^{+1}$	$4.60\times10^{+1}$	$4.87\times10^{+1}$	$5.07\times10^{+1}$	$4.75\times10^{+1}$	$4.50\times10^{+1}$	$4.18\times10^{+1}$	$3.94\times10^{+1}$	$3.63\times10^{+1}$
	24	$2.12\times10^{+1}$	$2.41\times10^{+1}$	$2.38\times10^{+1}$	$2.75\times10^{+1}$	$3.02\times10^{+1}$	$3.19\times10^{+1}$	$3.32\times10^{+1}$	$3.15\times10^{+1}$	$2.90\times10^{+1}$	$2.63\times10^{+1}$	$2.39\times10^{+1}$	$2.19\times10^{+1}$
	27	$1.31\times10^{+1}$	$1.48\times10^{+1}$	$1.51\times10^{+1}$	$1.64\times10^{+1}$	$1.89\times10^{+1}$	$2.06\times10^{+1}$	$2.13\times10^{+1}$	$1.98\times10^{+1}$	$1.74\times10^{+1}$	$1.58\times10^{+1}$	$1.44\times10^{+1}$	$1.31\times10^{+1}$
	30	8.47×10^{0}	9.58×10^{0}	9.24×10^{0}	$1.07\times10^{+1}$	$1.23\times10^{+1}$	$1.33\times10^{+1}$	$1.37\times10^{+1}$	$1.28\times10^{+1}$	$1.12\times10^{+1}$	9.82×10^{0}	8.69×10^{0}	7.90×10^{0}
	33	5.55×10^{0}	6.17×10^{0}	6.20×10^{0}	6.93×10^{0}	8.03×10^{0}	8.74×10^{0}	9.09×10^{0}	8.40×10^{0}	7.14×10^{0}	6.14×10^{0}	5.36×10^{0}	5.11×10^{0}
	36	3.44×10^{0}	3.74×10^{0}	3.71×10^{0}	4.53×10^{0}	5.24×10^{0}	5.83×10^{0}	6.05×10^{0}	5.51×10^{0}	4.64×10^{0}	3.76×10^{0}	3.38×10^{0}	3.17×10^{0}
	39	2.32×10^{0}	2.47×10^{0}	2.56×10^{0}	3.06×10^{0}	3.54×10^{0}	3.95×10^{0}	4.09×10^{0}	3.69×10^{0}	3.02×10^{0}	2.45×10^{0}	2.10×10^{0}	2.04×10^{0}
	42	1.50×10^{0}	1.64×10^{0}	1.58×10^{0}	1.97×10^{0}	2.37×10^{0}	2.65×10^{0}	2.74×10^{0}	2.44×10^{0}	1.95×10^{0}	1.53×10^{0}	1.26×10^{0}	1.29×10^{0}
	47	7.30×10^{-1}	7.39×10^{-1}	7.63×10^{-1}	1.03×10^{0}	1.25×10^{0}	1.44×10^{0}	1.49×10^{0}	1.29×10^{0}	9.72×10^{-1}	7.29×10^{-1}	6.26×10^{-1}	6.64×10^{-1}
	52	3.70×10^{-1}	3.77×10^{-1}	4.23×10^{-1}	5.49×10^{-1}	6.85×10^{-1}	7.96×10^{-1}	8.19×10^{-1}	7.10×10^{-1}	5.02×10^{-1}	3.71×10^{-1}	3.15×10^{-1}	3.14×10^{-1}
	60	1.15×10^{-1}	1.11×10^{-1}	1.37×10^{-1}	1.68×10^{-1}	2.47×10^{-1}	2.89×10^{-1}	3.01×10^{-1}	2.55×10^{-1}	1.76×10^{-1}	1.33×10^{-1}	1.06×10^{-1}	1.21×10^{-1}
90°N	12	$1.64\times10^{+2}$	$1.71\times10^{+2}$	$1.68\times10^{+2}$	$1.81\times10^{+2}$	$1.92\times10^{+2}$	$2.01\times10^{+2}$	$2.06\times10^{+2}$	$1.97\times10^{+2}$	$1.91\times10^{+2}$	$1.87\times10^{+2}$	$1.74\times10^{+2}$	$1.70\times10^{+2}$
	15	$9.93\times10^{+1}$	$1.04\times10^{+2}$	$1.04\times10^{+2}$	$1.16\times10^{+2}$	$1.23\times10^{+2}$	$1.26\times10^{+2}$	$1.36\times10^{+2}$	$1.25\times10^{+2}$	$1.20\times10^{+2}$	$1.14\times10^{+2}$	$1.08\times10^{+2}$	$1.03\times10^{+2}$
	18	$5.73\times10^{+1}$	$6.23\times10^{+1}$	$6.34\times10^{+1}$	$6.72\times10^{+1}$	$7.43\times10^{+1}$	$7.77\times10^{+1}$	$8.17\times10^{+1}$	$7.88\times10^{+1}$	$7.21\times10^{+1}$	$6.92\times10^{+1}$	$6.46\times10^{+1}$	$6.00\times10^{+1}$
	21	$3.48\times10^{+1}$	$3.75\times10^{+1}$	$3.78\times10^{+1}$	$4.26\times10^{+1}$	$4.62\times10^{+1}$	$4.92\times10^{+1}$	$5.10\times10^{+1}$	$4.75\times10^{+1}$	$4.55\times10^{+1}$	$4.22\times10^{+1}$	$3.86\times10^{+1}$	$3.60\times10^{+1}$
	24	$2.12\times10^{+1}$	$2.38\times10^{+1}$	$2.45\times10^{+1}$	$2.70\times10^{+1}$	$3.01\times10^{+1}$	$3.14\times10^{+1}$	$3.34\times10^{+1}$	$3.13\times10^{+1}$	$2.87\times10^{+1}$	$2.60\times10^{+1}$	$2.38\times10^{+1}$	$2.14\times10^{+1}$
	27	$1.36\times10^{+1}$	$1.42\times10^{+1}$	$1.44\times10^{+1}$	$1.68\times10^{+1}$	$1.90\times10^{+1}$	$2.06\times10^{+1}$	$2.12\times10^{+1}$	$1.99\times10^{+1}$	$1.73\times10^{+1}$	$1.59\times10^{+1}$	$1.42\times10^{+1}$	$1.28\times10^{+1}$
	30	8.58×10^{0}	9.52×10^{0}	9.37×10^{0}	$1.06\times10^{+1}$	$1.22\times10^{+1}$	$1.31\times10^{+1}$	$1.39\times10^{+1}$	$1.26\times10^{+1}$	$1.10\times10^{+1}$	9.93×10^{0}	8.52×10^{0}	7.63×10^{0}
	33	5.49×10^{0}	6.11×10^{0}	5.97×10^{0}	6.84×10^{0}	8.11×10^{0}	8.77×10^{0}	9.05×10^{0}	8.44×10^{0}	7.15×10^{0}	5.99×10^{0}	5.28×10^{0}	5.01×10^{0}
	36	3.64×10^{0}	3.71×10^{0}	3.81×10^{0}	4.55×10^{0}	5.25×10^{0}	5.76×10^{0}	6.11×10^{0}	5.50×10^{0}	4.64×10^{0}	3.83×10^{0}	3.33×10^{0}	3.12×10^{0}
	39	2.45×10^{0}	2.43×10^{0}	2.54×10^{0}	3.00×10^{0}	3.51×10^{0}	3.98×10^{0}	4.08×10^{0}	3.68×10^{0}	3.07×10^{0}	2.45×10^{0}	2.07×10^{0}	2.00×10^{0}
	42	1.53×10^{0}	1.65×10^{0}	1.58×10^{0}	1.93×10^{0}	2.39×10^{0}	2.66×10^{0}	2.78×10^{0}	2.45×10^{0}	1.96×10^{0}	1.53×10^{0}	1.28×10^{0}	1.32×10^{0}
	47	7.30×10^{-1}	7.14×10^{-1}	7.64×10^{-1}	1.03×10^{0}	1.26×10^{0}	1.44×10^{0}	1.52×10^{0}	1.30×10^{0}	9.84×10^{-1}	7.26×10^{-1}	6.10×10^{-1}	6.55×10^{-1}
	52	3.87×10^{-1}	3.76×10^{-1}	4.27×10^{-1}	5.44×10^{-1}	6.90×10^{-1}	8.17×10^{-1}	8.32×10^{-1}	7.13×10^{-1}	5.10×10^{-1}	3.82×10^{-1}	3.26×10^{-1}	3.11×10^{-1}
	60	1.02×10^{-1}	1.08×10^{-1}	1.38×10^{-1}	1.72×10^{-1}	2.51×10^{-1}	2.92×10^{-1}	3.07×10^{-1}	2.57×10^{-1}	1.84×10^{-1}	1.35×10^{-1}	1.04×10^{-1}	1.22×10^{-1}

Table A2
Monthly mean values of total air pressure p (hPa) obtained from the MIPAS data-set at 14 fixed levels from 12 to 60 km, for the 65°S, 70°S, 75°S, 80°S, 85°S and 90°S latitudes.

Latitude	Altitude (km)	Month											
		Jan.	Feb.	Mar.	Apr.	May	June	July	Aug.	Sep.	Oct.	Nov.	Dec.
65°S	12	$1.83\times10^{+2}$	$1.82\times10^{+2}$	$1.76\times10^{+2}$	$1.79\times10^{+2}$	$1.80\times10^{+2}$	$1.76\times10^{+2}$	$1.79\times10^{+2}$	$1.67\times10^{+2}$	$1.63\times10^{+2}$	$1.69\times10^{+2}$	$1.79\times10^{+2}$	$1.82\ 10^{+2}$
	15	$1.13\times10^{+2}$	$1.13\times10^{+2}$	$1.12\times10^{+2}$	$1.11\times10^{+2}$	$1.09\times10^{+2}$	$1.08\times10^{+2}$	$1.07\times10^{+2}$	$9.65\times10^{+1}$	$9.82\times10^{+1}$	$1.09\times10^{+2}$	$1.13\times10^{+2}$	$1.14\ 10^{+2}$
	18	$7.06\times10^{+1}$	$7.14\times10^{+1}$	$6.91\times10^{+1}$	$6.83\times10^{+1}$	$6.60\times10^{+1}$	$6.29\times10^{+1}$	$6.23\times10^{+1}$	$5.71\times10^{+1}$	$5.80\times10^{+1}$	$6.49\times10^{+1}$	$6.84\times10^{+1}$	$6.95\times10^{+1}$
	21	$4.41\times10^{+1}$	$4.34\times10^{+1}$	$4.20\times10^{+1}$	$4.10\times10^{+1}$	$3.90\times10^{+1}$	$3.77\times10^{+1}$	$3.73\times10^{+1}$	$3.34\times10^{+1}$	$3.52\times10^{+1}$	$3.95\times10^{+1}$	$4.18\times10^{+1}$	$4.35\times10^{+1}$
	24	$2.91\times10^{+1}$	$2.85\times10^{+1}$	$2.71\times10^{+1}$	$2.64\times10^{+1}$	$2.49\times10^{+1}$	$2.30\times10^{+1}$	$2.24\times10^{+1}$	$2.01\times10^{+1}$	$2.17\times10^{+1}$	$2.60\times10^{+1}$	$2.74\times10^{+1}$	$2.86\times10^{+1}$
	27	$1.86\times10^{+1}$	$1.84\times10^{+1}$	$1.72\times10^{+1}$	$1.61\times10^{+1}$	$1.48\times10^{+1}$	$1.32\times10^{+1}$	$1.26\times10^{+1}$	$1.20\times10^{+1}$	$1.39\times10^{+1}$	$1.56\times10^{+1}$	$1.73\times10^{+1}$	$1.83\times10^{+1}$
	30	$1.21\times10^{+1}$	$1.18\times10^{+1}$	$1.09\times10^{+1}$	9.83×10^{0}	8.89×10^{0}	7.86×10^{0}	7.48×10^{0}	7.07×10^{0}	8.65×10^{0}	9.97×10^{0}	$1.14\times10^{+1}$	$1.20\times10^{+1}$
	33	8.06×10^{0}	7.74×10^{0}	7.09×10^{0}	6.34×10^{0}	5.33×10^{0}	4.71×10^{0}	4.55×10^{0}	4.56×10^{0}	5.55×10^{0}	6.53×10^{0}	7.53×10^{0}	7.99×10^{0}
	36	5.38×10^{0}	5.14×10^{0}	4.61×10^{0}	4.01×10^{0}	3.53×10^{0}	2.91×10^{0}	3.06×10^{0}	2.99×10^{0}	3.62×10^{0}	4.41×10^{0}	5.04×10^{0}	5.38×10^{0}
	39	3.69×10^{0}	3.44×10^{0}	3.04×10^{0}	2.58×10^{0}	2.18×10^{0}	1.95×10^{0}	1.88×10^{0}	2.05×10^{0}	2.36×10^{0}	2.94×10^{0}	3.42×10^{0}	3.65×10^{0}
	42	2.53×10^{0}	2.34×10^{0}	2.02×10^{0}	1.63×10^{0}	1.35×10^{0}	1.18×10^{0}	1.18×10^{0}	1.24×10^{0}	1.61×10^{0}	2.03×10^{0}	2.32×10^{0}	2.52×10^{0}
	47	1.35×10^{0}	1.24×10^{0}	1.03×10^{0}	7.94×10^{-1}	6.79×10^{-1}	6.06×10^{-1}	6.52×10^{-1}	6.42×10^{-1}	8.59×10^{-1}	1.08×10^{0}	1.25×10^{0}	1.35×10^{0}
	52	7.35×10^{-1}	6.64×10^{-1}	5.30×10^{-1}	4.23×10^{-1}	3.40×10^{-1}	2.99×10^{-1}	3.06×10^{-1}	3.74×10^{-1}	4.54×10^{-1}	5.72×10^{-1}	6.61×10^{-1}	7.38×10^{-1}
	60	2.65×10^{-1}	2.33×10^{-1}	1.86×10^{-1}	1.35×10^{-1}	1.13×10^{-1}	1.13×10^{-1}	1.23×10^{-1}	1.27×10^{-1}	1.44×10^{-1}	1.99×10^{-1}	2.45×10^{-1}	2.65×10^{-1}
70°S	12	$1.81\times10^{+2}$	$1.78\times10^{+2}$	$1.73\times10^{+2}$	$1.73\times10^{+2}$	$1.73\times10^{+2}$	$1.79\times10^{+2}$	$1.74\times10^{+2}$	$1.63\times10^{+2}$	$1.63\times10^{+2}$	$1.62\times10^{+2}$	$1.78\times10^{+2}$	$1.83\times10^{+2}$
	15	$1.14\times10^{+2}$	$1.13\times10^{+2}$	$1.11\times10^{+2}$	$1.10\times10^{+2}$	$1.07\times10^{+2}$	$1.04\times10^{+2}$	$1.03\times10^{+2}$	$9.50\times10^{+1}$	$9.30\times10^{+1}$	$1.05\times10^{+2}$	$1.08\times10^{+2}$	$1.13\times10^{+2}$
	18	$7.03\times10^{+1}$	$7.01\times10^{+1}$	$6.82\times10^{+1}$	$6.69\times10^{+1}$	$6.40\times10^{+1}$	$6.19\times10^{+1}$	$6.00\times10^{+1}$	$5.45\times10^{+1}$	$5.38\times10^{+1}$	$6.32\times10^{+1}$	$6.97\times10^{+1}$	$6.85\times10^{+1}$
	21	$4.41\times10^{+1}$	$4.34\times10^{+1}$	$4.15\times10^{+1}$	$4.02\times10^{+1}$	$3.82\times10^{+1}$	$3.71\times10^{+1}$	$3.48\times10^{+1}$	$3.05\times10^{+1}$	$3.41\times10^{+1}$	$3.80\times10^{+1}$	$4.04\times10^{+1}$	$4.35\times10^{+1}$
	24	$2.90\times10^{+1}$	$2.84\times10^{+1}$	$2.70\times10^{+1}$	$2.52\times10^{+1}$	$2.29\times10^{+1}$	$2.11\times10^{+1}$	$2.04\times10^{+1}$	$1.92\times10^{+1}$	$2.01\times10^{+1}$	$2.43\times10^{+1}$	$2.66\times10^{+1}$	$2.83\times10^{+1}$
	27	$1.88\times10^{+1}$	$1.84\times10^{+1}$	$1.71\times10^{+1}$	$1.58\times10^{+1}$	$1.42\times10^{+1}$	$1.27\times10^{+1}$	$1.16\times10^{+1}$	$1.09\times10^{+1}$	$1.29\times10^{+1}$	$1.54\times10^{+1}$	$1.73\times10^{+1}$	$1.85\times10^{+1}$
	30	$1.23\times10^{+1}$	$1.19\times10^{+1}$	$1.07\times10^{+1}$	9.38×10^{0}	8.20×10^{0}	7.01×10^{0}	6.71×10^{0}	6.48×10^{0}	7.99×10^{0}	9.49×10^{0}	$1.13\times10^{+1}$	$1.22\times10^{+1}$
	33	8.16×10^{0}	7.78×10^{0}	7.11×10^{0}	6.11×10^{0}	4.99×10^{0}	4.49×10^{0}	4.28×10^{0}	4.11×10^{0}	5.14×10^{0}	6.34×10^{0}	7.51×10^{0}	8.08×10^{0}
	36	5.48×10^{0}	5.19×10^{0}	4.56×10^{0}	3.80×10^{0}	3.31×10^{0}	2.79×10^{0}	2.71×10^{0}	2.78×10^{0}	3.42×10^{0}	4.39×10^{0}	5.07×10^{0}	5.47×10^{0}
	39	3.74×10^{0}	3.44×10^{0}	3.01×10^{0}	2.47×10^{0}	2.00×10^{0}	1.80×10^{0}	1.72×10^{0}	1.85×10^{0}	2.21×10^{0}	2.85×10^{0}	3.42×10^{0}	3.71×10^{0}
	42	2.54×10^{0}	2.32×10^{0}	1.98×10^{0}	1.51×10^{0}	1.23×10^{0}	1.07×10^{0}	1.11×10^{0}	1.18×10^{0}	1.50×10^{0}	2.01×10^{0}	2.32×10^{0}	2.52×10^{0}
	47	1.37×10^{0}	1.24×10^{0}	1.01×10^{0}	7.75×10^{-1}	6.59×10^{-1}	5.63×10^{-1}	5.99×10^{-1}	5.96×10^{-1}	8.16×10^{-1}	1.07×10^{0}	1.27×10^{0}	1.37×10^{0}
	52	7.46×10^{-1}	6.65×10^{-1}	5.21×10^{-1}	3.85×10^{-1}	3.13×10^{-1}	2.96×10^{-1}	2.92×10^{-1}	3.37×10^{-1}	4.31×10^{-1}	5.67×10^{-1}	6.70×10^{-1}	7.54×10^{-1}
	60	2.71×10^{-1}	2.34×10^{-1}	1.82×10^{-1}	1.29×10^{-1}	1.13×10^{-1}	1.03×10^{-1}	1.12×10^{-1}	1.20×10^{-1}	1.39×10^{-1}	1.98×10^{-1}	2.50×10^{-1}	2.75×10^{-1}
75°S	12	$1.80\times10^{+2}$	$1.77\times10^{+2}$	$1.72\times10^{+2}$	$1.69\times10^{+2}$	$1.71\times10^{+2}$	$1.76\times10^{+2}$	$1.71\times10^{+2}$	$1.61\times10^{+2}$	$1.60\times10^{+2}$	$1.62\times10^{+2}$	$1.76\times10^{+2}$	$1.84\times10^{+2}$
	15	$1.13\times10^{+2}$	$1.12\times10^{+2}$	$1.09\times10^{+2}$	$1.10\times10^{+2}$	$1.04\times10^{+2}$	$1.01\times10^{+2}$	$9.87\times10^{+1}$	$9.11\times10^{+1}$	$9.15\times10^{+1}$	$1.00\times10^{+2}$	$1.04\times10^{+2}$	$1.10\times10^{+2}$
	18	$6.99\times10^{+1}$	$6.94\times10^{+1}$	$6.75\times10^{+1}$	$6.40\times10^{+1}$	$6.20\times10^{+1}$	$5.84\times10^{+1}$	$5.78\times10^{+1}$	$5.04\times10^{+1}$	$5.15\times10^{+1}$	$5.75\times10^{+1}$	$6.76\times10^{+1}$	$6.82\times10^{+1}$
	21	$4.42\times10^{+1}$	$4.34\times10^{+1}$	$4.11\times10^{+1}$	$3.98\times10^{+1}$	$3.67\times10^{+1}$	$3.46\times10^{+1}$	$3.32\times10^{+1}$	$2.87\times10^{+1}$	$3.12\times10^{+1}$	$3.75\times10^{+1}$	$3.99\times10^{+1}$	$4.33\times10^{+1}$
	24	$2.88\times10^{+1}$	$2.83\times10^{+1}$	$2.68\times10^{+1}$	$2.41\times10^{+1}$	$2.18\times10^{+1}$	$1.96\times10^{+1}$	$1.86\times10^{+1}$	$1.79\times10^{+1}$	$1.90\times10^{+1}$	$2.25\times10^{+1}$	$2.57\times10^{+1}$	$2.81\times10^{+1}$
	27	$1.87\times10^{+1}$	$1.82\times10^{+1}$	$1.67\times10^{+1}$	$1.51\times10^{+1}$	$1.31\times10^{+1}$	$1.17\times10^{+1}$	$1.11\times10^{+1}$	9.93×10^{0}	$1.17\times10^{+1}$	$1.50\times10^{+1}$	$1.69\times10^{+1}$	$1.84\times10^{+1}$
	30	$1.23\times10^{+1}$	$1.18\times10^{+1}$	$1.06\times10^{+1}$	9.19×10^{0}	7.60×10^{0}	6.61×10^{0}	6.26×10^{0}	6.03×10^{0}	7.49×10^{0}	9.00×10^{0}	$1.10\times10^{+1}$	$1.22\times10^{+1}$
	33	8.15×10^{0}	7.75×10^{0}	6.95×10^{0}	5.68×10^{0}	4.85×10^{0}	4.11×10^{0}	4.02×10^{0}	3.90×10^{0}	4.77×10^{0}	6.14×10^{0}	7.38×10^{0}	8.07×10^{0}
	36	5.48×10^{0}	5.15×10^{0}	4.46×10^{0}	3.66×10^{0}	2.95×10^{0}	2.63×10^{0}	2.60×10^{0}	2.56×10^{0}	3.21×10^{0}	4.30×10^{0}	5.01×10^{0}	5.51×10^{0}
	39	3.72×10^{0}	3.42×10^{0}	2.94×10^{0}	2.29×10^{0}	1.97×10^{0}	1.72×10^{0}	1.58×10^{0}	1.66×10^{0}	2.09×10^{0}	2.81×10^{0}	3.37×10^{0}	3.72×10^{0}
	42	2.55×10^{0}	2.31×10^{0}	1.92×10^{0}	1.47×10^{0}	1.14×10^{0}	9.86×10^{-1}	1.03×10^{0}	1.13×10^{0}	1.40×10^{0}	1.97×10^{0}	2.32×10^{0}	2.53×10^{0}
	47	1.38×10^{0}	1.23×10^{0}	9.81×10^{-1}	7.24×10^{-1}	6.12×10^{-1}	5.35×10^{-1}	5.66×10^{-1}	5.76×10^{-1}	7.62×10^{-1}	1.05×10^{0}	1.27×10^{0}	1.39×10^{0}
	52	7.54×10^{-1}	6.65×10^{-1}	5.02×10^{-1}	3.65×10^{-1}	3.06×10^{-1}	2.78×10^{-1}	2.78×10^{-1}	2.95×10^{-1}	4.21×10^{-1}	5.72×10^{-1}	6.72×10^{-1}	7.66×10^{-1}
	60	2.80×10^{-1}	2.39×10^{-1}	1.78×10^{-1}	1.30×10^{-1}	1.06×10^{-1}	9.83×10^{-2}	1.03×10^{-1}	1.13×10^{-1}	1.43×10^{-1}	1.83×10^{-1}	2.58×10^{-1}	2.85×10^{-1}

80°S	12	$1.79\times10^{+2}$	$1.76\times10^{+2}$	$1.70\times10^{+2}$	$1.69\times10^{+2}$	$1.71\times10^{+2}$	$1.71\times10^{+2}$	$1.64\times10^{+2}$	$1.53\times10^{+2}$	$1.61\times10^{+2}$	$1.57\times10^{+2}$	$1.75\times10^{+2}$	$1.85\times10^{+2}$
	15	$1.13\times10^{+2}$	$1.11\times10^{+2}$	$1.08\times10^{+2}$	$1.08\times10^{+2}$	$1.02\times10^{+2}$	$9.72\times10^{+1}$	$9.11\times10^{+1}$	$8.84\times10^{+1}$	$9.07\times10^{+1}$	$9.56\times10^{+1}$	$1.02\times10^{+2}$	$1.10\times10^{+2}$
	18	$6.98\times10^{+1}$	$6.91\times10^{+1}$	$6.66\times10^{+1}$	$6.23\times10^{+1}$	$6.06\times10^{+1}$	$5.79\times10^{+1}$	$5.19\times10^{+1}$	$4.86\times10^{+1}$	$5.04\times10^{+1}$	$5.58\times10^{+1}$	$6.62\times10^{+1}$	$6.79\times10^{+1}$
	21	$4.41\times10^{+1}$	$4.30\times10^{+1}$	$4.07\times10^{+1}$	$3.92\times10^{+1}$	$3.55\times10^{+1}$	$3.46\times10^{+1}$	$3.18\times10^{+1}$	$2.78\times10^{+1}$	$2.94\times10^{+1}$	$3.58\times10^{+1}$	$3.99\times10^{+1}$	$4.30\times10^{+1}$
	24	$2.87\times10^{+1}$	$2.82\times10^{+1}$	$2.65\times10^{+1}$	$2.36\times10^{+1}$	$2.06\times10^{+1}$	$1.87\times10^{+1}$	$1.72\times10^{+1}$	$1.67\times10^{+1}$	$1.80\times10^{+1}$	$2.18\times10^{+1}$	$2.51\times10^{+1}$	$2.80\times10^{+1}$
	27	$1.87\times10^{+1}$	$1.81\times10^{+1}$	$1.63\times10^{+1}$	$1.44\times10^{+1}$	$1.25\times10^{+1}$	$1.07\times10^{+1}$	$1.05\times10^{+1}$	9.72×10^{0}	$1.11\times10^{+1}$	$1.41\times10^{+1}$	$1.68\times10^{+1}$	$1.83\times10^{+1}$
	30	$1.23\times10^{+1}$	$1.18\times10^{+1}$	$1.05\times10^{+1}$	8.94×10^{0}	7.30×10^{0}	6.53×10^{0}	6.13×10^{0}	5.86×10^{0}	7.01×10^{0}	8.98×10^{0}	$1.08\times10^{+1}$	$1.23\times10^{+1}$
	33	8.17×10^{0}	7.69×10^{0}	6.90×10^{0}	5.51×10^{0}	4.56×10^{0}	3.95×10^{0}	3.74×10^{0}	3.65×10^{0}	4.52×10^{0}	6.11×10^{0}	7.39×10^{0}	8.07×10^{0}
	36	5.49×10^{0}	5.14×10^{0}	4.41×10^{0}	3.49×10^{0}	2.86×10^{0}	2.49×10^{0}	2.48×10^{0}	2.44×10^{0}	3.08×10^{0}	4.15×10^{0}	4.96×10^{0}	5.50×10^{0}
	39	3.74×10^{0}	3.44×10^{0}	2.90×10^{0}	2.26×10^{0}	1.87×10^{0}	1.60×10^{0}	1.57×10^{0}	1.60×10^{0}	1.99×10^{0}	2.81×10^{0}	3.39×10^{0}	3.74×10^{0}
	42	2.55×10^{0}	2.29×10^{0}	1.90×10^{0}	1.39×10^{0}	1.09×10^{0}	9.61×10^{-1}	9.64×10^{-1}	1.06×10^{0}	1.34×10^{0}	1.97×10^{0}	2.31×10^{0}	2.57×10^{0}
	47	1.39×10^{0}	1.23×10^{0}	9.56×10^{-1}	6.92×10^{-1}	5.80×10^{-1}	5.06×10^{-1}	5.30×10^{-1}	5.45×10^{-1}	7.22×10^{-1}	1.04×10^{0}	1.28×10^{0}	1.40×10^{0}
	52	7.62×10^{-1}	6.64×10^{-1}	4.90×10^{-1}	3.52×10^{-1}	2.91×10^{-1}	2.65×10^{-1}	2.71×10^{-1}	2.72×10^{-1}	4.04×10^{-1}	5.71×10^{-1}	6.79×10^{-1}	7.73×10^{-1}
	60	2.82×10^{-1}	2.40×10^{-1}	1.74×10^{-1}	1.23×10^{-1}	1.03×10^{-1}	9.27×10^{-2}	9.62×10^{-2}	1.10×10^{-1}	1.49×10^{-1}	1.84×10^{-1}	2.64×10^{-1}	2.92×10^{-1}
85°S	12	$1.79\times10^{+2}$	$1.77\times10^{+2}$	$1.67\times10^{+2}$	$1.68\times10^{+2}$	$1.70\times10^{+2}$	$1.65\times10^{+2}$	$1.60\times10^{+2}$	$1.47\times10^{+2}$	$1.60\times10^{+2}$	$1.50\times10^{+2}$	$1.73\times10^{+2}$	$1.85\times10^{+2}$
	15	$1.12\times10^{+2}$	$1.11\times10^{+2}$	$1.08\times10^{+2}$	$1.06\times10^{+2}$	$1.02\times10^{+2}$	$9.65\times10^{+1}$	$9.50\times10^{+1}$	$8.74\times10^{+1}$	$9.32\times10^{+1}$	$1.01\times10^{+2}$	$1.02\times10^{+2}$	$1.09\times10^{+2}$
	18	$6.96\times10^{+1}$	$6.92\times10^{+1}$	$6.64\times10^{+1}$	$6.24\times10^{+1}$	$5.91\times10^{+1}$	$5.54\times10^{+1}$	$5.33\times10^{+1}$	$4.67\times10^{+1}$	$4.99\times10^{+1}$	$5.20\times10^{+1}$	$6.52\times10^{+1}$	$6.77\times10^{+1}$
	21	$4.38\times10^{+1}$	$4.27\times10^{+1}$	$4.01\times10^{+1}$	$3.80\times10^{+1}$	$3.50\times10^{+1}$	$3.32\times10^{+1}$	$2.97\times10^{+1}$	$2.81\times10^{+1}$	$2.88\times10^{+1}$	$3.44\times10^{+1}$	$3.93\times10^{+1}$	$4.29\times10^{+1}$
	24	$2.87\times10^{+1}$	$2.82\times10^{+1}$	$2.62\times10^{+1}$	$2.31\times10^{+1}$	$1.99\times10^{+1}$	$1.77\times10^{+1}$	$1.65\times10^{+1}$	$1.60\times10^{+1}$	$1.76\times10^{+1}$	$2.13\times10^{+1}$	$2.49\times10^{+1}$	$2.79\times10^{+1}$
	27	$1.88\times10^{+1}$	$1.81\times10^{+1}$	$1.60\times10^{+1}$	$1.41\times10^{+1}$	$1.21\times10^{+1}$	$1.00\times10^{+1}$	$1.02\times10^{+1}$	9.37×10^{0}	$1.07\times10^{+1}$	$1.38\times10^{+1}$	$1.65\times10^{+1}$	$1.83\times10^{+1}$
	30	$1.23\times10^{+1}$	$1.18\times10^{+1}$	$1.04\times10^{+1}$	8.73×10^{0}	6.98×10^{0}	6.38×10^{0}	5.95×10^{0}	5.65×10^{0}	6.79×10^{0}	8.80×10^{0}	$1.08\times10^{+1}$	$1.23\times10^{+1}$
	33	8.20×10^{0}	7.71×10^{0}	6.81×10^{0}	5.39×10^{0}	4.51×10^{0}	$3.87\ 10^{0}$	3.73×10^{0}	3.57×10^{0}	$4.28\ 10^{0}$	6.07×10^{0}	7.36×10^{0}	8.13×10^{0}
	36	5.51×10^{0}	5.17×10^{0}	4.36×10^{0}	3.42×10^{0}	2.78×10^{0}	2.45×10^{0}	2.40×10^{0}	2.43×10^{0}	3.01×10^{0}	4.14×10^{0}	4.95×10^{0}	5.54×10^{0}
	39	3.78×10^{0}	3.46×10^{0}	2.90×10^{0}	2.15×10^{0}	1.80×10^{0}	1.50×10^{0}	1.53×10^{0}	1.54×10^{0}	1.97×10^{0}	2.86×10^{0}	3.39×10^{0}	3.77×10^{0}
	42	2.59×10^{0}	2.32×10^{0}	1.89×10^{0}	1.37×10^{0}	1.07×10^{0}	9.63×10^{-1}	9.56×10^{-1}	1.01×10^{0}	1.30×10^{0}	1.97×10^{0}	2.33×10^{0}	2.61×10^{0}
	47	1.41×10^{0}	1.25×10^{0}	9.53×10^{-1}	6.69×10^{-1}	5.72×10^{-1}	5.03×10^{-1}	5.02×10^{-1}	5.28×10^{-1}	7.10×10^{-1}	1.04×10^{0}	1.29×10^{0}	1.42×10^{0}
	52	7.75×10^{-1}	6.75×10^{-1}	4.91×10^{-1}	3.41×10^{-1}	2.75×10^{-1}	2.48×10^{-1}	2.71×10^{-1}	2.74×10^{-1}	3.91×10^{-1}	5.85×10^{-1}	6.93×10^{-1}	7.90×10^{-1}
	60	2.90×10^{-1}	2.50×10^{-1}	1.72×10^{-1}	1.22×10^{-1}	1.00×10^{-1}	9.40×10^{-2}	8.91×10^{-2}	1.03×10^{-1}	1.54×10^{-1}	1.86×10^{-1}	2.64×10^{-1}	2.96×10^{-1}
90°S	12	$1.81\times10^{+2}$	$1.77\times10^{+2}$	$1.67\times10^{+2}$	$1.68\times10^{+2}$	$1.71\times10^{+2}$	$1.73\times10^{+2}$	$1.72\times10^{+2}$	$1.68\times10^{+2}$	$1.56\times10^{+2}$	$1.43\times10^{+2}$	$1.68\times10^{+2}$	$1.85\times10^{+2}$
	15	$1.13\times10^{+2}$	$1.11\times10^{+2}$	$1.08\times10^{+2}$	$1.08\times10^{+2}$	$1.01\times10^{+2}$	$8.88\times10^{+1}$	$9.43\times10^{+1}$	$8.21\times10^{+1}$	$9.03\times10^{+1}$	$1.05\times10^{+2}$	$1.07\times10^{+2}$	$1.09\times10^{+2}$
	18	$7.01\times10^{+1}$	$6.92\times10^{+1}$	$6.59\times10^{+1}$	$6.29\times10^{+1}$	$5.78\times10^{+1}$	$5.61\times10^{+1}$	$5.04\times10^{+1}$	$4.66\times10^{+1}$	$4.97\times10^{+1}$	$5.19\times10^{+1}$	$6.30\times10^{+1}$	$6.80\times10^{+1}$
	21	$4.41\times10^{+1}$	$4.29\times10^{+1}$	$4.03\times10^{+1}$	$3.76\times10^{+1}$	$3.61\times10^{+1}$	$3.32\times10^{+1}$	$2.95\times10^{+1}$	$2.76\times10^{+1}$	$2.93\times10^{+1}$	$3.36\times10^{+1}$	$3.95\times10^{+1}$	$4.30\times10^{+1}$
	24	$2.87\times10^{+1}$	$2.83\times10^{+1}$	$2.61\times10^{+1}$	$2.31\times10^{+1}$	$1.90\times10^{+1}$	$1.68\times10^{+1}$	$1.63\times10^{+1}$	$1.58\times10^{+1}$	$1.70\times10^{+1}$	$2.10\times10^{+1}$	$2.52\times10^{+1}$	$2.77\times10^{+1}$
	27	$1.89\times10^{+1}$	$1.80\times10^{+1}$	$1.60\times10^{+1}$	$1.43\times10^{+1}$	$1.24\times10^{+1}$	$1.08\times10^{+1}$	$1.05\times10^{+1}$	9.49×10^{0}	$1.05\times10^{+1}$	$1.39\times10^{+1}$	$1.63\times10^{+1}$	$1.83\times10^{+1}$
	30	$1.25\times10^{+1}$	$1.19\times10^{+1}$	$1.04\times10^{+1}$	8.57×10^{0}	6.96×10^{0}	6.15×10^{0}	5.80×10^{0}	5.68×10^{0}	6.76×10^{0}	8.74×10^{0}	$1.10\times10^{+1}$	$1.23\times10^{+1}$
	33	8.22×10^{0}	7.71×10^{0}	6.84×10^{0}	5.47×10^{0}	4.49×10^{0}	3.88×10^{0}	3.75×10^{0}	3.53×10^{0}	4.25×10^{0}	6.11×10^{0}	$7.36\ 10^{0}$	8.17×10^{0}
	36	5.53×10^{0}	5.17×10^{0}	4.34×10^{0}	3.40×10^{0}	2.71×10^{0}	2.51×10^{0}	2.50×10^{0}	2.41×10^{0}	2.99×10^{0}	4.16×10^{0}	4.96×10^{0}	5.55×10^{0}
	39	3.78×10^{0}	3.45×10^{0}	2.91×10^{0}	2.08×10^{0}	1.79×10^{0}	1.46×10^{0}	1.47×10^{0}	1.54×10^{0}	1.95×10^{0}	2.88×10^{0}	3.39×10^{0}	3.77×10^{0}
	42	2.59×10^{0}	2.31×10^{0}	1.86×10^{0}	1.41×10^{0}	1.08×10^{0}	9.48×10^{-1}	9.61×10^{-1}	9.98×10^{-1}	1.29×10^{0}	1.94×10^{0}	2.33×10^{0}	2.59×10^{0}
	47	1.41×10^{0}	1.24×10^{0}	9.40×10^{-1}	6.46×10^{-1}	5.47×10^{-1}	4.98×10^{-1}	4.98×10^{-1}	5.23×10^{-1}	6.97×10^{-1}	1.02×10^{0}	1.29×10^{0}	1.42×10^{0}
	52	7.78×10^{-1}	6.69×10^{-1}	4.88×10^{-1}	3.43×10^{-1}	2.79×10^{-1}	2.50×10^{-1}	2.68×10^{-1}	2.73×10^{-1}	3.83×10^{-1}	5.87×10^{-1}	6.91×10^{-1}	7.85×10^{-1}
	60	2.86×10^{-1}	2.47×10^{-1}	1.71×10^{-1}	1.23×10^{-1}	9.74×10^{-2}	9.15×10^{-2}	9.09×10^{-2}	1.01×10^{-1}	1.50×10^{-1}	1.96×10^{-1}	2.67×10^{-1}	2.98×10^{-1}

Table A3
Monthly mean values of air temperature T (K) obtained from the MIPAS data-set at 14 fixed levels from 12 to 60 km, for the 65°N, 70°N, 75°N, 80°N, 85°N and 90°N latitudes.

Latitude	Altitude (km)	Month											
		Jan.	Feb.	Mar.	Apr.	May	June	July	Aug.	Sep.	Oct.	Nov.	Dec.
65°N	12	216.9	219.6	221.7	222.6	225.1	227.0	227.1	225.5	223.6	220.8	219.3	217.6
	15	215.9	219.1	220.3	221.8	223.7	225.5	225.9	224.8	222.6	219.7	217.7	215.8
	18	216.0	219.5	219.5	221.1	223.2	225.1	225.5	224.4	221.4	218.1	215.5	214.8
	21	218.7	220.3	219.1	220.9	223.6	226.0	226.6	224.7	220.6	216.6	214.0	214.9
	24	221.7	221.3	218.9	221.0	224.4	227.9	228.7	225.8	220.4	216.2	213.3	216.1
	27	226.4	224.1	220.0	222.3	227.2	231.2	232.0	228.5	222.1	217.5	213.7	219.3
	30	230.6	225.9	221.8	225.7	231.7	235.9	236.7	233.1	225.6	219.5	214.7	222.7
	33	234.2	228.1	225.2	231.2	237.3	243.3	242.3	238.7	229.6	222.0	216.5	227.3
	36	238.9	233.2	231.4	237.5	246.8	249.3	249.6	244.8	235.2	227.4	220.6	233.3
	39	243.1	238.3	237.6	247.9	254.0	259.2	257.2	253.2	242.3	233.2	226.5	238.8
	42	247.7	240.7	246.0	254.6	262.1	266.6	265.9	259.2	248.4	239.2	235.0	243.5
	47	252.7	244.2	254.9	264.2	271.2	274.6	273.1	267.6	257.3	247.9	246.4	249.6
	52	251.7	244.4	257.1	264.9	272.0	275.6	274.5	268.0	258.2	250.8	254.7	256.1
	60	244.2	242.2	245.3	249.1	258.7	263.1	261.7	253.9	240.8	245.6	251.1	249.0
70°N	12	215.2	218.6	220.7	222.8	226.0	228.0	228.2	226.4	223.9	220.7	218.4	216.2
	15	213.7	218.1	219.8	222.2	224.7	226.7	227.3	225.9	223.1	219.5	216.5	213.6
	18	213.3	218.6	218.7	221.6	224.5	226.6	227.0	225.6	221.7	217.1	213.8	211.8
	21	216.6	219.4	218.7	221.4	225.0	227.6	228.1	225.8	220.6	215.2	211.9	211.4
	24	220.4	220.3	218.3	221.4	225.8	229.4	229.9	226.6	220.0	214.2	210.6	212.5
	27	226.4	223.5	219.2	222.9	228.3	232.3	232.8	228.9	221.2	214.9	210.7	215.9
	30	231.7	226.4	221.8	225.7	232.5	236.8	237.5	233.3	224.4	217.0	211.5	220.6
	33	235.6	228.2	224.7	230.6	237.6	243.7	243.1	238.9	228.8	220.2	213.2	225.9
	36	240.0	232.4	230.3	237.0	246.7	250.2	250.3	245.0	233.6	224.5	217.7	231.5
	39	244.2	236.8	236.0	247.1	253.9	258.9	258.1	253.2	241.3	230.0	224.8	237.3
	42	249.0	238.7	244.2	253.8	262.0	267.7	267.1	259.3	247.4	236.8	232.5	243.6
	47	253.0	242.9	254.0	263.7	271.8	276.0	274.6	268.6	257.2	246.9	246.3	252.2
	52	253.1	243.5	255.4	265.1	273.3	278.2	277.0	270.1	258.5	250.8	252.9	257.1
	60	245.9	240.3	246.5	249.5	259.7	266.3	265.6	256.4	244.3	246.4	251.2	250.0
75°N	12	213.1	217.7	219.9	223.0	226.8	228.6	229.6	227.4	224.1	220.9	217.5	214.6
	15	211.4	216.8	218.7	222.3	225.7	227.7	228.6	227.0	223.5	219.3	215.2	211.3
	18	210.4	217.0	218.0	221.9	225.7	227.8	228.6	226.7	222.0	216.4	211.6	208.6
	21	212.7	217.9	217.7	221.9	226.3	228.9	229.5	226.9	220.3	213.9	208.9	207.3
	24	218.6	219.8	217.4	221.9	227.0	230.5	230.9	227.4	219.7	212.3	207.5	207.7
	27	225.4	223.0	218.7	222.9	229.2	233.1	233.5	229.7	220.6	212.5	207.7	211.4
	30	230.8	226.0	221.4	226.0	232.8	237.3	238.0	233.4	223.4	214.5	208.7	216.2
	33	236.1	228.4	224.2	231.5	238.1	244.3	243.8	238.9	227.9	217.3	210.4	223.0
	36	240.7	232.6	229.0	236.6	246.4	251.0	251.2	245.0	232.3	222.2	215.4	230.9
	39	246.2	235.5	236.1	246.2	253.9	259.3	259.0	253.1	239.5	228.0	223.6	236.6
	42	250.2	237.4	243.2	252.9	261.5	268.8	267.3	259.4	245.9	234.0	231.9	243.9
	47	253.0	241.8	253.1	263.9	272.5	277.5	276.6	269.7	256.1	245.8	246.0	253.3
	52	253.7	241.7	254.0	266.0	275.7	280.4	279.7	272.1	259.0	251.0	252.5	257.4
	60	248.4	240.8	245.5	249.2	260.4	268.1	266.9	259.0	244.5	247.2	252.9	252.8
80°N	12	212.1	216.8	219.0	222.7	227.7	229.6	230.3	228.7	225.2	221.0	217.0	213.1
	15	209.0	215.4	217.2	222.4	226.5	228.7	229.6	228.1	223.9	218.9	213.7	209.3

	18	207.9	215.2	216.7	222.0	226.7	228.9	229.6	227.6	222.2	215.4	209.8	205.3
	21	209.4	216.1	216.8	222.2	227.3	230.0	230.4	227.7	220.4	212.5	206.4	203.1
	24	214.8	218.3	216.7	222.4	227.8	231.4	231.5	228.0	219.6	210.4	204.3	202.9
	27	223.5	222.1	218.8	223.2	229.8	233.7	233.9	229.6	220.5	210.2	204.5	206.7
	30	230.7	225.0	221.1	226.1	233.2	237.7	238.3	233.2	222.6	211.9	206.0	212.6
	33	236.1	227.9	223.5	231.5	238.3	243.8	244.1	239.0	226.7	214.8	208.8	219.8
	36	242.5	231.7	228.2	237.2	246.6	251.6	251.9	245.0	231.5	219.4	213.1	228.6
	39	247.5	234.2	234.7	245.3	254.0	260.2	258.7	253.1	237.9	225.6	220.9	237.7
	42	251.0	236.2	241.4	253.8	261.6	269.4	267.2	259.5	244.5	231.5	231.4	245.8
	47	254.0	241.0	252.3	263.9	273.5	279.1	278.3	270.6	254.9	243.2	244.7	255.7
	52	255.5	239.9	252.5	266.5	276.6	281.7	281.0	274.0	260.0	250.3	251.8	259.5
	60	247.8	240.9	246.3	248.8	262.4	267.9	266.8	261.2	247.6	248.3	253.5	251.3
85°N	12	211.1	215.9	217.9	222.5	228.4	230.2	230.7	229.5	225.9	220.7	216.8	212.3
	15	207.1	214.4	215.9	222.1	227.2	229.2	230.1	228.8	224.4	218.6	213.1	208.0
	18	205.3	213.9	215.3	222.2	227.4	229.6	230.2	228.4	222.4	214.9	208.2	203.3
	21	207.1	214.6	215.7	222.0	227.9	230.8	231.0	228.4	220.5	211.6	204.6	199.7
	24	212.3	216.7	216.7	222.5	228.4	232.0	232.0	228.4	219.6	209.0	202.0	199.3
	27	221.6	221.3	218.3	224.0	230.2	233.9	234.2	230.1	220.4	208.7	201.9	204.6
	30	229.2	224.8	220.6	226.1	233.6	237.9	238.5	233.3	222.3	210.0	203.6	211.5
	33	236.1	227.5	223.4	231.1	238.5	244.1	244.4	239.0	225.9	212.6	207.1	217.9
	36	243.1	231.2	228.6	237.4	246.8	252.1	252.4	245.0	230.3	217.5	211.8	226.3
	39	247.3	233.4	233.6	245.1	254.2	260.8	260.0	253.3	236.6	223.3	219.4	236.6
	42	251.5	234.7	240.6	254.2	262.0	270.2	269.2	259.7	243.5	229.6	229.7	245.5
	47	255.7	239.8	251.7	264.1	274.3	280.4	279.5	271.5	254.2	243.1	243.2	256.9
	52	256.4	239.7	252.9	267.0	277.2	282.8	282.2	275.5	260.7	250.1	253.1	263.0
	60	245.5	239.5	247.7	250.4	262.0	268.5	268.0	261.4	246.9	249.9	251.1	252.1
90°N	12	211.4	215.4	217.5	222.5	228.5	230.3	230.5	229.7	225.9	220.5	216.5	212.3
	15	207.7	213.5	215.3	222.0	227.5	229.5	230.2	229.1	224.5	218.5	212.8	207.7
	18	206.3	213.0	215.0	222.1	227.6	229.9	230.3	228.5	222.5	214.9	207.8	202.1
	21	208.9	213.9	215.9	222.1	228.1	231.0	231.2	228.6	220.5	211.1	203.8	198.5
	24	213.6	216.2	216.4	222.5	228.7	232.2	232.1	228.5	219.7	208.5	200.8	198.3
	27	223.6	220.0	218.8	223.8	230.4	234.0	234.2	230.4	220.5	208.0	201.0	203.1
	30	231.7	224.6	221.3	226.6	234.2	237.9	238.5	233.7	222.1	209.2	202.9	210.6
	33	238.4	227.5	223.9	231.1	238.6	245.2	244.5	238.8	225.8	212.0	206.6	218.4
	36	244.0	230.8	228.3	237.6	246.9	252.3	252.5	244.9	230.2	216.3	212.3	226.6
	39	246.9	232.7	233.1	245.2	254.4	260.9	259.7	253.4	236.6	222.2	219.5	235.8
	42	251.2	233.8	240.1	254.4	262.1	270.3	268.3	259.8	242.9	228.7	228.8	244.6
	47	255.5	239.1	251.6	264.4	274.1	280.9	278.7	271.5	253.9	242.0	243.2	257.4
	52	254.6	239.5	252.6	267.5	277.3	281.8	282.4	275.7	260.5	249.4	251.6	264.3
	60	242.2	238.7	248.1	254.9	261.0	268.4	266.7	262.2	249.0	250.3	254.2	252.2

Table A4
Monthly mean values of air temperature T (K) obtained from the MIPAS data-set at 14 fixed levels from 12 to 60 km, for the 65°S, 70°S, 75°S, 80°S, 85°S and 90°S latitudes.

Latitude	Altitude (km)	Month											
		Jan.	Feb.	Mar.	Apr.	May	June	July	Aug.	Sep.	Oct.	Nov.	Dec.
65°S	12	226.9	227.2	226.0	221.8	216.8	212.8	209.5	204.7	206.0	215.0	220.3	224.1
	15	227.7	227.0	224.6	219.4	213.6	208.5	205.4	201.2	205.6	219.0	222.0	225.8
	18	229.3	227.1	223.2	216.7	209.8	203.8	201.4	199.1	209.5	226.5	226.4	229.3
	21	231.4	228.2	222.8	214.9	207.1	200.2	198.2	198.8	215.4	231.4	231.1	232.6
	24	233.2	229.3	223.0	213.4	204.8	197.7	196.3	200.3	221.4	234.8	234.7	235.3
	27	236.8	231.8	224.4	213.9	204.4	198.1	198.4	206.1	228.8	238.9	238.3	238.4
	30	241.2	236.1	227.2	215.6	206.1	201.0	205.2	215.6	235.7	242.9	241.2	242.6
	33	247.5	240.9	232.2	218.4	209.8	207.4	214.1	226.4	241.1	247.2	246.1	248.0
	36	253.7	248.1	236.5	223.1	216.0	216.6	224.1	236.8	249.7	252.7	251.1	254.1
	39	262.2	255.1	244.4	229.3	224.4	226.9	236.4	248.2	256.6	258.1	257.8	262.7
	42	269.2	261.4	249.8	236.6	234.1	235.7	247.7	259.3	263.2	262.0	265.0	270.1
	47	276.9	269.1	258.4	247.9	247.7	252.2	260.7	270.0	267.0	267.2	272.2	277.8
	52	277.2	270.1	259.3	250.8	254.3	260.5	269.7	264.6	264.4	266.3	273.0	278.4
	60	263.2	255.7	242.6	246.0	251.6	255.8	254.1	248.8	247.0	249.3	258.6	266.0
70°S	12	226.7	227.3	225.6	221.2	214.6	210.0	206.8	201.9	201.7	210.0	216.7	223.1
	15	228.4	227.7	224.8	218.6	211.0	205.4	201.5	197.1	199.2	213.4	219.9	225.9
	18	230.8	228.2	223.5	215.3	206.3	200.7	197.4	194.2	201.6	223.3	225.2	230.7
	21	233.1	229.3	223.0	213.2	202.6	197.0	194.0	193.5	208.4	232.0	232.2	234.9
	24	234.7	230.2	222.8	211.4	200.8	194.6	192.2	195.2	217.8	236.7	237.2	237.8
	27	238.1	232.4	224.0	211.4	201.0	195.1	196.1	203.0	228.1	242.1	241.5	240.7
	30	241.9	236.4	226.4	213.3	204.4	200.3	203.9	214.2	236.5	246.7	245.0	244.6
	33	248.6	241.1	230.9	216.1	209.8	208.1	214.9	226.7	244.9	251.1	249.4	249.8
	36	254.4	248.1	235.4	221.2	215.6	216.7	225.9	238.5	252.0	257.4	253.9	255.8
	39	263.4	255.1	242.6	227.5	224.4	227.6	238.4	249.1	260.9	262.2	260.2	264.4
	42	270.5	261.4	248.2	236.4	236.4	240.6	250.3	260.7	267.0	265.7	266.7	272.0
	47	278.6	269.6	257.3	248.1	248.1	253.9	262.6	272.2	271.7	269.8	274.0	280.2
	52	279.9	271.7	258.7	254.8	256.7	259.0	268.6	268.0	269.6	268.7	275.7	281.3
	60	266.9	258.0	244.9	246.3	250.1	254.0	255.0	252.6	249.2	251.1	260.9	268.6
75°S	12	226.8	227.2	225.3	219.8	211.8	207.7	204.0	199.9	199.3	205.5	213.3	221.7
	15	229.1	228.1	224.7	216.9	207.0	203.1	198.8	194.6	195.3	206.5	216.7	225.6
	18	231.9	229.0	223.5	213.4	202.3	198.4	194.0	190.7	195.7	215.8	225.4	231.5
	21	234.4	230.1	222.9	210.7	199.2	194.8	190.8	189.5	200.9	229.0	234.0	236.4
	24	235.7	230.8	222.6	209.2	197.4	192.2	189.1	191.0	211.8	239.0	238.6	239.9
	27	238.8	232.8	223.7	209.3	198.7	193.7	193.5	200.1	225.1	245.3	244.1	242.5
	30	242.5	236.6	225.8	210.9	202.6	199.7	202.8	212.1	235.1	250.7	247.8	246.1
	33	249.3	241.1	229.9	214.6	208.8	208.1	213.8	224.0	244.7	256.2	252.4	251.2
	36	255.2	248.1	234.8	219.7	217.6	217.9	225.7	238.6	254.8	260.7	256.6	256.7
	39	263.5	254.9	241.0	226.4	226.2	229.0	240.0	250.5	263.3	265.6	262.9	265.8
	42	271.7	261.3	247.1	234.7	238.4	241.4	250.2	260.3	271.7	269.5	269.3	273.6
	47	280.1	270.5	256.6	248.7	250.1	254.4	260.8	270.9	275.0	272.5	276.2	282.2
	52	282.6	273.2	259.4	256.2	255.7	258.6	266.1	271.6	271.3	270.3	278.3	283.9
	60	268.1	259.8	246.1	248.3	250.2	253.7	255.8	257.2	253.6	252.1	262.6	271.0

80°S	12	227.3	227.6	225.1	218.1	210.0	206.0	200.1	195.4	197.6	202.0	210.7	220.8
	15	229.8	228.6	224.6	215.0	204.8	201.0	194.6	191.1	192.4	200.5	213.7	225.1
	18	232.8	229.6	223.4	211.6	199.7	196.1	189.5	188.0	191.1	208.0	223.0	231.8
	21	235.2	230.7	222.7	208.8	196.6	192.2	186.8	186.6	195.5	223.0	233.8	237.8
	24	236.3	231.3	222.4	207.3	195.1	189.8	186.7	188.4	206.1	237.3	240.9	241.1
	27	239.2	233.0	223.6	207.8	196.6	192.6	191.9	196.7	218.2	247.9	245.7	243.6
	30	242.9	236.7	225.6	209.5	201.6	198.3	201.5	210.0	232.2	253.9	250.6	247.1
	33	249.9	241.2	229.1	213.0	208.4	207.5	213.0	223.2	245.0	259.7	254.6	252.3
	36	256.0	248.1	233.6	219.0	216.7	218.0	224.5	235.8	254.5	264.8	258.8	257.9
	39	264.5	254.9	239.5	225.2	227.1	229.9	237.4	249.5	266.1	268.6	265.0	267.1
	42	273.0	262.0	245.8	233.5	238.5	242.2	248.4	257.9	272.6	272.3	271.3	275.1
	47	281.7	271.8	256.1	248.2	249.8	254.8	259.4	270.5	278.0	275.2	278.3	283.6
	52	284.7	275.4	260.1	255.8	255.8	258.7	262.5	273.2	273.5	272.4	280.6	286.1
	60	269.5	261.9	247.9	249.5	249.7	254.6	255.1	260.4	256.6	253.5	264.3	271.4
85°S	12	227.6	227.7	224.9	216.8	208.7	204.6	190.5	193.0	196.3	200.3	209.5	220.2
	15	230.3	228.8	224.1	213.9	203.5	199.4	188.1	189.9	190.7	196.6	211.6	224.5
	18	233.4	230.0	223.2	209.9	198.3	193.4	185.9	186.5	188.9	203.2	221.6	231.9
	21	235.7	231.0	222.6	207.1	194.9	189.8	184.5	184.4	191.9	218.9	233.2	238.1
	24	236.6	231.4	222.3	206.0	193.4	188.2	185.7	186.5	202.1	233.6	241.8	241.9
	27	239.2	232.9	223.7	206.5	196.0	192.3	191.8	196.5	216.0	247.1	246.5	244.2
	30	242.9	236.5	225.7	208.6	201.3	198.6	201.5	208.7	227.7	256.6	252.0	247.7
	33	250.2	241.2	228.7	212.5	208.3	206.3	212.4	220.6	242.9	262.7	255.9	252.9
	36	256.5	248.2	233.2	218.1	215.9	217.5	223.3	232.7	254.4	267.4	260.2	258.7
	39	264.7	255.1	238.5	225.7	226.1	228.8	235.7	246.7	265.2	270.8	266.3	267.3
	42	273.8	261.8	244.7	232.2	237.2	240.7	246.0	257.2	272.7	274.3	272.5	274.9
	47	282.6	272.5	255.3	247.5	248.4	252.9	257.7	269.5	278.8	277.0	279.7	284.8
	52	285.4	276.6	260.2	254.9	255.4	260.1	259.7	271.2	274.9	273.1	281.7	286.8
	60	270.5	264.3	249.5	249.5	248.8	253.7	256.8	258.8	260.4	253.8	265.6	271.8
90°S	12	227.6	227.9	224.8	216.3	208.2	199.6	188.5	189.4	195.1	200.0	209.4	220.3
	15	230.5	229.0	224.1	213.5	203.2	195.7	187.1	187.3	190.0	195.7	210.9	224.3
	18	233.6	230.2	223.1	209.6	198.0	191.4	185.2	185.8	188.4	201.4	220.9	231.9
	21	235.8	231.1	222.5	206.7	194.1	188.6	184.4	183.8	190.8	216.9	232.7	238.6
	24	236.7	231.4	222.2	205.3	193.4	188.1	185.5	186.1	201.1	234.3	241.4	242.1
	27	239.3	233.0	223.6	206.1	195.5	190.6	191.1	196.0	215.5	246.6	246.9	244.5
	30	242.8	236.6	225.3	208.5	200.9	198.5	202.5	208.2	226.4	257.8	252.4	247.4
	33	250.4	241.2	228.5	212.0	208.1	206.1	211.9	220.0	241.7	263.7	256.3	253.1
	36	256.6	248.3	232.9	217.5	217.2	216.9	222.7	232.4	254.8	267.9	260.7	258.9
	39	264.4	255.3	238.1	225.4	225.5	229.1	236.0	245.2	264.8	272.1	266.8	267.7
	42	274.1	262.1	245.2	231.9	236.2	240.3	245.3	256.2	272.7	275.1	273.1	276.4
	47	283.3	273.1	255.4	247.2	248.2	252.1	256.9	269.8	279.2	278.1	280.4	285.3
	52	285.9	277.8	260.5	254.4	254.5	259.3	259.1	270.8	276.4	274.3	282.4	287.4
	60	270.9	264.1	250.1	249.4	249.7	254.1	257.1	260.0	260.6	253.6	269.1	272.1

Table A5
Monthly mean values of water vapour volume mixing ratio Q (measured in ppmv) obtained from the MIPAS data-set at 14 fixed levels from 12 to 60 km, for the 65°N, 70°N, 75°N, 80°N, 85°N and 90°N latitudes.

Latitude	Altitude (km)	Month											
		Jan.	Feb.	Mar.	Apr.	May	June	July	Aug.	Sep.	Oct.	Nov.	Dec.
65°N	12	4.7	4.4	4.3	4.4	4.1	4.7	9.1	8.7	7.8	6.8	6.0	5.1
	15	4.7	4.4	4.0	4.6	3.9	3.8	4.0	4.6	4.5	4.7	4.7	4.4
	18	4.5	4.4	4.3	4.6	4.3	4.0	4.0	4.3	4.3	4.2	4.2	4.4
	21	4.8	5.0	4.7	4.8	4.7	4.6	4.6	4.6	4.7	4.7	4.7	4.9
	24	5.4	5.2	5.1	5.1	5.0	5.2	5.2	5.2	5.2	5.3	5.3	5.4
	27	5.5	5.5	5.6	5.4	5.5	5.5	5.6	5.6	5.7	5.7	5.6	5.4
	30	5.7	5.9	5.9	6.0	5.9	5.9	6.0	6.1	6.2	6.0	5.9	5.7
	33	6.2	6.2	6.3	6.4	6.3	6.4	6.4	6.5	6.6	6.5	6.3	6.3
	36	6.4	6.2	6.5	6.6	6.6	6.6	6.6	6.8	6.9	7.1	6.8	6.6
	39	6.7	6.3	6.7	7.0	6.8	7.0	6.9	7.1	7.4	7.2	7.4	6.9
	42	6.6	6.6	6.9	7.2	7.1	7.3	7.4	7.5	7.8	7.5	7.4	6.9
	47	6.2	7.1	6.5	7.0	7.1	7.5	7.6	7.7	7.8	7.7	7.0	6.9
	52	5.6	6.1	5.5	6.1	6.4	6.9	7.2	7.2	7.1	6.9	5.8	5.4
	60	3.3	3.5	4.2	4.8	5.3	5.9	6.0	5.9	6.3	6.5	5.1	4.6
70°N	12	4.7	4.5	4.3	4.7	4.4	4.6	5.1	7.1	5.4	6.2	5.9	5.0
	15	4.6	4.4	4.4	4.6	4.0	4.0	4.0	4.2	4.4	4.7	4.6	4.2
	18	4.4	4.4	4.4	4.5	4.2	4.2	4.0	4.2	4.3	4.2	4.3	4.3
	21	4.6	4.9	4.8	4.8	4.7	4.6	4.6	4.7	4.7	4.7	4.7	4.9
	24	5.7	5.3	5.3	5.1	5.1	5.2	5.2	5.2	5.2	5.3	5.4	5.5
	27	5.7	5.5	5.6	5.5	5.5	5.5	5.6	5.7	5.7	5.8	5.7	5.6
	30	5.8	6.0	6.0	6.0	5.9	5.9	6.0	6.1	6.3	6.2	6.0	5.8
	33	6.3	6.3	6.3	6.3	6.2	6.3	6.3	6.5	6.7	6.7	6.5	6.1
	36	6.4	6.4	6.6	6.6	6.6	6.5	6.6	6.8	7.0	7.2	7.0	6.4
	39	6.6	6.3	6.8	6.9	6.9	6.9	6.9	7.2	7.6	7.6	7.6	6.8
	42	6.5	6.6	6.8	7.1	7.2	7.3	7.3	7.5	7.9	7.9	7.4	7.0
	47	6.3	7.0	6.3	6.9	7.2	7.5	7.6	7.8	7.8	7.8	6.8	6.7
	52	5.3	6.0	5.5	6.0	6.6	7.1	7.3	7.4	7.3	7.1	6.3	5.5
	60	3.3	3.3	3.8	4.2	5.4	5.9	6.1	5.9	6.5	6.3	4.9	4.2
75°N	12	4.5	4.2	4.5	4.4	4.3	5.6	4.9	5.5	6.3	6.1	5.6	4.8
	15	4.5	4.6	4.5	4.7	4.1	4.0	4.0	4.2	4.6	4.6	4.3	4.1
	18	4.6	4.4	4.5	4.6	4.3	4.1	4.1	4.2	4.2	4.1	4.3	4.2
	21	4.8	5.0	4.9	4.8	4.7	4.7	4.6	4.6	4.7	4.7	4.8	4.9
	24	5.7	5.4	5.4	5.2	5.0	5.2	5.3	5.2	5.3	5.3	5.5	5.6
	27	5.8	5.7	5.7	5.5	5.5	5.6	5.7	5.8	5.8	5.9	5.8	5.8
	30	5.9	5.9	6.0	6.0	5.9	5.9	6.1	6.1	6.3	6.3	6.2	6.2
	33	6.4	6.3	6.3	6.3	6.2	6.2	6.3	6.5	6.7	6.8	6.7	6.5
	36	6.5	6.4	6.6	6.5	6.5	6.5	6.6	6.8	6.9	7.3	7.1	6.5
	39	6.5	6.3	6.7	6.9	6.8	6.9	6.9	7.1	7.6	7.8	7.4	6.7
	42	6.5	6.4	6.7	7.1	7.1	7.3	7.2	7.4	7.9	7.9	7.2	6.7
	47	6.3	6.7	6.1	6.7	7.2	7.5	7.6	7.7	7.8	7.6	6.6	6.6
	52	5.2	5.4	5.1	5.9	6.4	7.1	7.3	7.4	7.3	6.9	6.0	5.5
	60	3.8	3.4	3.4	4.6	5.8	5.9	6.2	6.2	6.4	6.0	4.7	4.1

80°N	12	4.2	4.3	4.3	4.1	4.3	4.5	4.9	5.7	5.4	5.8	5.3	4.6
	15	4.2	4.4	4.3	4.7	4.1	4.3	4.1	4.5	4.3	4.5	4.2	4.0
	18	4.6	4.5	4.6	4.6	4.4	4.3	4.1	4.2	4.2	4.2	4.3	4.3
	21	5.0	5.1	5.1	4.9	4.7	4.7	4.6	4.7	4.7	4.7	4.9	5.0
	24	6.1	5.6	5.6	5.2	5.1	5.2	5.3	5.3	5.3	5.4	5.7	5.7
	27	6.0	5.8	5.8	5.6	5.6	5.6	5.7	5.8	5.9	5.9	6.1	6.0
	30	6.0	6.0	6.1	6.0	5.9	5.9	6.1	6.2	6.4	6.4	6.5	6.5
	33	6.3	6.2	6.3	6.2	6.2	6.2	6.3	6.5	6.7	6.8	7.0	6.8
	36	6.5	6.4	6.5	6.6	6.5	6.5	6.6	6.8	7.0	7.3	7.4	6.6
	39	6.6	6.4	6.8	7.0	6.8	6.9	6.9	7.2	7.6	8.0	7.7	6.5
	42	6.7	6.5	6.7	7.1	7.2	7.3	7.3	7.5	8.0	8.1	7.2	6.5
	47	6.4	6.7	5.9	6.7	7.3	7.5	7.6	7.8	8.0	7.7	6.5	6.5
	52	5.3	5.2	5.1	6.0	6.6	7.2	7.4	7.5	7.4	7.3	5.9	5.5
	60	3.7	3.8	3.3	4.6	5.7	6.0	6.2	6.4	6.7	6.3	5.1	4.1
85°N	12	4.3	4.5	4.4	4.1	4.3	4.2	4.4	5.3	4.8	6.1	5.3	4.5
	15	4.1	4.4	4.4	4.6	4.2	4.3	4.1	4.5	4.2	4.6	4.2	4.1
	18	4.6	4.6	4.8	4.6	4.4	4.4	4.1	4.2	4.2	4.2	4.2	4.2
	21	5.5	5.2	5.4	4.8	4.7	4.7	4.6	4.7	4.7	4.7	4.8	5.0
	24	6.4	5.8	5.6	5.3	5.1	5.2	5.3	5.2	5.4	5.4	5.7	5.9
	27	6.3	5.9	5.9	5.7	5.6	5.6	5.7	5.8	6.0	6.1	6.2	6.3
	30	6.2	6.0	6.2	6.0	5.9	5.9	6.0	6.2	6.4	6.5	6.6	6.8
	33	6.4	6.3	6.4	6.2	6.2	6.2	6.3	6.4	6.6	6.9	7.1	7.0
	36	6.5	6.5	6.5	6.5	6.5	6.5	6.5	6.7	7.0	7.4	7.5	6.8
	39	6.6	6.2	6.8	7.0	6.8	6.9	6.8	7.2	7.6	8.0	7.8	6.6
	42	6.7	6.3	6.7	7.0	7.1	7.2	7.2	7.5	7.8	8.1	7.2	6.6
	47	6.3	6.5	5.6	6.5	7.2	7.5	7.5	7.7	7.9	7.5	6.4	6.2
	52	5.3	5.1	4.7	5.8	6.6	7.1	7.3	7.4	7.3	6.9	6.0	5.2
	60	3.8	4.1	3.2	5.5	5.6	6.0	6.2	6.4	6.8	6.9	4.6	4.8
90°N	12	4.2	4.3	4.2	4.8	4.3	4.0	5.0	5.3	5.4	6.3	5.0	4.5
	15	4.2	4.3	4.1	4.4	4.2	4.6	4.3	4.4	4.3	4.6	4.1	4.0
	18	4.5	4.4	4.6	4.7	4.3	4.5	4.1	4.1	4.2	4.3	4.3	4.2
	21	5.4	5.1	5.4	4.9	4.7	4.7	4.7	4.7	4.7	4.8	5.0	5.1
	24	6.1	5.8	5.7	5.3	5.1	5.1	5.3	5.2	5.4	5.6	5.7	5.9
	27	6.1	6.0	6.0	5.8	5.6	5.6	5.7	5.9	6.1	6.1	6.2	6.5
	30	6.0	6.1	6.1	6.1	6.0	6.0	6.1	6.2	6.4	6.5	6.6	6.6
	33	6.2	6.3	6.3	6.3	6.2	6.3	6.3	6.5	6.7	6.9	7.1	6.9
	36	6.4	6.5	6.3	6.6	6.5	6.5	6.6	6.7	7.0	7.4	7.4	6.7
	39	6.6	6.2	6.6	6.9	6.8	6.9	6.8	7.1	7.7	8.2	7.4	6.6
	42	6.6	6.3	6.6	6.9	7.1	7.3	7.2	7.5	7.9	8.2	7.0	6.6
	47	6.2	6.2	5.3	6.5	7.3	7.5	7.7	7.8	8.0	7.5	6.4	6.1
	52	5.5	4.9	4.7	5.9	6.7	7.3	7.4	7.5	7.6	6.8	5.4	5.0
	60	3.5	3.8	3.5	5.5	5.3	5.8	6.3	6.4	7.0	6.5	4.8	5.3

Table A6
Monthly mean values of water vapour volume mixing ratio Q (measured in ppmv) obtained from the MIPAS data-set at 14 fixed levels from 12 to 60 km, for the 65°S, 70°S, 75°S, 80°S, 85°S and 90°S latitudes.

Latitude	Altitude (km)	Month											
		Jan.	Feb.	Mar.	Apr.	May	June	July	Aug.	Sep.	Oct.	Nov.	Dec.
65°S	12	5.3	5.0	4.8	4.8	4.4	3.9	3.8	3.2	3.3	4.1	4.3	4.8
	15	4.7	4.5	4.2	4.0	3.8	3.5	3.7	3.3	3.6	4.5	4.4	4.4
	18	4.5	4.2	4.0	3.9	3.9	4.0	4.1	3.4	3.9	4.8	4.6	4.6
	21	4.8	4.8	4.7	4.6	4.6	4.7	4.6	4.6	5.3	5.1	5.1	4.9
	24	5.1	5.1	5.2	5.1	5.1	5.3	5.4	5.9	5.8	5.3	5.3	5.1
	27	5.3	5.4	5.4	5.5	5.6	5.9	6.2	6.3	5.8	5.4	5.4	5.2
	30	5.5	5.7	5.7	6.0	6.1	6.5	6.4	6.3	6.0	5.8	5.5	5.4
	33	5.8	6.0	6.3	6.6	6.8	7.0	6.5	6.3	6.5	6.2	5.9	5.7
	36	6.2	6.5	6.7	7.3	7.5	6.8	6.7	6.7	6.8	6.5	6.3	6.1
	39	6.9	7.1	7.5	8.1	8.1	7.2	6.6	7.1	6.9	6.8	6.7	6.7
	42	7.4	7.5	7.9	8.3	7.7	7.0	6.4	6.9	6.9	7.1	7.2	7.2
	47	7.6	7.8	7.9	7.9	7.2	6.4	6.7	6.5	6.8	7.2	7.5	7.4
	52	7.4	7.4	7.4	7.8	6.5	5.9	5.7	6.5	6.1	6.4	6.9	7.2
	60	6.0	6.1	6.8	6.2	5.4	5.6	5.8	4.7	5.0	6.1	6.0	6.1
70°S	12	5.0	4.7	4.9	4.7	4.3	3.6	3.6	2.8	2.7	3.4	4.0	4.9
	15	4.6	4.6	4.4	4.1	3.8	3.9	3.4	2.6	2.6	4.0	4.0	4.3
	18	4.5	4.3	4.2	4.1	4.0	4.1	3.7	2.7	3.3	4.8	4.6	4.5
	21	4.8	4.8	4.8	4.6	4.8	4.7	4.6	4.3	5.1	5.4	5.3	5.0
	24	5.0	5.1	5.2	5.2	5.3	5.4	5.7	6.2	6.4	5.6	5.5	5.1
	27	5.3	5.4	5.4	5.6	5.8	5.9	6.4	6.7	6.1	5.5	5.5	5.3
	30	5.5	5.7	5.8	6.1	6.6	6.8	6.4	6.3	6.2	5.9	5.6	5.4
	33	5.8	6.0	6.4	6.7	7.1	7.0	6.4	6.2	6.6	6.3	5.9	5.7
	36	6.2	6.5	6.9	7.6	7.8	7.0	6.6	6.8	6.8	6.6	6.3	6.1
	39	6.8	7.0	7.5	8.2	8.1	6.9	6.4	7.1	6.8	6.8	6.7	6.7
	42	7.3	7.5	7.9	8.3	7.4	6.5	6.4	6.9	6.9	6.9	7.1	7.1
	47	7.5	7.8	8.0	7.9	7.0	6.2	6.6	6.3	6.7	7.0	7.4	7.4
	52	7.3	7.4	7.5	7.4	6.3	5.9	5.6	6.3	6.0	6.1	6.8	7.2
	60	6.2	6.2	6.5	5.9	4.3	5.1	6.0	4.9	4.9	5.9	6.1	6.2
75°S	12	5.0	4.8	5.0	4.5	4.0	3.5	3.6	2.7	2.4	3.5	4.1	5.0
	15	4.6	4.6	4.5	3.8	3.6	3.6	3.4	2.3	2.0	3.3	3.8	4.2
	18	4.6	4.3	4.3	4.1	4.1	4.2	3.6	2.4	2.7	4.3	4.7	4.6
	21	4.9	4.8	4.7	4.7	4.8	4.8	4.2	3.8	4.7	5.7	5.5	5.1
	24	5.0	5.1	5.2	5.2	5.4	5.5	5.8	5.9	6.5	5.9	5.6	5.2
	27	5.3	5.4	5.5	5.6	6.0	6.5	6.7	6.5	6.4	5.8	5.6	5.3
	30	5.5	5.7	5.8	6.2	6.7	6.8	6.5	6.2	6.5	6.0	5.7	5.5
	33	5.9	6.0	6.4	7.0	7.4	7.0	6.4	6.3	6.7	6.4	6.0	5.8
	36	6.3	6.6	6.9	7.6	7.9	7.0	6.7	6.8	6.9	6.7	6.4	6.1
	39	6.8	7.0	7.5	8.2	7.8	7.0	6.4	6.9	6.9	6.8	6.7	6.7
	42	7.3	7.4	7.9	8.3	7.2	6.6	6.2	6.9	6.8	7.0	7.1	7.1
	47	7.6	7.8	8.0	7.7	6.7	6.0	6.5	6.5	6.6	7.0	7.5	7.4
	52	7.4	7.4	7.5	7.1	6.4	6.0	5.7	5.9	6.1	6.2	6.8	7.2
	60	6.2	6.1	6.7	5.7	4.3	4.9	5.5	5.6	4.7	5.3	6.1	6.2

80°S	12	4.6	4.7	5.0	4.4	4.0	3.2	3.4	2.3	2.3	3.0	3.7	5.4
	15	4.6	4.6	4.6	3.8	3.7	3.3	3.3	1.9	2.0	2.3	3.4	4.1
	18	4.6	4.4	4.2	4.2	4.0	4.2	3.2	1.9	2.2	3.3	4.5	4.6
	21	4.8	4.8	4.8	4.6	4.8	4.8	3.5	3.0	4.1	5.9	5.7	5.2
	24	5.0	5.1	5.2	5.3	5.5	5.9	5.5	6.0	6.4	6.3	5.7	5.2
	27	5.3	5.4	5.6	5.8	6.1	6.4	6.6	6.6	6.5	5.9	5.7	5.3
	30	5.5	5.7	5.9	6.4	6.9	7.0	6.7	6.2	6.4	6.2	5.8	5.5
	33	5.9	6.0	6.5	7.1	7.4	7.0	6.4	6.3	6.8	6.5	6.1	5.8
	36	6.3	6.6	7.0	7.8	7.9	6.9	6.6	6.8	6.9	6.7	6.4	6.1
	39	6.8	7.1	7.5	8.4	7.8	6.8	6.5	6.9	6.8	6.8	6.7	6.7
	42	7.2	7.4	8.0	8.4	7.1	6.3	6.2	6.9	6.8	7.0	7.1	7.2
	47	7.6	7.8	8.0	7.5	6.6	6.1	6.3	6.4	6.5	6.9	7.4	7.4
	52	7.4	7.4	7.6	6.9	6.3	5.6	5.9	5.5	6.0	6.1	6.8	7.1
	60	6.2	6.5	7.0	5.9	4.5	5.0	4.6	6.0	4.7	5.2	6.0	6.3
85°S	12	4.4	4.7	4.9	4.6	4.1	3.2	4.4	2.3	2.2	2.6	3.6	5.3
	15	4.6	4.7	4.4	3.9	3.6	3.3	3.3	2.0	2.0	1.7	3.2	4.1
	18	4.7	4.5	4.3	4.2	4.1	4.3	2.7	2.0	2.1	3.2	4.5	4.5
	21	4.8	4.8	4.8	4.8	4.8	5.0	3.4	3.2	3.9	5.7	5.7	5.1
	24	5.0	5.1	5.2	5.4	5.6	6.0	5.7	6.2	6.5	6.5	5.8	5.2
	27	5.4	5.5	5.7	5.8	6.3	6.5	6.7	6.5	6.5	6.3	5.7	5.3
	30	5.5	5.8	6.0	6.4	6.9	6.8	6.8	5.9	6.4	6.3	5.8	5.5
	33	5.9	6.1	6.5	7.1	7.6	7.1	6.4	6.3	6.7	6.5	6.1	5.8
	36	6.3	6.6	7.0	7.8	8.1	6.9	6.7	6.9	6.9	6.7	6.4	6.2
	39	6.8	7.1	7.5	8.2	7.8	6.7	6.4	6.8	7.0	6.9	6.8	6.7
	42	7.3	7.5	7.9	8.4	7.1	6.4	6.3	6.7	6.9	7.0	7.1	7.2
	47	7.7	7.9	8.0	7.4	6.6	6.1	6.4	6.5	6.5	6.9	7.5	7.5
	52	7.4	7.5	7.6	6.7	6.2	5.5	6.1	5.7	6.1	6.2	6.9	7.2
	60	6.1	6.5	7.1	5.8	4.3	4.9	4.7	5.8	4.9	4.8	6.0	6.3
90°S	12	4.4	4.6	5.0	4.7	4.2	3.5	6.5	2.9	2.4	2.6	3.3	4.3
	15	4.7	4.7	4.4	3.9	3.7	3.3	6.5	1.8	1.7	1.4	2.8	3.9
	18	4.7	4.6	4.3	4.1	4.2	4.0	4.1	2.1	1.9	3.0	4.2	4.6
	21	4.8	4.8	4.8	4.8	4.7	4.8	3.7	3.1	3.9	5.7	5.8	5.2
	24	5.0	5.1	5.2	5.4	5.9	5.9	5.8	6.1	6.4	6.6	5.8	5.2
	27	5.4	5.4	5.7	5.9	6.2	6.6	6.9	6.3	6.4	6.4	5.7	5.3
	30	5.5	5.8	6.0	6.4	7.0	6.9	6.3	6.1	6.4	6.4	5.9	5.5
	33	5.9	6.0	6.5	7.2	7.4	7.0	6.6	6.2	6.7	6.5	6.1	5.8
	36	6.3	6.6	7.0	7.9	7.9	7.3	6.5	6.9	6.9	6.7	6.4	6.2
	39	6.8	7.1	7.5	8.1	7.8	6.7	6.4	6.8	7.0	6.8	6.7	6.7
	42	7.3	7.4	8.0	8.1	7.3	6.2	6.2	6.6	6.8	6.9	7.1	7.2
	47	7.6	7.8	7.9	7.4	6.3	6.2	6.3	6.3	6.4	6.7	7.4	7.4
	52	7.4	7.4	7.7	6.8	6.1	5.7	6.1	5.6	5.9	6.1	6.9	7.1
	60	6.2	6.7	7.2	5.9	4.4	5.1	4.6	5.7	5.1	5.5	6.1	6.2

Table A7
Monthly mean values of absolute humidity ρ_w (g m^{-3}) obtained from the MIPAS data given in Tables A1–A6 at 14 fixed levels from 12 to 60 km, for the 65°N, 70°N, 75°N, 80°N, 85°N and 90°N latitudes.

Latitude	Altitude (km)	Month											
		Jan.	Feb.	Mar.	Apr.	May	June	July	Aug.	Sep.	Oct.	Nov.	Dec.
65°N	12	8.5×10^{-4}	8.0×10^{-4}	7.7×10^{-4}	8.4×10^{-4}	7.7×10^{-4}	9.3×10^{-4}	1.8×10^{-3}	1.8×10^{-3}	1.5×10^{-3}	1.3×10^{-3}	1.1×10^{-3}	9.3×10^{-4}
	15	5.0×10^{-4}	4.8×10^{-4}	4.4×10^{-4}	5.0×10^{-4}	4.6×10^{-4}	4.7×10^{-4}	5.2×10^{-4}	5.7×10^{-4}	5.4×10^{-4}	5.5×10^{-4}	5.2×10^{-4}	4.8×10^{-4}
	18	2.9×10^{-4}	2.8×10^{-4}	2.8×10^{-4}	3.1×10^{-4}	3.1×10^{-4}	3.0×10^{-4}	3.2×10^{-4}	3.2×10^{-4}	3.1×10^{-4}	3.0×10^{-4}	2.9×10^{-4}	2.9×10^{-4}
	21	1.8×10^{-4}	2.0×10^{-4}	1.9×10^{-4}	2.0×10^{-4}	2.1×10^{-4}	2.2×10^{-4}	2.2×10^{-4}	2.2×10^{-4}	2.1×10^{-4}	2.1×10^{-4}	2.0×10^{-4}	2.0×10^{-4}
	24	1.3×10^{-4}	1.3×10^{-4}	1.3×10^{-4}	1.4×10^{-4}	1.4×10^{-4}	1.5×10^{-4}	1.6×10^{-4}	1.6×10^{-4}	1.5×10^{-4}	1.5×10^{-4}	1.4×10^{-4}	1.3×10^{-4}
	27	8.1×10^{-5}	8.2×10^{-5}	9.0×10^{-5}	9.3×10^{-5}	9.8×10^{-5}	1.0×10^{-4}	1.1×10^{-4}	1.1×10^{-4}	1.0×10^{-4}	9.8×10^{-5}	9.2×10^{-5}	8.5×10^{-5}
	30	5.1×10^{-5}	5.8×10^{-5}	5.8×10^{-5}	6.3×10^{-5}	6.6×10^{-5}	7.0×10^{-5}	7.5×10^{-5}	7.2×10^{-5}	6.9×10^{-5}	6.3×10^{-5}	5.9×10^{-5}	5.3×10^{-5}
	33	3.5×10^{-5}	3.9×10^{-5}	4.0×10^{-5}	4.3×10^{-5}	4.5×10^{-5}	4.8×10^{-5}	5.1×10^{-5}	4.9×10^{-5}	4.7×10^{-5}	4.5×10^{-5}	3.9×10^{-5}	3.6×10^{-5}
	36	2.4×10^{-5}	2.1×10^{-5}	2.5×10^{-5}	2.8×10^{-5}	2.9×10^{-5}	3.2×10^{-5}	3.4×10^{-5}	3.3×10^{-5}	3.1×10^{-5}	3.0×10^{-5}	2.6×10^{-5}	2.3×10^{-5}
	39	1.5×10^{-5}	1.5×10^{-5}	1.6×10^{-5}	1.8×10^{-5}	2.0×10^{-5}	2.2×10^{-5}	2.3×10^{-5}	2.2×10^{-5}	2.1×10^{-5}	1.9×10^{-5}	1.7×10^{-5}	1.5×10^{-5}
	42	9.3×10^{-6}	1.0×10^{-5}	1.0×10^{-5}	1.2×10^{-5}	1.3×10^{-5}	1.5×10^{-5}	1.6×10^{-5}	1.5×10^{-5}	1.4×10^{-5}	1.2×10^{-5}	1.0×10^{-5}	9.6×10^{-6}
	47	4.2×10^{-6}	5.4×10^{-6}	4.9×10^{-6}	6.0×10^{-6}	6.9×10^{-6}	8.1×10^{-6}	8.6×10^{-6}	8.1×10^{-6}	7.0×10^{-6}	6.0×10^{-6}	4.6×10^{-6}	4.7×10^{-6}
	52	1.9×10^{-6}	2.2×10^{-6}	2.1×10^{-6}	2.8×10^{-6}	3.4×10^{-6}	4.1×10^{-6}	4.4×10^{-6}	4.1×10^{-6}	3.3×10^{-6}	2.7×10^{-6}	1.8×10^{-6}	1.7×10^{-6}
	60	3.3×10^{-7}	4.5×10^{-7}	5.8×10^{-7}	7.5×10^{-7}	1.1×10^{-6}	1.3×10^{-6}	1.4×10^{-6}	1.2×10^{-6}	1.1×10^{-6}	9.5×10^{-7}	5.9×10^{-7}	4.8×10^{-7}
70°N	12	8.4×10^{-4}	8.1×10^{-4}	7.5×10^{-4}	8.7×10^{-4}	8.1×10^{-4}	8.9×10^{-4}	1.0×10^{-3}	1.4×10^{-3}	1.0×10^{-3}	1.2×10^{-3}	1.1×10^{-3}	9.1×10^{-4}
	15	4.7×10^{-4}	4.8×10^{-4}	4.6×10^{-4}	5.1×10^{-4}	4.8×10^{-4}	4.9×10^{-4}	5.2×10^{-4}	5.2×10^{-4}	5.3×10^{-4}	5.5×10^{-4}	5.2×10^{-4}	4.6×10^{-4}
	18	2.9×10^{-4}	2.8×10^{-4}	2.9×10^{-4}	3.0×10^{-4}	3.0×10^{-4}	3.1×10^{-4}	3.1×10^{-4}	3.1×10^{-4}	3.1×10^{-4}	3.0×10^{-4}	2.9×10^{-4}	2.8×10^{-4}
	21	1.7×10^{-4}	2.0×10^{-4}	1.9×10^{-4}	2.0×10^{-4}	2.1×10^{-4}	2.2×10^{-4}	2.2×10^{-4}	2.2×10^{-4}	2.1×10^{-4}	2.1×10^{-4}	2.0×10^{-4}	2.0×10^{-4}
	24	1.3×10^{-4}	1.3×10^{-4}	1.3×10^{-4}	1.4×10^{-4}	1.5×10^{-4}	1.6×10^{-4}	1.6×10^{-4}	1.6×10^{-4}	1.5×10^{-4}	1.5×10^{-4}	1.4×10^{-4}	1.3×10^{-4}
	27	7.9×10^{-5}	8.5×10^{-5}	9.0×10^{-5}	9.2×10^{-5}	9.9×10^{-5}	1.0×10^{-4}	1.1×10^{-4}	1.1×10^{-4}	1.0×10^{-4}	9.9×10^{-5}	9.4×10^{-5}	8.8×10^{-5}
	30	4.9×10^{-5}	5.5×10^{-5}	5.7×10^{-5}	6.3×10^{-5}	6.6×10^{-5}	7.1×10^{-5}	7.5×10^{-5}	7.2×10^{-5}	7.0×10^{-5}	6.4×10^{-5}	5.9×10^{-5}	5.4×10^{-5}
	33	3.5×10^{-5}	4.0×10^{-5}	3.9×10^{-5}	4.2×10^{-5}	4.5×10^{-5}	4.8×10^{-5}	5.0×10^{-5}	4.9×10^{-5}	4.7×10^{-5}	4.4×10^{-5}	4.0×10^{-5}	3.3×10^{-5}
	36	2.2×10^{-5}	2.2×10^{-5}	2.5×10^{-5}	2.7×10^{-5}	3.0×10^{-5}	3.3×10^{-5}	3.4×10^{-5}	3.3×10^{-5}	3.1×10^{-5}	2.9×10^{-5}	2.6×10^{-5}	2.1×10^{-5}
	39	1.4×10^{-5}	1.4×10^{-5}	1.7×10^{-5}	1.8×10^{-5}	2.0×10^{-5}	2.2×10^{-5}	2.3×10^{-5}	2.2×10^{-5}	2.1×10^{-5}	1.9×10^{-5}	1.7×10^{-5}	1.5×10^{-5}
	42	8.7×10^{-6}	1.0×10^{-5}	1.0×10^{-5}	1.2×10^{-5}	1.4×10^{-5}	1.5×10^{-5}	1.6×10^{-5}	1.5×10^{-5}	1.4×10^{-5}	1.2×10^{-5}	1.0×10^{-5}	9.2×10^{-6}
	47	4.2×10^{-6}	5.2×10^{-6}	4.5×10^{-6}	5.9×10^{-6}	7.0×10^{-6}	8.2×10^{-6}	8.8×10^{-6}	8.1×10^{-6}	6.8×10^{-6}	5.7×10^{-6}	4.1×10^{-6}	4.3×10^{-6}
	52	1.7×10^{-6}	2.2×10^{-6}	2.1×10^{-6}	2.8×10^{-6}	3.5×10^{-6}	4.2×10^{-6}	4.5×10^{-6}	4.2×10^{-6}	3.3×10^{-6}	2.6×10^{-6}	2.0×10^{-6}	1.6×10^{-6}
	60	3.1×10^{-7}	4.3×10^{-7}	5.0×10^{-7}	6.1×10^{-7}	1.1×10^{-6}	1.3×10^{-6}	1.4×10^{-6}	1.2×10^{-6}	1.1×10^{-6}	8.8×10^{-7}	4.8×10^{-7}	4.6×10^{-7}
75°N	12	7.9×10^{-4}	7.3×10^{-4}	7.7×10^{-4}	8.0×10^{-4}	8.0×10^{-4}	1.1×10^{-3}	9.7×10^{-4}	1.1×10^{-3}	1.2×10^{-3}	1.1×10^{-3}	1.0×10^{-3}	8.5×10^{-4}
	15	4.6×10^{-4}	4.8×10^{-4}	4.8×10^{-4}	5.2×10^{-4}	4.9×10^{-4}	5.0×10^{-4}	5.1×10^{-4}	5.1×10^{-4}	5.3×10^{-4}	5.2×10^{-4}	4.9×10^{-4}	4.5×10^{-4}
	18	2.9×10^{-4}	2.7×10^{-4}	2.8×10^{-4}	3.1×10^{-4}	3.0×10^{-4}	3.1×10^{-4}	3.1×10^{-4}	3.1×10^{-4}	3.0×10^{-4}	2.9×10^{-4}	2.9×10^{-4}	2.7×10^{-4}
	21	1.8×10^{-4}	2.0×10^{-4}	1.9×10^{-4}	2.0×10^{-4}	2.1×10^{-4}	2.1×10^{-4}	2.2×10^{-4}	2.1×10^{-4}	2.1×10^{-4}	2.0×10^{-4}	2.1×10^{-4}	2.0×10^{-4}
	24	1.2×10^{-4}	1.3×10^{-4}	1.3×10^{-4}	1.4×10^{-4}	1.5×10^{-4}	1.6×10^{-4}	1.6×10^{-4}	1.6×10^{-4}	1.5×10^{-4}	1.5×10^{-4}	1.4×10^{-4}	1.4×10^{-4}
	27	7.9×10^{-5}	8.5×10^{-5}	8.7×10^{-5}	9.2×10^{-5}	9.9×10^{-5}	1.0×10^{-4}	1.1×10^{-4}	1.1×10^{-4}	1.0×10^{-4}	9.9×10^{-5}	9.3×10^{-5}	8.5×10^{-5}
	30	4.9×10^{-5}	5.4×10^{-5}	5.6×10^{-5}	6.3×10^{-5}	6.7×10^{-5}	7.1×10^{-5}	7.6×10^{-5}	7.2×10^{-5}	7.0×10^{-5}	6.5×10^{-5}	6.0×10^{-5}	5.5×10^{-5}
	33	3.4×10^{-5}	3.9×10^{-5}	3.9×10^{-5}	4.1×10^{-5}	4.5×10^{-5}	4.8×10^{-5}	5.1×10^{-5}	5.0×10^{-5}	4.6×10^{-5}	4.4×10^{-5}	4.0×10^{-5}	3.4×10^{-5}
	36	2.1×10^{-5}	2.2×10^{-5}	2.5×10^{-5}	2.7×10^{-5}	2.9×10^{-5}	3.2×10^{-5}	3.4×10^{-5}	3.3×10^{-5}	3.1×10^{-5}	2.9×10^{-5}	2.6×10^{-5}	2.0×10^{-5}
	39	1.3×10^{-5}	1.4×10^{-5}	1.6×10^{-5}	1.9×10^{-5}	2.0×10^{-5}	2.2×10^{-5}	2.3×10^{-5}	2.2×10^{-5}	2.1×10^{-5}	1.9×10^{-5}	1.6×10^{-5}	1.3×10^{-5}
	42	8.6×10^{-6}	9.7×10^{-6}	9.6×10^{-6}	1.2×10^{-5}	1.4×10^{-5}	1.5×10^{-5}	1.6×10^{-5}	1.5×10^{-5}	1.4×10^{-5}	1.2×10^{-5}	9.2×10^{-6}	8.4×10^{-6}
	47	4.2×10^{-6}	4.8×10^{-6}	4.3×10^{-6}	5.7×10^{-6}	7.1×10^{-6}	8.3×10^{-6}	8.7×10^{-6}	8.0×10^{-6}	6.7×10^{-6}	5.3×10^{-6}	3.8×10^{-6}	4.0×10^{-6}
	52	1.7×10^{-6}	1.9×10^{-6}	1.9×10^{-6}	2.6×10^{-6}	3.4×10^{-6}	4.2×10^{-6}	4.5×10^{-6}	4.1×10^{-6}	3.2×10^{-6}	2.4×10^{-6}	1.8×10^{-6}	1.6×10^{-6}
	60	3.6×10^{-7}	3.2×10^{-7}	4.4×10^{-7}	6.6×10^{-7}	1.2×10^{-6}	1.3×10^{-6}	1.5×10^{-6}	1.3×10^{-6}	1.1×10^{-6}	7.9×10^{-7}	4.4×10^{-7}	4.2×10^{-7}

80°N	12	7.2×10^{-4}	7.6×10^{-4}	7.1×10^{-4}	7.4×10^{-4}	7.9×10^{-4}	8.4×10^{-4}	9.5×10^{-4}	1.1×10^{-3}	1.0×10^{-3}	1.1×10^{-3}	9.5×10^{-4}	8.1×10^{-4}
	15	4.3×10^{-4}	4.7×10^{-4}	4.6×10^{-4}	5.1×10^{-4}	4.9×10^{-4}	5.2×10^{-4}	5.2×10^{-4}	5.3×10^{-4}	5.0×10^{-4}	5.1×10^{-4}	4.6×10^{-4}	4.3×10^{-4}
	18	2.8×10^{-4}	2.8×10^{-4}	2.8×10^{-4}	3.1×10^{-4}	3.1×10^{-4}	3.2×10^{-4}	3.2×10^{-4}	3.1×10^{-4}	3.0×10^{-4}	3.0×10^{-4}	2.9×10^{-4}	2.7×10^{-4}
	21	1.9×10^{-4}	2.0×10^{-4}	2.0×10^{-4}	2.0×10^{-4}	2.1×10^{-4}	2.1×10^{-4}	2.2×10^{-4}	2.1×10^{-4}	2.1×10^{-4}	2.0×10^{-4}	2.1×10^{-4}	2.0×10^{-4}
	24	1.3×10^{-4}	1.4×10^{-4}	1.4×10^{-4}	1.4×10^{-4}	1.5×10^{-4}	1.6×10^{-4}	1.6×10^{-4}	1.6×10^{-4}	1.5×10^{-4}	1.5×10^{-4}	1.4×10^{-4}	1.4×10^{-4}
	27	7.9×10^{-5}	8.5×10^{-5}	8.7×10^{-5}	9.4×10^{-5}	9.9×10^{-5}	1.1×10^{-4}	1.1×10^{-4}	1.1×10^{-4}	1.0×10^{-4}	1.0×10^{-4}	9.5×10^{-5}	8.5×10^{-5}
	30	4.8×10^{-5}	5.4×10^{-5}	5.5×10^{-5}	6.2×10^{-5}	6.8×10^{-5}	7.2×10^{-5}	7.6×10^{-5}	7.3×10^{-5}	7.0×10^{-5}	6.5×10^{-5}	6.0×10^{-5}	5.5×10^{-5}
	33	3.2×10^{-5}	3.8×10^{-5}	3.8×10^{-5}	4.0×10^{-5}	4.6×10^{-5}	4.8×10^{-5}	5.1×10^{-5}	5.0×10^{-5}	4.5×10^{-5}	4.3×10^{-5}	4.0×10^{-5}	3.5×10^{-5}
	36	2.1×10^{-5}	2.3×10^{-5}	2.4×10^{-5}	2.7×10^{-5}	3.0×10^{-5}	3.3×10^{-5}	3.4×10^{-5}	3.3×10^{-5}	3.0×10^{-5}	2.9×10^{-5}	2.6×10^{-5}	2.0×10^{-5}
	39	1.3×10^{-5}	1.4×10^{-5}	1.6×10^{-5}	1.9×10^{-5}	2.1×10^{-5}	2.3×10^{-5}	2.4×10^{-5}	2.3×10^{-5}	2.1×10^{-5}	1.9×10^{-5}	1.6×10^{-5}	1.2×10^{-5}
	42	8.6×10^{-6}	9.8×10^{-6}	9.6×10^{-6}	1.2×10^{-5}	1.4×10^{-5}	1.5×10^{-5}	1.6×10^{-5}	1.5×10^{-5}	1.4×10^{-5}	1.2×10^{-5}	8.7×10^{-6}	7.6×10^{-6}
	47	4.2×10^{-6}	4.6×10^{-6}	3.9×10^{-6}	5.6×10^{-6}	7.1×10^{-6}	8.4×10^{-6}	8.8×10^{-6}	8.1×10^{-6}	6.7×10^{-6}	5.3×10^{-6}	3.6×10^{-6}	3.7×10^{-6}
	52	1.6×10^{-6}	1.8×10^{-6}	1.9×10^{-6}	2.7×10^{-6}	3.5×10^{-6}	4.4×10^{-6}	4.7×10^{-6}	4.2×10^{-6}	3.2×10^{-6}	2.5×10^{-6}	1.7×10^{-6}	1.6×10^{-6}
	60	3.9×10^{-7}	4.1×10^{-7}	4.0×10^{-7}	6.6×10^{-7}	1.2×10^{-6}	1.4×10^{-6}	1.5×10^{-6}	1.3×10^{-6}	1.1×10^{-6}	7.9×10^{-7}	4.6×10^{-7}	4.2×10^{-7}
85°N	12	7.3×10^{-4}	$7.9\ 10^{-4}$	7.4×10^{-4}	7.3×10^{-4}	7.6×10^{-4}	7.9×10^{-4}	8.5×10^{-4}	1.0×10^{-3}	8.8×10^{-4}	1.1×10^{-3}	9.3×10^{-4}	7.9×10^{-4}
	15	4.3×10^{-4}	$4.6\ 10^{-4}$	4.6×10^{-4}	5.1×10^{-4}	4.9×10^{-4}	5.2×10^{-4}	5.2×10^{-4}	$5.3\times\ 10^{-4}$	4.9×10^{-4}	5.2×10^{-4}	4.6×10^{-4}	4.4×10^{-4}
	18	2.8×10^{-4}	$2.9\ 10^{-4}$	3.0×10^{-4}	3.0×10^{-4}	3.1×10^{-4}	3.3×10^{-4}	3.1×10^{-4}	3.1×10^{-4}	2.9×10^{-4}	2.9×10^{-4}	2.9×10^{-4}	2.7×10^{-4}
	21	2.0×10^{-4}	$2.0\ 10^{-4}$	2.0×10^{-4}	2.0×10^{-4}	2.1×10^{-4}	2.2×10^{-4}	2.2×10^{-4}	2.1×10^{-4}	2.1×10^{-4}	2.0×10^{-4}	2.0×10^{-4}	2.0×10^{-4}
	24	1.4×10^{-4}	1.4×10^{-4}	1.3×10^{-4}	1.4×10^{-4}	1.5×10^{-4}	$1.5\ 10^{-4}$	1.6×10^{-4}	1.6×10^{-4}	1.5×10^{-4}	1.5×10^{-4}	1.4×10^{-4}	1.4×10^{-4}
	27	8.1×10^{-5}	8.5×10^{-5}	8.8×10^{-5}	9.1×10^{-5}	9.9×10^{-5}	1.1×10^{-4}	1.1×10^{-4}	1.1×10^{-4}	1.0×10^{-4}	1.0×10^{-4}	9.6×10^{-5}	8.8×10^{-5}
	30	5.0×10^{-5}	5.5×10^{-5}	5.6×10^{-5}	6.2×10^{-5}	6.8×10^{-5}	7.2×10^{-5}	7.5×10^{-5}	7.3×10^{-5}	7.0×10^{-5}	6.6×10^{-5}	6.1×10^{-5}	5.5×10^{-5}
	33	$3.3\ 10^{-5}$	3.7×10^{-5}	3.8×10^{-5}	4.1×10^{-5}	4.5×10^{-5}	4.8×10^{-5}	5.1×10^{-5}	4.9×10^{-5}	4.6×10^{-5}	4.3×10^{-5}	4.0×10^{-5}	3.6×10^{-5}
	36	2.0×10^{-5}	2.3×10^{-5}	2.3×10^{-5}	$2.7\ 10^{-5}$	3.0×10^{-5}	3.3×10^{-5}	3.4×10^{-5}	3.3×10^{-5}	3.0×10^{-5}	2.8×10^{-5}	2.6×10^{-5}	2.1×10^{-5}
	39	1.4×10^{-5}	1.4×10^{-5}	1.6×10^{-5}	1.9×10^{-5}	2.1×10^{-5}	2.3×10^{-5}	2.3×10^{-5}	2.3×10^{-5}	2.1×10^{-5}	1.9×10^{-5}	1.6×10^{-5}	1.2×10^{-5}
	42	8.6×10^{-6}	9.5×10^{-6}	9.5×10^{-6}	1.2×10^{-5}	1.4×10^{-5}	1.5×10^{-5}	1.6×10^{-5}	1.5×10^{-5}	1.4×10^{-5}	1.2×10^{-5}	8.5×10^{-6}	7.5×10^{-6}
	47	3.9×10^{-6}	4.4×10^{-6}	3.7×10^{-6}	5.5×10^{-6}	7.1×10^{-6}	8.4×10^{-6}	8.7×10^{-6}	8.0×10^{-6}	6.5×10^{-6}	4.8×10^{-6}	3.6×10^{-6}	3.5×10^{-6}
	52	1.7×10^{-6}	1.7×10^{-6}	1.7×10^{-6}	2.6×10^{-6}	3.5×10^{-6}	4.4×10^{-6}	4.6×10^{-6}	4.1×10^{-6}	3.0×10^{-6}	2.2×10^{-6}	1.6×10^{-6}	1.3×10^{-6}
	60	3.9×10^{-7}	4.1×10^{-7}	3.9×10^{-7}	8.0×10^{-7}	1.1×10^{-6}	1.4×10^{-6}	1.5×10^{-6}	1.3×10^{-6}	1.0×10^{-6}	8.0×10^{-7}	4.2×10^{-7}	5.0×10^{-7}
90°N	12	7.1×10^{-4}	7.4×10^{-4}	7.0×10^{-4}	8.4×10^{-4}	7.9×10^{-4}	7.5×10^{-4}	9.6×10^{-4}	9.9×10^{-4}	9.8×10^{-4}	1.1×10^{-3}	8.6×10^{-4}	7.7×10^{-4}
	15	4.3×10^{-4}	4.6×10^{-4}	4.2×10^{-4}	5.0×10^{-4}	4.9×10^{-4}	5.4×10^{-4}	5.4×10^{-4}	5.2×10^{-4}	5.0×10^{-4}	5.1×10^{-4}	4.6×10^{-4}	4.3×10^{-4}
	18	2.7×10^{-4}	2.8×10^{-4}	2.9×10^{-4}	3.1×10^{-4}	3.1×10^{-4}	3.3×10^{-4}	3.2×10^{-4}	3.1×10^{-4}	2.9×10^{-4}	3.0×10^{-4}	2.9×10^{-4}	2.7×10^{-4}
	21	1.9×10^{-4}	2.0×10^{-4}	2.1×10^{-4}	2.0×10^{-4}	2.1×10^{-4}	2.2×10^{-4}	2.2×10^{-4}	2.1×10^{-4}	2.1×10^{-4}	2.1×10^{-4}	2.0×10^{-4}	2.0×10^{-4}
	24	1.3×10^{-4}	1.4×10^{-4}	1.4×10^{-4}	1.4×10^{-4}	1.4×10^{-4}	1.5×10^{-4}	1.6×10^{-4}	1.6×10^{-4}	1.5×10^{-4}	1.5×10^{-4}	1.5×10^{-4}	1.4×10^{-4}
	27	8.1×10^{-5}	8.3×10^{-5}	8.6×10^{-5}	9.4×10^{-5}	1.0×10^{-4}	1.1×10^{-4}	1.1×10^{-4}	1.1×10^{-4}	1.0×10^{-4}	1.0×10^{-4}	9.5×10^{-5}	8.9×10^{-5}
	30	4.8×10^{-5}	5.6×10^{-5}	5.6×10^{-5}	6.2×10^{-5}	6.7×10^{-5}	7.2×10^{-5}	7.7×10^{-5}	7.2×10^{-5}	6.9×10^{-5}	6.7×10^{-5}	6.0×10^{-5}	5.2×10^{-5}
	33	3.1×10^{-5}	3.7×10^{-5}	3.6×10^{-5}	4.0×10^{-5}	4.6×10^{-5}	4.9×10^{-5}	$5.1\ 10^{-5}$	4.9×10^{-5}	4.6×10^{-5}	4.2×10^{-5}	3.9×10^{-5}	3.4×10^{-5}
	36	2.1×10^{-5}	2.3×10^{-5}	2.3×10^{-5}	2.7×10^{-5}	3.0×10^{-5}	3.2×10^{-5}	3.4×10^{-5}	3.3×10^{-5}	3.1×10^{-5}	2.8×10^{-5}	$2.5\ \times10^{-5}$	2.0×10^{-5}
	39	1.4×10^{-5}	1.4×10^{-5}	1.5×10^{-5}	1.8×10^{-5}	2.0×10^{-5}	2.3×10^{-5}	2.3×10^{-5}	2.2×10^{-5}	2.2×10^{-5}	2.0×10^{-5}	1.5×10^{-5}	1.2×10^{-5}
	42	8.7×10^{-6}	9.6×10^{-6}	9.4×10^{-6}	1.1×10^{-5}	1.4×10^{-5}	1.6×10^{-5}	1.6×10^{-5}	1.5×10^{-5}	1.4×10^{-5}	1.2×10^{-5}	8.5×10^{-6}	7.7×10^{-6}
	47	3.8×10^{-6}	4.0×10^{-6}	3.5×10^{-6}	5.5×10^{-6}	7.2×10^{-6}	8.3×10^{-6}	9.0×10^{-6}	8.1×10^{-6}	6.7×10^{-6}	4.9×10^{-6}	3.5×10^{-6}	3.4×10^{-6}
	52	1.8×10^{-6}	1.7×10^{-6}	1.7×10^{-6}	2.6×10^{-6}	3.6×10^{-6}	4.6×10^{-6}	4.7×10^{-6}	4.2×10^{-6}	3.2×10^{-6}	2.3×10^{-6}	1.5×10^{-6}	1.3×10^{-6}
	60	3.2×10^{-7}	3.7×10^{-7}	4.2×10^{-7}	8.0×10^{-7}	1.1×10^{-6}	1.4×10^{-6}	1.6×10^{-6}	1.4×10^{-6}	1.1×10^{-6}	7.6×10^{-7}	4.2×10^{-7}	5.5×10^{-7}

Table A8
Monthly mean values of absolute humidity ρ_w (g m^{-3}) obtained from the MIPAS data given in Tables A1–A6 at 14 fixed levels from 12 to 60 km, for the 65°S, 70°S, 75°S, 80°S, 85°S and 90°S latitudes.

Latitude	Altitude (km)	Month											
		Jan.	Feb.	Mar.	Apr.	May	June	July	Aug.	Sep.	Oct.	Nov.	Dec.
65°S	12	9.3×10^{-4}	8.6×10^{-4}	8.2×10^{-4}	8.3×10^{-4}	7.9×10^{-4}	7.0×10^{-4}	7.0×10^{-4}	5.6×10^{-4}	5.6×10^{-4}	7.1×10^{-4}	7.6×10^{-4}	8.3×10^{-4}
	15	5.1×10^{-4}	4.9×10^{-4}	4.6×10^{-4}	4.4×10^{-4}	4.2×10^{-4}	4.0×10^{-4}	4.1×10^{-4}	3.4×10^{-4}	3.7×10^{-4}	4.8×10^{-4}	4.8×10^{-4}	4.9×10^{-4}
	18	3.0×10^{-4}	2.8×10^{-4}	2.7×10^{-4}	2.7×10^{-4}	2.6×10^{-4}	2.6×10^{-4}	2.7×10^{-4}	2.1×10^{-4}	2.4×10^{-4}	3.0×10^{-4}	3.0×10^{-4}	3.0×10^{-4}
	21	2.0×10^{-4}	2.0×10^{-4}	1.9×10^{-4}	1.9×10^{-4}	1.9×10^{-4}	1.9×10^{-4}	1.9×10^{-4}	1.7×10^{-4}	1.9×10^{-4}	1.9×10^{-4}	2.0×10^{-4}	2.0×10^{-4}
	24	1.4×10^{-4}	1.4×10^{-4}	1.4×10^{-4}	1.4×10^{-4}	1.3×10^{-4}	1.3×10^{-4}	1.3×10^{-4}	1.3×10^{-4}	1.2×10^{-4}	1.3×10^{-4}	1.3×10^{-4}	1.3×10^{-4}
	27	9.0×10^{-5}	9.2×10^{-5}	9.0×10^{-5}	9.0×10^{-5}	8.7×10^{-5}	8.5×10^{-5}	8.6×10^{-5}	8.0×10^{-5}	7.6×10^{-5}	7.6×10^{-5}	8.4×10^{-5}	8.7×10^{-5}
	30	6.0×10^{-5}	6.2×10^{-5}	5.9×10^{-5}	5.9×10^{-5}	5.7×10^{-5}	5.5×10^{-5}	5.0×10^{-5}	4.5×10^{-5}	4.8×10^{-5}	5.1×10^{-5}	5.6×10^{-5}	5.8×10^{-5}
	33	4.1×10^{-5}	4.2×10^{-5}	4.2×10^{-5}	4.1×10^{-5}	3.7×10^{-5}	3.4×10^{-5}	3.0×10^{-5}	2.8×10^{-5}	3.2×10^{-5}	3.6×10^{-5}	3.9×10^{-5}	4.0×10^{-5}
	36	2.8×10^{-5}	2.9×10^{-5}	2.9×10^{-5}	2.9×10^{-5}	2.7×10^{-5}	2.0×10^{-5}	2.0×10^{-5}	1.8×10^{-5}	2.1×10^{-5}	2.5×10^{-5}	2.7×10^{-5}	2.8×10^{-5}
	39	2.1×10^{-5}	2.1×10^{-5}	2.0×10^{-5}	2.0×10^{-5}	1.7×10^{-5}	1.3×10^{-5}	1.1×10^{-5}	1.3×10^{-5}	1.4×10^{-5}	1.7×10^{-5}	1.9×10^{-5}	2.0×10^{-5}
	42	1.5×10^{-5}	1.5×10^{-5}	1.4×10^{-5}	1.2×10^{-5}	9.6×10^{-6}	7.6×10^{-6}	6.6×10^{-6}	7.1×10^{-6}	9.2×10^{-6}	1.2×10^{-5}	1.4×10^{-5}	1.4×10^{-5}
	47	8.0×10^{-6}	7.8×10^{-6}	6.9×10^{-6}	5.5×10^{-6}	4.3×10^{-6}	3.3×10^{-6}	3.6×10^{-6}	3.4×10^{-6}	4.7×10^{-6}	6.3×10^{-6}	7.5×10^{-6}	7.8×10^{-6}
	52	4.2×10^{-6}	3.9×10^{-6}	3.3×10^{-6}	2.8×10^{-6}	1.9×10^{-6}	1.5×10^{-6}	1.4×10^{-6}	2.0×10^{-6}	2.3×10^{-6}	3.0×10^{-6}	3.6×10^{-6}	4.2×10^{-6}
	60	1.3×10^{-6}	1.2×10^{-6}	1.1×10^{-6}	7.4×10^{-7}	5.2×10^{-7}	5.4×10^{-7}	6.1×10^{-7}	5.2×10^{-7}	6.4×10^{-7}	1.0×10^{-6}	1.2×10^{-6}	1.3×10^{-6}
70°S	12	8.6×10^{-4}	8.0×10^{-4}	8.1×10^{-4}	7.9×10^{-4}	7.5×10^{-4}	6.6×10^{-4}	6.6×10^{-4}	4.8×10^{-4}	4.8×10^{-4}	5.7×10^{-4}	7.1×10^{-4}	8.7×10^{-4}
	15	5.0×10^{-4}	4.9×10^{-4}	4.7×10^{-4}	4.5×10^{-4}	4.2×10^{-4}	4.3×10^{-4}	3.8×10^{-4}	2.7×10^{-4}	2.6×10^{-4}	4.2×10^{-4}	4.2×10^{-4}	4.6×10^{-4}
	18	3.0×10^{-4}	2.9×10^{-4}	2.8×10^{-4}	2.7×10^{-4}	2.7×10^{-4}	2.8×10^{-4}	2.4×10^{-4}	1.7×10^{-4}	1.9×10^{-4}	3.0×10^{-4}	3.1×10^{-4}	2.9×10^{-4}
	21	2.0×10^{-4}	2.0×10^{-4}	1.9×10^{-4}	1.9×10^{-4}	2.0×10^{-4}	1.9×10^{-4}	1.8×10^{-4}	1.5×10^{-4}	1.8×10^{-4}	1.9×10^{-4}	2.0×10^{-4}	2.0×10^{-4}
	24	1.4×10^{-4}	1.4×10^{-4}	1.4×10^{-4}	1.3×10^{-4}	1.3×10^{-4}	1.3×10^{-4}	1.3×10^{-4}	1.3×10^{-4}	1.3×10^{-4}	1.2×10^{-4}	1.3×10^{-4}	1.3×10^{-4}
	27	9.1×10^{-5}	9.2×10^{-5}	9.0×10^{-5}	9.1×10^{-5}	8.9×10^{-5}	8.4×10^{-5}	8.2×10^{-5}	7.8×10^{-5}	7.5×10^{-5}	7.6×10^{-5}	8.5×10^{-5}	8.7×10^{-5}
	30	6.0×10^{-5}	6.2×10^{-5}	6.0×10^{-5}	5.8×10^{-5}	5.7×10^{-5}	5.1×10^{-5}	4.6×10^{-5}	4.1×10^{-5}	4.6×10^{-5}	4.9×10^{-5}	5.6×10^{-5}	5.9×10^{-5}
	33	4.2×10^{-5}	4.2×10^{-5}	4.2×10^{-5}	4.1×10^{-5}	3.7×10^{-5}	3.3×10^{-5}	2.8×10^{-5}	2.4×10^{-5}	3.0×10^{-5}	3.4×10^{-5}	3.9×10^{-5}	4.0×10^{-5}
	36	2.9×10^{-5}	3.0×10^{-5}	2.9×10^{-5}	2.8×10^{-5}	2.6×10^{-5}	2.0×10^{-5}	1.7×10^{-5}	1.7×10^{-5}	2.0×10^{-5}	2.4×10^{-5}	2.7×10^{-5}	2.8×10^{-5}
	39	2.1×10^{-5}	2.1×10^{-5}	2.0×10^{-5}	1.9×10^{-5}	1.6×10^{-5}	1.2×10^{-5}	1.0×10^{-5}	1.1×10^{-5}	1.3×10^{-5}	1.6×10^{-5}	1.9×10^{-5}	2.0×10^{-5}
	42	1.5×10^{-5}	1.4×10^{-5}	1.4×10^{-5}	1.2×10^{-5}	8.3×10^{-6}	6.3×10^{-6}	6.1×10^{-6}	6.7×10^{-6}	8.3×10^{-6}	1.1×10^{-5}	1.3×10^{-5}	1.4×10^{-5}
	47	8.0×10^{-6}	7.8×10^{-6}	6.8×10^{-6}	5.4×10^{-6}	4.0×10^{-6}	3.0×10^{-6}	3.3×10^{-6}	3.0×10^{-6}	4.4×10^{-6}	6.1×10^{-6}	7.5×10^{-6}	7.8×10^{-6}
	52	4.2×10^{-6}	3.9×10^{-6}	3.3×10^{-6}	2.4×10^{-6}	1.7×10^{-6}	1.5×10^{-6}	1.3×10^{-6}	1.7×10^{-6}	2.1×10^{-6}	2.8×10^{-6}	3.6×10^{-6}	4.2×10^{-6}
	60	1.4×10^{-6}	1.2×10^{-6}	1.0×10^{-6}	6.7×10^{-7}	4.2×10^{-7}	4.5×10^{-7}	5.7×10^{-7}	5.1×10^{-7}	5.9×10^{-7}	1.0×10^{-6}	1.3×10^{-6}	1.4×10^{-6}
75°S	12	8.5×10^{-4}	8.1×10^{-4}	8.2×10^{-4}	7.5×10^{-4}	7.1×10^{-4}	6.5×10^{-4}	6.5×10^{-4}	4.6×10^{-4}	4.1×10^{-4}	6.0×10^{-4}	7.3×10^{-4}	9.0×10^{-4}
	15	4.9×10^{-4}	4.9×10^{-4}	4.8×10^{-4}	4.1×10^{-4}	4.0×10^{-4}	3.8×10^{-4}	3.7×10^{-4}	2.3×10^{-4}	2.0×10^{-4}	$3.4\ 10^{-4}$	3.9×10^{-4}	4.5×10^{-4}
	18	3.0×10^{-4}	2.9×10^{-4}	2.8×10^{-4}	2.7×10^{-4}	2.7×10^{-4}	2.7×10^{-4}	2.3×10^{-4}	1.4×10^{-4}	1.6×10^{-4}	2.5×10^{-4}	3.0×10^{-4}	2.9×10^{-4}
	21	2.0×10^{-4}	2.0×10^{-4}	1.9×10^{-4}	1.9×10^{-4}	1.9×10^{-4}	1.9×10^{-4}	1.6×10^{-4}	1.2×10^{-4}	1.6×10^{-4}	2.0×10^{-4}	2.0×10^{-4}	2.0×10^{-4}
	24	1.3×10^{-4}	1.3×10^{-4}	1.3×10^{-4}	1.3×10^{-4}	1.3×10^{-4}	1.2×10^{-4}	1.2×10^{-4}	1.2×10^{-4}	1.3×10^{-4}	1.2×10^{-4}	1.3×10^{-4}	1.3×10^{-4}
	27	9.1×10^{-5}	9.1×10^{-5}	8.8×10^{-5}	8.8×10^{-5}	8.5×10^{-5}	8.5×10^{-5}	8.4×10^{-5}	7.0×10^{-5}	7.2×10^{-5}	7.6×10^{-5}	8.4×10^{-5}	8.6×10^{-5}
	30	6.1×10^{-5}	6.1×10^{-5}	5.9×10^{-5}	5.9×10^{-5}	5.4×10^{-5}	4.9×10^{-5}	4.3×10^{-5}	3.8×10^{-5}	4.5×10^{-5}	4.7×10^{-5}	5.5×10^{-5}	5.9×10^{-5}
	33	4.2×10^{-5}	4.2×10^{-5}	4.2×10^{-5}	4.0×10^{-5}	3.7×10^{-5}	3.0×10^{-5}	2.6×10^{-5}	2.4×10^{-5}	2.8×10^{-5}	3.3×10^{-5}	3.8×10^{-5}	4.0×10^{-5}
	36	2.9×10^{-5}	3.0×10^{-5}	2.9×10^{-5}	2.8×10^{-5}	2.3×10^{-5}	1.8×10^{-5}	1.7×10^{-5}	1.6×10^{-5}	1.9×10^{-5}	2.4×10^{-5}	2.7×10^{-5}	2.8×10^{-5}
	39	2.1×10^{-5}	2.0×10^{-5}	2.0×10^{-5}	1.8×10^{-5}	1.5×10^{-5}	1.1×10^{-5}	9.0×10^{-6}	9.8×10^{-6}	1.2×10^{-5}	1.6×10^{-5}	1.9×10^{-5}	2.0×10^{-5}
	42	1.5×10^{-5}	1.4×10^{-5}	1.3×10^{-5}	1.1×10^{-5}	7.4×10^{-6}	5.8×10^{-6}	5.5×10^{-6}	6.5×10^{-6}	7.6×10^{-6}	1.1×10^{-5}	1.3×10^{-5}	1.4×10^{-5}
	47	8.1×10^{-6}	7.7×10^{-6}	6.6×10^{-6}	4.9×10^{-6}	3.5×10^{-6}	2.7×10^{-6}	3.1×10^{-6}	3.0×10^{-6}	3.9×10^{-6}	5.9×10^{-6}	7.5×10^{-6}	8.0×10^{-6}
	52	4.3×10^{-6}	3.9×10^{-6}	3.2×10^{-6}	2.2×10^{-6}	1.7×10^{-6}	1.4×10^{-6}	1.3×10^{-6}	1.4×10^{-6}	2.0×10^{-6}	2.8×10^{-6}	3.6×10^{-6}	4.2×10^{-6}
	60	1.4×10^{-6}	1.2×10^{-6}	1.0×10^{-6}	6.5×10^{-7}	4.0×10^{-7}	4.1×10^{-7}	4.8×10^{-7}	5.3×10^{-7}	5.7×10^{-7}	8.4×10^{-7}	1.3×10^{-6}	1.4×10^{-6}

80°S	12	7.9×10^{-4}	7.8×10^{-4}	8.2×10^{-4}	7.4×10^{-4}	7.0×10^{-4}	5.7×10^{-4}	6.0×10^{-4}	3.9×10^{-4}	4.1×10^{-4}	5.1×10^{-4}	6.7×10^{-4}	9.8×10^{-4}
	15	4.8×10^{-4}	4.8×10^{-4}	4.8×10^{-4}	4.2×10^{-4}	4.0×10^{-4}	3.5×10^{-4}	3.3×10^{-4}	1.9×10^{-4}	2.0×10^{-4}	2.4×10^{-4}	3.5×10^{-4}	4.4×10^{-4}
	18	3.0×10^{-4}	2.9×10^{-4}	2.7×10^{-4}	2.6×10^{-4}	2.6×10^{-4}	2.7×10^{-4}	1.9×10^{-4}	1.1×10^{-4}	1.2×10^{-4}	1.9×10^{-4}	2.9×10^{-4}	2.9×10^{-4}
	21	2.0×10^{-4}	1.9×10^{-4}	1.9×10^{-4}	1.9×10^{-4}	1.9×10^{-4}	1.9×10^{-4}	1.3×10^{-4}	9.8×10^{-5}	1.3×10^{-4}	2.0×10^{-4}	2.1×10^{-4}	2.0×10^{-4}
	24	1.3×10^{-4}	1.3×10^{-4}	1.3×10^{-4}	1.3×10^{-4}	1.3×10^{-4}	1.3×10^{-4}	1.1×10^{-4}	1.2×10^{-4}	1.2×10^{-4}	1.2×10^{-4}	1.3×10^{-4}	1.3×10^{-4}
	27	9.0×10^{-5}	9.1×10^{-5}	8.8×10^{-5}	8.7×10^{-5}	8.4×10^{-5}	7.7×10^{-5}	7.8×10^{-5}	7.1×10^{-5}	7.1×10^{-5}	7.3×10^{-5}	8.4×10^{-5}	8.6×10^{-5}
	30	6.1×10^{-5}	6.1×10^{-5}	6.0×10^{-5}	5.9×10^{-5}	5.4×10^{-5}	5.0×10^{-5}	4.4×10^{-5}	3.7×10^{-5}	4.2×10^{-5}	4.7×10^{-5}	5.4×10^{-5}	5.9×10^{-5}
	33	4.2×10^{-5}	4.2×10^{-5}	4.2×10^{-5}	4.0×10^{-5}	3.5×10^{-5}	2.9×10^{-5}	2.4×10^{-5}	2.2×10^{-5}	$2.7\times10^{--5}$	3.3×10^{-5}	3.8×10^{-5}	4.0×10^{-5}
	36	2.9×10^{-5}	3.0×10^{-5}	2.8×10^{-5}	2.7×10^{-5}	2.3×10^{-5}	1.7×10^{-5}	1.6×10^{-5}	1.5×10^{-5}	1.8×10^{-5}	2.3×10^{-5}	2.6×10^{-5}	2.8×10^{-5}
	39	2.1×10^{-5}	2.1×10^{-5}	2.0×10^{-5}	1.8×10^{-5}	1.4×10^{-5}	1.0×10^{-5}	9.3×10^{-6}	9.5×10^{-6}	1.1×10^{-5}	1.5×10^{-5}	1.9×10^{-5}	2.0×10^{-5}
	42	1.5×10^{-5}	1.4×10^{-5}	1.3×10^{-5}	1.1×10^{-5}	7.0×10^{-6}	5.4×10^{-6}	5.2×10^{-6}	6.1×10^{-6}	7.2×10^{-6}	1.1×10^{-5}	1.3×10^{-5}	1.4×10^{-5}
	47	8.2×10^{-6}	7.7×10^{-6}	6.5×10^{-6}	4.5×10^{-6}	3.3×10^{-6}	2.6×10^{-6}	2.8×10^{-6}	2.8×10^{-6}	3.6×10^{-6}	5.6×10^{-6}	7.4×10^{-6}	7.9×10^{-6}
	52	4.3×10^{-6}	3.9×10^{-6}	3.1×10^{-6}	2.1×10^{-6}	1.5×10^{-6}	1.3×10^{-6}	1.3×10^{-6}	1.2×10^{-6}	1.9×10^{-6}	2.7×10^{-6}	3.6×10^{-6}	4.2×10^{-6}
	60	1.4×10^{-6}	1.3×10^{-6}	1.1×10^{-6}	6.3×10^{-7}	4.0×10^{-7}	3.9×10^{-7}	3.8×10^{-7}	5.5×10^{-7}	5.9×10^{-7}	8.1×10^{-7}	1.3×10^{-6}	1.5×10^{-6}
85°S	12	7.6×10^{-4}	7.9×10^{-4}	7.9×10^{-4}	7.7×10^{-4}	7.2×10^{-4}	5.6×10^{-4}	8.1×10^{-4}	3.7×10^{-4}	3.9×10^{-4}	4.2×10^{-4}	6.4×10^{-4}	9.6×10^{-4}
	15	4.9×10^{-4}	4.9×10^{-4}	4.6×10^{-4}	4.2×10^{-4}	3.9×10^{-4}	3.5×10^{-4}	3.6×10^{-4}	2.0×10^{-4}	2.1×10^{-4}	1.9×10^{-4}	3.4×10^{-4}	4.3×10^{-4}
	18	3.0×10^{-4}	2.9×10^{-4}	2.8×10^{-4}	2.7×10^{-4}	2.6×10^{-4}	2.7×10^{-4}	1.7×10^{-4}	1.1×10^{-4}	1.2×10^{-4}	1.8×10^{-4}	2.8×10^{-4}	2.9×10^{-4}
	21	1.9×10^{-4}	1.9×10^{-4}	1.9×10^{-4}	1.9×10^{-4}	1.9×10^{-4}	1.9×10^{-4}	1.2×10^{-4}	1.1×10^{-4}	1.3×10^{-4}	2.0×10^{-4}	2.1×10^{-4}	2.0×10^{-4}
	24	1.3×10^{-4}	1.3×10^{-4}	1.3×10^{-4}	1.3×10^{-4}	1.2×10^{-4}	1.2×10^{-4}	1.1×10^{-4}	1.1×10^{-4}	1.2×10^{-4}	1.3×10^{-4}	1.3×10^{-4}	1.3×10^{-4}
	27	9.2×10^{-5}	9.2×10^{-5}	8.8×10^{-5}	8.6×10^{-5}	8.5×10^{-5}	7.3×10^{-5}	7.8×10^{-5}	6.8×10^{-5}	7.0×10^{-5}	7.6×10^{-5}	8.2×10^{-5}	8.5×10^{-5}
	30	6.1×10^{-5}	6.2×10^{-5}	5.9×10^{-5}	5.8×10^{-5}	5.2×10^{-5}	4.7×10^{-5}	4.3×10^{-5}	3.5×10^{-5}	4.1×10^{-5}	4.7×10^{-5}	5.4×10^{-5}	5.9×10^{-5}
	33	4.2×10^{-5}	4.2×10^{-5}	4.2×10^{-5}	3.9×10^{-5}	3.5×10^{-5}	2.9×10^{-5}	2.5×10^{-5}	2.2×10^{-5}	2.5×10^{-5}	3.3×10^{-5}	3.8×10^{-5}	4.0×10^{-5}
	36	2.9×10^{-5}	3.0×10^{-5}	2.8×10^{-5}	2.6×10^{-5}	2.2×10^{-5}	1.7×10^{-5}	1.6×10^{-5}	1.6×10^{-5}	1.8×10^{-5}	2.3×10^{-5}	2.7×10^{-5}	2.9×10^{-5}
	39	2.1×10^{-5}	2.1×10^{-5}	2.0×10^{-5}	1.7×10^{-5}	1.3×10^{-5}	9.5×10^{-6}	9.0×10^{-6}	9.2×10^{-6}	1.1×10^{-5}	1.6×10^{-5}	1.9×10^{-5}	2.1×10^{-5}
	42	1.5×10^{-5}	1.4×10^{-5}	1.3×10^{-5}	1.1×10^{-5}	6.9×10^{-6}	5.5×10^{-6}	5.3×10^{-6}	5.7×10^{-6}	7.1×10^{-6}	1.1×10^{-5}	1.3×10^{-5}	1.5×10^{-5}
	47	8.3×10^{-6}	7.8×10^{-6}	6.5×10^{-6}	4.3×10^{-6}	3.3×10^{-6}	2.6×10^{-6}	2.7×10^{-6}	2.7×10^{-6}	3.6×10^{-6}	5.6×10^{-6}	7.5×10^{-6}	8.1×10^{-6}
	52	4.4×10^{-6}	4.0×10^{-6}	3.1×10^{-6}	2.0×10^{-6}	1.4×10^{-6}	1.1×10^{-6}	1.4×10^{-6}	1.3×10^{-6}	1.9×10^{-6}	2.9×10^{-6}	3.7×10^{-6}	4.3×10^{-6}
	60	1.4×10^{-6}	1.3×10^{-6}	1.1×10^{-6}	6.1×10^{-7}	3.7×10^{-7}	3.9×10^{-7}	3.5×10^{-7}	5.1×10^{-7}	6.3×10^{-7}	7.6×10^{-7}	1.3×10^{-6}	1.5×10^{-6}
90°S	12	7.6×10^{-4}	7.7×10^{-4}	8.0×10^{-4}	7.8×10^{-4}	7.4×10^{-4}	6.6×10^{-4}	1.3×10^{-3}	5.6×10^{-4}	4.1×10^{-4}	4.0×10^{-4}	5.7×10^{-4}	7.9×10^{-4}
	15	4.9×10^{-4}	4.9×10^{-4}	4.6×10^{-4}	4.3×10^{-4}	4.0×10^{-4}	3.3×10^{-4}	7.1×10^{-4}	1.7×10^{-4}	1.8×10^{-4}	1.6×10^{-4}	3.1×10^{-4}	4.1×10^{-4}
	18	3.1×10^{-4}	3.0×10^{-4}	2.7×10^{-4}	2.6×10^{-4}	2.6×10^{-4}	2.6×10^{-4}	2.4×10^{-4}	1.1×10^{-4}	1.1×10^{-4}	1.7×10^{-4}	2.6×10^{-4}	2.9×10^{-4}
	21	2.0×10^{-4}	1.9×10^{-4}	1.9×10^{-4}	1.9×10^{-4}	1.9×10^{-4}	1.8×10^{-4}	1.3×10^{-4}	1.0×10^{-4}	1.3×10^{-4}	1.9×10^{-4}	2.1×10^{-4}	2.0×10^{-4}
	24	1.3×10^{-4}	1.3×10^{-4}	1.3×10^{-4}	1.3×10^{-4}	1.2×10^{-4}	1.1×10^{-4}	1.1×10^{-4}	1.1×10^{-4}	1.2×10^{-4}	1.3×10^{-4}	1.3×10^{-4}	1.3×10^{-4}
	27	9.2×10^{-5}	9.1×10^{-5}	8.8×10^{-5}	8.8×10^{-5}	8.5×10^{-5}	8.1×10^{-5}	8.2×10^{-5}	6.6×10^{-5}	6.8×10^{-5}	7.8×10^{-5}	8.2×10^{-5}	8.6×10^{-5}
	30	6.2×10^{-5}	6.3×10^{-5}	6.0×10^{-5}	5.7×10^{-5}	5.3×10^{-5}	4.7×10^{-5}	3.9×10^{-5}	3.6×10^{-5}	4.1×10^{-5}	4.7×10^{-5}	5.5×10^{-5}	5.9×10^{-5}
	33	4.2×10^{-5}	4.2×10^{-5}	4.2×10^{-5}	4.0×10^{-5}	3.5×10^{-5}	2.9×10^{-5}	2.5×10^{-5}	2.1×10^{-5}	2.5×10^{-5}	3.3×10^{-5}	3.8×10^{-5}	4.1×10^{-5}
	36	2.9×10^{-5}	3.0×10^{-5}	2.8×10^{-5}	2.7×10^{-5}	2.1×10^{-5}	1.8×10^{-5}	1.6×10^{-5}	1.6×10^{-5}	1.8×10^{-5}	2.3×10^{-5}	$2.6\ 10^{-5}$	$2.9\ 10^{-5}$
	39	2.1×10^{-5}	2.1×10^{-5}	2.0×10^{-5}	1.6×10^{-5}	1.3×10^{-5}	9.2×10^{-6}	8.7×10^{-6}	9.3×10^{-6}	1.1×10^{-5}	1.6×10^{-5}	1.9×10^{-5}	2.0×10^{-5}
	42	1.5×10^{-5}	1.4×10^{-5}	1.3×10^{-5}	1.1×10^{-5}	7.2×10^{-6}	5.3×10^{-6}	5.3×10^{-6}	5.6×10^{-6}	7.0×10^{-6}	1.1×10^{-5}	1.3×10^{-5}	1.5×10^{-5}
	47	8.2×10^{-6}	7.7×10^{-6}	6.3×10^{-6}	4.2×10^{-6}	3.0×10^{-6}	2.6×10^{-6}	2.6×10^{-6}	2.6×10^{-6}	3.5×10^{-6}	5.4×10^{-6}	7.4×10^{-6}	8.0×10^{-6}
	52	4.3×10^{-6}	3.9×10^{-6}	3.1×10^{-6}	2.0×10^{-6}	1.5×10^{-6}	1.2×10^{-6}	1.4×10^{-6}	1.2×10^{-6}	1.8×10^{-6}	2.8×10^{-6}	3.6×10^{-6}	4.2×10^{-6}
	60	1.4×10^{-6}	1.4×10^{-6}	1.1×10^{-6}	6.3×10^{-7}	3.7×10^{-7}	3.9×10^{-7}	3.5×10^{-7}	4.8×10^{-7}	6.3×10^{-7}	9.2×10^{-7}	1.3×10^{-6}	1.5×10^{-6}

and millimetric radiation are usually observed at the high-altitude sites of the Antarctic Plateau (Martin, 2007).

7. Conclusions

The present results obtained from the analysis of a numerous MIPAS data-set provide realistic evaluations of the monthly mean profiles of the thermodynamic parameters of the polar stratosphere and low mesosphere, for which reliable radiative transfer calculations can be performed. For this purpose, the data reported in Tables A1–A8 of Appendix A, which define the monthly mean vertical profiles of air pressure, temperature, water vapour VMR and absolute humidity over the 12–60 km altitude range, can be used for the 12 selected polar latitudes taken in steps of 5° from 65° to 90°. The data will be made available to readers on the POLAR-AOD web site (http://polaraod.isti.cnr.it:8080/Polar/), with the relative errors given in Fig. 3 for pressure, Fig. 7 for temperature and Fig. 11 for water vapour mixing ratio. In addition, the monthly mean values of stratospheric water vapour content over the 12–50 km altitude range have been calculated in the present study to complete the characterisation of the moisture conditions of the polar atmosphere provided by radiosounding measurements. Such measurements of relative humidity are not usually reliable at altitudes higher than 12 km, because the relative humidity is so low at these stratospheric levels as to be comparable with the accuracy of the radiosondes throughout the year.

The MIPAS data pertaining to the minor species of the polar atmosphere have been not examined, to avoid an excessive length of the article, and only the vertical distributions of water vapour VMR and the other moisture parameters have been investigated, as they are closely related to the air temperature and pressure conditions.

The analysis of the MIPAS data-set containing the measurements of the VMRs of the five "high priority" atmospheric constituents, O_3, HNO_3, CH_4, N_2O and NO_2, recorded in the period from July 2002 to April 2010 will be the focus of a future paper, in which the set of monthly mean vertical profiles of these gaseous volume mixing ratios will be proposed at the same 12 polar latitudes chosen in the present paper. This information will be completed by supplemental data defining the vertical profiles of the VMRs of both CO and CO_2 molecules, as obtained at different polar latitudes and for various seasonal periods of the year during the SABER/TIMED (Mertens et al., 2009) satellite mission, the ACE-FTS satellite-borne experiment (Foucher et al., 2011) or from TIME-GCM simulations (López-Puertas et al., 2000).

Table B1
List of the experiments/campaigns performed at 5 of the six selected Arctic latitudes, using different satellite-borne radiometric techniques, air-borne measurements, and number of vertical profiles of water vapour volume mixing ratio $Q(z)$ obtained for the various months.

Experiment/campaign	Satellite sensor/Instrument	Reference	Monthly number of profiles at 5 of the six selected Arctic latitudes				
			70°N	75°N	80°N	85°N	90°N
Limb Infrared Monitor of the Stratosphere Experiment (LIMSE)	NIMBUS 7 satellite	Russell et al. (1984)	1 (January)	1 (January)	1 (January)	1 (January)	-
Early phase of the SAGE II experiment	Earth Radiation Budget Satellite (ERBS)	Rind et al. (1993)	1 (April)	1 (April)	–	–	–
Early phase of the HALOE experiment	Solar occultation limb infrared sounder onboard the Upper Atmosphere Research Satellite (UARS)	Harries et al. (1996)	2 (January)	2 (January)	2 (January)	–	–
Microwave Limb Sounder (MLS) Experiment	UARS satellite	Lahoz et al. (1996)	–	–	1 (January)	–	–
					1 (February)		
					1 (March)		
					1(May)		
					1 (October)		
					1 (December)		
Second 5-year phase of the SAGE II experiment	Earth Radiation Budget Satellite (ERBS)	Chiou et al. (1997)	1 (April)	–	–	–	–
			1 (July)				
			1 (October)				
Airborne Millimetre- and Submillimeter-Wave Observing System (AMSWOS)	Learjet of the Swiss Air Force	Peter (1998)	4 (March)	3 (March)	3 (March)	–	–
					1 (August)		
					1 (October)		
			2 (August)	1 (August)			
			2 (October)	1 (October)			
Campaign of late winters 1992 and 1993, using MLS data	UARS satellite	Morrey and Harwood (1998)	1 (February)	1 (February)	1 (February)	1 (February)	1 (February)
HALOE observations from 1991 to 2000 & climatological MLS data	UARS satellite	Randel et al. (2001)	2 (January)	2 (January)	2 (January)	–	–
			2 (July) +1 for all the other months	2 (July) +1 for all the other months	2 (July) +1 for all the other months		
Arctic campaigns at Ny Ålesund (Svalbards)	Balloon-borne frost-point hygrometers	Müller et al. (2003)	–	–	1 (January)		–
					1 (February)		
LAPBIAT validation project	MIAWARA radiometric measurements of water vapour content	Deuber et al. (2005)	1 (January)	–	–		–
			1 (February)				

Acknowledgments

The research activity was supported by the Programma Nazionale di Ricerche in Antartide (PNRA) and developed as a part of Subproject 2006/6.01: "POLAR-AOD: a network to characterize the means, variability and trends of the climate-forcing properties of aerosols in polar regions". The authors gratefully acknowledge the International Centre for Theoretical Physics, Trieste, Italy, for its support of the participation of B. Petkov in the framework of the Programme for Training and Research in Italian Laboratories. E. Arnone and E. Papandrea acknowledge the support by ESA within the framework of the Changing Earth Science Network Initiative. The MLS data-set used in this work was acquired as part of the activities of NASA's Science Mission Directorate, and is archived and distributed by the Goddard Earth Sciences (GES) Data and Information Services Center (DISC).

Appendix A. Tables of the monthly mean vertical profiles of pressure, temperature, water vapour volume mixing ratio and absolute humidity

Appendix A presents Tables A1–A8 giving the monthly mean values of air pressure $p(z)$, air temperature $T(z)$, water vapour VMR $Q(z)$ and absolute humidity $\rho_w(z)$ at the 14 fixed MIPAS levels from 12 to 60 km, for the six selected Arctic latitudes of 70°N, 75°N, 80°N, 85°N and 90°N, and the six selected Antarctic latitudes of 70°S, 75°S, 80°S, 85°S and 90°S. All the data can be downloaded from the POLAR-AOD website (http://polaraod.isti.cnr.it:8080/Polar/) on request of the access password made to the corresponding author Claudio Tomasi (e-mail address: c.tomasi@isac.cnr.it) or second author Boyan Petkov (e-mail address: b.petkov@isac.cnr.it).

Appendix B. Vertical profiles of water vapour volume mixing ratio in the polar stratosphere from satellite-based radiometer, air-borne and ground-based lidar measurements for comparison with MIPAS results.

During the present study, a great number of monthly mean vertical profiles of water vapour VMR $Q(z)$ were calculated at the polar latitudes of the two hemispheres, within the altitude range from 8 km to more than 50 km. It was done by examining various sets of measurements of this moisture parameter performed with different satellite-borne radiometric techniques, air-borne measurements and ground-based lidar measurements in the Arctic and Antarctic atmospheres.

A large set of 89 vertical profiles of $Q(z)$ measured at the Arctic latitudes in various months were derived from stratospheric measurements performed during the 10 experiments listed in Table B1:

(a) The 70°N data-set consisted of an overall number of 32 stratospheric vertical profiles of $Q(z)$, of which 6 profiles were measured in January, 5 in March, 4 in October, 3 in February, April, July and August and only 1 in May, June, September, November and December. The vertical profiles obtained in January, April, July and October are shown in Fig. B1 for comparison with the corresponding monthly mean vertical profiles of $Q(z)$ obtained from the MIPAS data. All the vertical profiles in Fig. B1 provide evidence of the rapid decrease of $Q(z)$ from more than 7 to about 3 ppmv throughout the altitude range from 8 to 15 km, and of the subsequent increase to values close to 6 ppmv at the 40–50 km levels, followed by a gradual decrease at the mesospheric levels. The MIPAS profiles are in good agreement with the evaluations of $Q(z)$ derived from the experimental results obtained through the activities listed in Table B1, which present relevant discrepancies of 1.5 ppmv in October only, at altitudes ranging between 35 and 60 km.

(b) The 75°N latitude data-set consisted of 24 vertical stratospheric profiles of $Q(z)$ including 5 profiles for January, 4 for March, 2 for February, April, July, August and October, and only 1 for May, June, September, November and December. The vertical profiles obtained in January, April, July and October are shown in Fig. B2 and compared with the corresponding MIPAS monthly mean vertical profiles of $Q(z)$. They exhibit values gradually increasing with altitude from 15 to 50 km, presenting similar characteristics to the MIPAS data up to 25 km and then differing by 1–2 ppmv throughout the 30–50 km altitude range, where the MIPAS profiles describe a pronounced maximum close to the stratopause level.

(c) The 80°N data-set was found to consist of 31 vertical profiles of $Q(z)$, of which 7 pertain to January, 5 to March, 4 to February, 3 to October, 2 to May, July, August and December and 1 to April, June, September and November. Some of these vertical profiles obtained in January, July and October are presented in Fig. B3, showing a clear minimum at about 15 km and a subsequent increase with altitude to describe a maximum at about 40–50 km. They present a good agreement with the MIPAS profiles from 12 to 30 km in January and July and differ from the MIPAS values only in October at the 30–60 km altitudes by 1.5 ppmv on average.

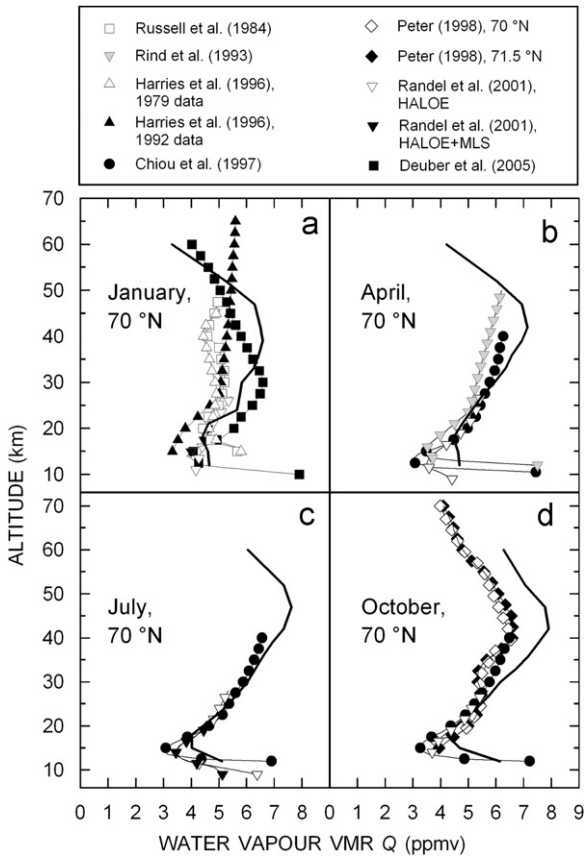

Fig. B1. Comparison of the vertical profiles of water vapour volume mixing ratio $Q(z)$ determined at 70°N latitude from various sets of experimental data with the corresponding monthly mean vertical profiles of $Q(z)$ (solid curve) obtained at the 15 fixed MIPAS levels for January (a), April (b), July (c) and October (d).

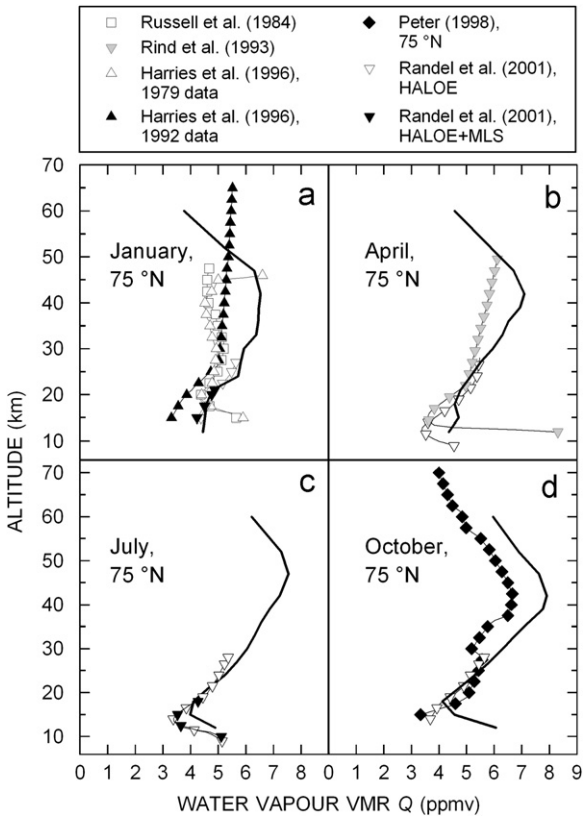

Fig. B2. As in Figure B.1 at 75°N latitude, for January (a), April (b), July (c) and October (d).

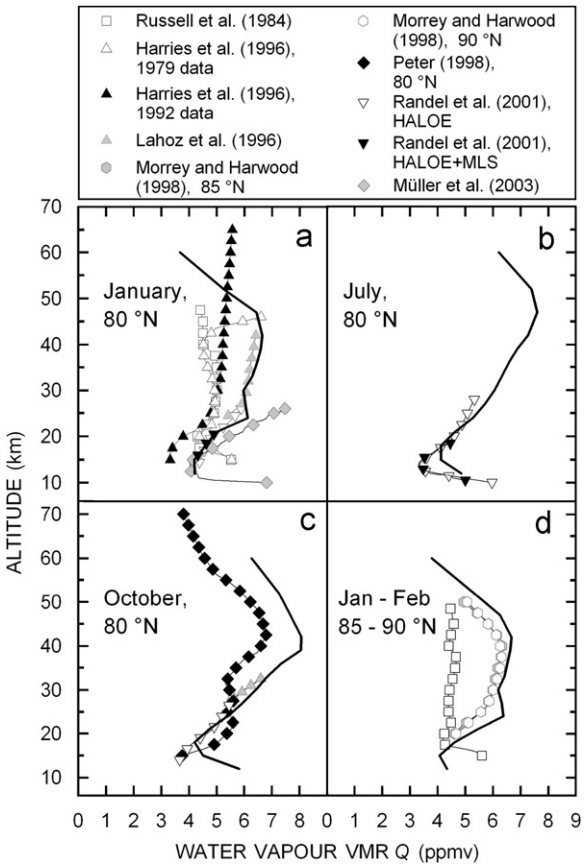

Fig. B3. As in Fig. B1 at 80°N latitude, for January (a), July (b) and October (c), for comparison with the present monthly mean profiles of $Q(z)$ (solid curves). Part (d) presents the vertical profiles of $Q(z)$ determined at 85°N latitude for January (Russell et al., 1984) and February (Morrey and Harwood, 1998), and the vertical profile of $Q(z)$ defined for February at 90°N latitude (Morrey and Harwood, 1998).

(d) Only 2 vertical profiles of $Q(z)$ were collected at the 85°N latitude, the first defined by Russell et al. (1984) in January 1979, and the second by Morrey and Harwood (1998) in February 1992 and 1993. The latter shows a close agreement with the MIPAS profile, which assumes rather stable values gradually increasing from 4 to 6 ppmv as the altitude increases from 20 to 50 km.

(e) Only 1 profile was collected at the 90°N latitude, determined by Morrey and Harwood (1998) from data measured in February 1992 and 1993. It was found to be in substantial agreement with the one measured by them at the 85°N latitude.

An overall set of 104 vertical profiles of $Q(z)$ were collected at the Antarctic latitudes in the various months of the year. These stratospheric measurements were performed during the 9 experiments listed in Table B2:

(a) The 70°S data set consisted of 33 stratospheric vertical profiles of $Q(z)$, of which 6 pertain to October, 4 to January, 3 to April, July, August, September and November, 2 to March and December and 1 to February. The January, April, July and October profiles are shown in Fig. B4, providing evidence of the increase of $Q(z)$ throughout the stratosphere, passing from values of 2–3 ppmv at about 12 km to values close to 6 ppmv at the stratopause level. The comparison of these satellite-borne profiles with the corresponding monthly mean profiles of $Q(z)$ derived from MIPAS data shows for all the four months a very good agreement at levels lower than 40 km, with differences of 1–2 ppmv at altitudes higher than 40 km.

(b) The 75°S data-set consisted of 30 vertical profiles of $Q(z)$, including 5 profiles for October, 4 for August and September, 3 for January and July, 2 for February, March, April and November and only 1 for May, June and December. The vertical profiles collected in January, April, July and October are presented in Fig. B5, where they are compared with the corresponding MIPAS monthly mean profiles. It can be seen that the values of $Q(z)$ obtained from the satellite- and airborne measurements listed in Table B2 increase in general from 2–3 ppmv at 15 km to 5–7 ppmv at 50 km. Fig. B5 provides evidence of the good agreement between these profiles of $Q(z)$ and those obtained from the MIPAS data up to 40 km, presenting appreciable discrepancies only in January at altitudes from 40 to 60 km.

(c) The 80°S latitude data-set consisted of 27 stratospheric vertical profiles of $Q(z)$, of which 5 profiles were pertinent to October, 4 to April, July, August and September, 3 to January and November, 2 to March and 1 to February, May, June and December. The profiles for January, April, July and October are shown in Fig. B6, confirming that $Q(z)$ increases rapidly with height in all months, from 2–3 ppmv at around 12 km to more than 6 ppmv at 40 km, and then decreases slightly at higher levels. These profiles present a substantial agreement with the MIPAS profiles up to 30 km and then exhibit appreciable differences of 1–2 ppmv only in January, from 30 to 50 km.

(d) Only 1 vertical profile of $Q(z)$ was found at 85°S latitude, determined by Morrey and Harwood (1998) from measurements taken in August 1992, with values increasing from

Table B2
List of the experiments/campaigns performed at 5 of the six selected Antarctic latitudes, using different satellite-borne radiometric techniques, air-borne measurements and ground-based lidar measurements, and number of vertical profiles of water vapour volume mixing ratio $Q(z)$ obtained for the various months.

Experiment/campaign	Satellite sensor/ Instrument	Reference	Monthly number of profiles at 5 of the six selected Antarctic latitudes				
			70°S	75°S	80°S	85°S	90°S
Measurement campaign at South Pole	Frost point sounding	Rosen et al. (1991)	–	–	–	–	1 (May) 1 (June 1 (August) 1 (October)
Measurement campaigns at South Pole	Ground-based lidar	Fuà et al. (1992), Fiocco et al. (1996), Cacciani et al. (1997)	–	–	–	–	1 (May) 3 (June) 2 (July) 1 (August) 1 (September)
Early phase of the SAGE II experiment	Earth Radiation Budget Satellite (ERBS)	Rind et al. (1993)	1 (October)	1 (March) 1 (October)	–	–	–
Early phase of the HALOE experiment	Solar occultation limb infrared sounder onboard the Upper Atmosphere Research Satellite (UARS)	Harries et al. (1996)	1 (January) 1 (October)	1 (January) 2 (October)	1 (January) 1 (October)	–	–
Microwave Limb Sounder (MLS) Experiment	UARS satellite	Lahoz et al. (1996)	1 (April) 1 (July) 1 (August) 1 (September) 1 (October) 1 (November)	1 (April) 1 (July) 1 (August) 1 (September) 1 (October) 1 (November)	1 (April) 1 (July) 1 (August) 1 (September) 1 (October) 1 (November)	–	–
Second 5-year phase of the SAGE II experiment	Earth Radiation Budget Satellite (ERBS)	Chiou et al. (1997)	1 (January) 1 (April) 1 (September) 2 (October)	2 (September)	–	–	–
Campaign of late winters 1992 and 1993, using Microwave Limb Sounder (MLS) data	UARS satellite	Morrey and Harwood (1998)	1 (August)	1 (August)	1 (August)	1 (August)	1 (August)
HALOE observations from 1991 to 2000 & climatological MLS data	UARS satellite	Randel et al. (2001)	2 (January) 2 (July)+ 1 for all the other months	2 (January) 2 (July)+ 1 for all the other months	2 (January) 2 (July)+ 1 for all the other months	–	–
Dehydration measurement campaign in Antarctica	POAM III (Polar Ozone and Aerosol Measurement) onboard the MOZAIC aircraft	Nedoluha et al. (2002)	1 (May) 1 (June) 1 (November) 1 (December)	1 (February 1 (August)	1 (March) 1 (April) 1 (September) 1 (October)	–	–

2 ppmv at 20 km to 6 ppmv at about 30 km and then decreasing to about 5 ppmv at 50 km. This profile is shown in Fig. B7, presenting a very good agreement with the MIPAS monthly mean profile of August at the 85°S latitude.

(e) An overall set of 13 stratospheric vertical profiles were collected from measurements performed at South Pole (Rosen et al., 1991; Fuà et al., 1992; Fiocco et al., 1996; Cacciani et al., 1997; Morrey and Harwood, 1998), of which 4 profiles were for June, 3 for August, 2 for May and July and 1 for September and October. The May, June, August and October profiles are presented in Fig. B7, yielding values of $Q(z)$ gradually decreasing from 10 to 4 ppmv as the altitude increases from 10 to 25 km, and then increasing from about 2 ppmv to nearly 6 ppmv at 50 km, in the case of August at the 90°S latitude, presenting a close agreement with the corresponding MIPAS profile.

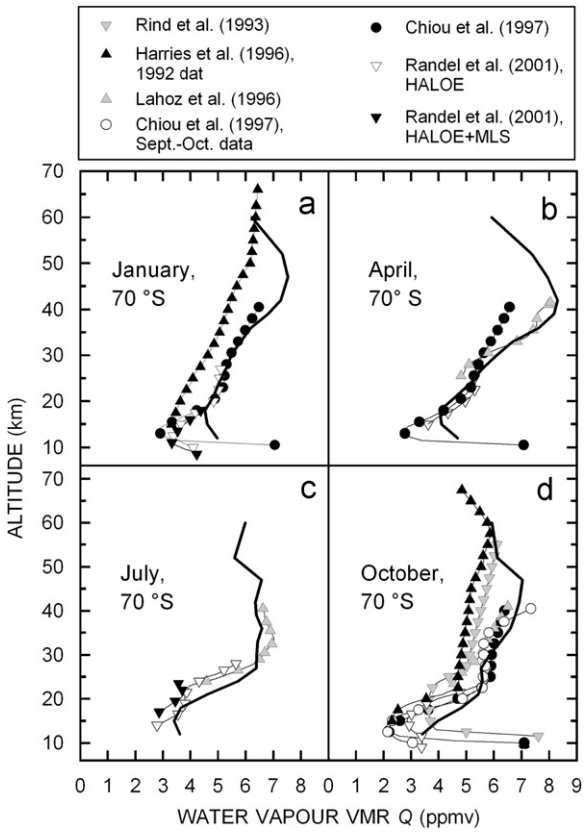

Fig. B4. As in Figure B.1 at 70°S latitude, for January (a), April (b), July (c) and October (d).

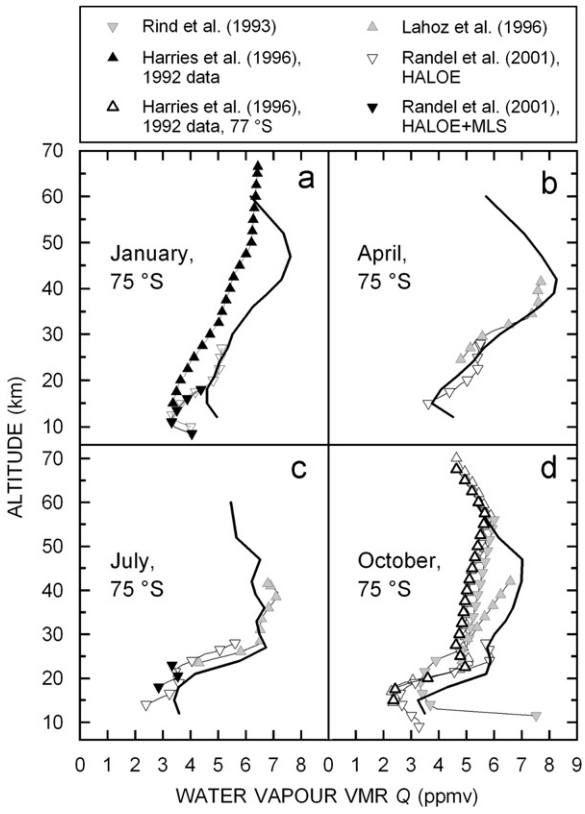

Fig. B5. As in Figure B.1 at 75°S latitude, for January (a), April (b), July (c) and October (d).

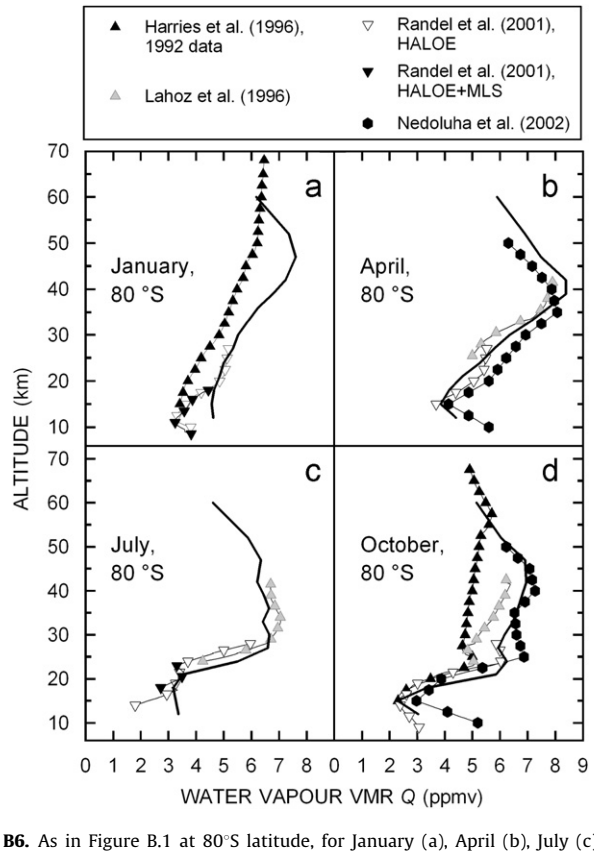

Fig. B6. As in Figure B.1 at 80°S latitude, for January (a), April (b), July (c) and October (d).

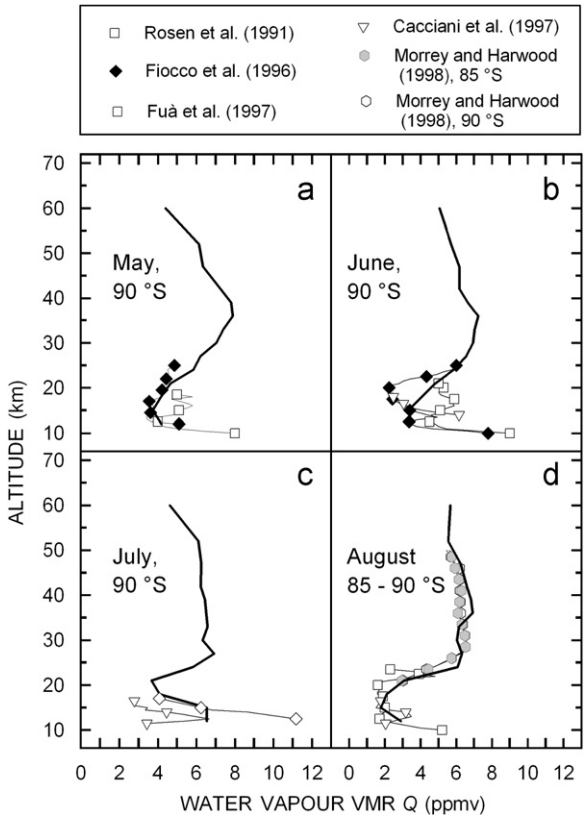

Fig. B7. As in Fig. B1 at 90°S latitude, for May (a), June (b) and July (c). Part (d) shows the vertical profiles determined at 85°S latitude in August (Morrey and Harwood, 1998) and at 90°S latitude (Rosen et al., 1991; Cacciani et al., 1997; Morrey and Harwood, 1998).

References

Anderson, G.P., et al., 1986. AFGL Atmospheric Constituent Profiles (0–120 km), Environmental Research Papers, No. 954, AFGL-TR-86-0110. Optical Physics Division (Air Force Geophysics Laboratory), Hanscom Air Force Base, Mass.

Cacciani, M., et al., 1997. Lidar observations of polar stratospheric clouds at the South Pole. I. Stratospheric unperturbed conditions, 1990. J. Geophys. Res. 102, 12937–12943.

Carlotti, M., et al., 2001. Geo-fit approach to the analysis of limb-scanning satellite measurements. Appl. Opt. 40, 1872–1885.

Carlotti, M., et al., 2006. GMTR: two-dimensional geo-fit multitarget retrieval model for Michelson Interferometer for Passive Atmospheric Sounding/Environmental Satellite observations. Appl. Opt. 45, 716–727.

Chamberlin, R.A., et al., 1997. The 492 GHz atmospheric opacity at the geographic South Pole. J. Astrophys. 476, 428–433.

Chiou, E.-W., et al., 1997. Global water vapor distributions in the stratosphere and upper troposphere derived from 5.5 years of SAGE II observations (1986–1991). J. Geophys. Res. 102, 19105–19118.

CIRA 1986, 1988. COSPAR International Reference Atmosphere 1986. In: D. Rees (Ed.), Adv. Space Res. 8, Number 5–6.

Deuber, B., et al., 2005. Middle Atmospheric Water Vapour radiometer (MIAWARA): validation and first results of the LAPBIAT Upper tropospheric Lower Stratospheric Water Vapour Validation Project. J. Geophys. Res. 110, D13306. doi:10.1029/2004JD005543.

Dinelli, B.M., et al., 2004. Multi-target retrieval (MTR): the simultaneous retrieval of pressure, temperature and volume mixing ratio profiles from limb-scanning atmospheric measurements. J. Quant. Spectrosc. Radiat. Transfer 84, 141–157.

Dinelli, B.M., et al., 2010. The MIPAS2D database of MIPAS/ENVISAT measurements retrieved with a multi-target 2-dimensional tomographic approach. Atmos. Meas. Techn. Discuss. (AMTD) 2, 2639–2688.

Foucher, P.Y., et al., 2011. Carbon dioxide atmospheric vertical profiles retrieved from space observation using ACE-FTS solar occultation instrument. Atmos. Chem. Phys 11, 2445–2470.

Fiocco, G., et al., 1996. The evolution of the Pinatubo stratospheric aerosol layer observed by lidar at South Pole, Rome, Thule: a summary of results. In: Fiocco, G., Fuà, D., Visconti, G. (Eds.), The Mt. Pinatubo Eruption: Effects on the Atmosphere and Climate, NATO/ASI Series, Vol. I. Springer-Verlag, Berlin, pp. 17–32.

Fleming, E.L., et al., 1990. Zonal mean temperature, pressure, zonal wind and geopotential heights as function of latitude. Adv. Space Res. 10, 11–59.

Fuà, D., et al., 1992. Stratospheric clouds at South Pole during 1988. 2. Their evolution in relation to atmospheric structure and composition. J. Geophys. Res. 97, 5947–5952.

Gettelman, A., et al., 2006. Relative humidity over Antarctica from radiosondes, satellites, and a general circulation model. J. Geophys. Res., 111. doi:10.1029/2005JD006636.

Harries, J.E., et al., 1996. Validation of measurements of water vapor from the Halogen Occultation Experiment (HALOE). J. Geophys. Res. 101, 10205–10216.

Hurst, D.F., et al., 2011. Stratospheric water vapor trends over Boulder, Colorado: analysis of the 30 year Boulder record. J. Geophys. Res. 116, D02306. doi:10.1029/2010JD015065.

Kenyon, S.L., Storey, J.W.V., 2006. A review of optical sky brightness and extinction at Dome C, Antarctica. **Publ.** Astron. **Soc.** Pacific (PASP) 118, 489–502.

Lahoz, W.A., et al., 1996. Vortex dynamics and the evolution of water vapour in the stratosphere of the southern hemisphere. Quart. J. Roy. Met. Soc. (QJRMS) 122, 423–450.

Lanconelli, C., et al., 2009. Estimation of fractional sky cover, cloud type and cloud forcing effects at Mario Zucchelli and Concordia Stations (75°S) from broadband radiation measurements. SIF Conf. Proc 97, 85–94.

Lawrence, J.S., et al., 2004. Exceptional astronomical seeing conditions above Dome C in Antarctica. Nature 431, 278–281.

Liu, Y., et al., 2009. Atmospheric tracers during the 2003–2004 stratospheric warming event and impact of ozone intrusions in the troposphere. Atmos. Chem. Phys 9, 2157–2170.

López-Puertas, M., López-Valverde M.Á., Garcia R.R., Roble G., 2000. A review of CO_2 and CO abundances in the middle atmosphere. Atmospheric Science Across the Stratopause, AGU Chapman Conference, Annapolis (Maryland, USA). In:Geophysical Monograph Series, Vol. 123. American Geophysical UnionWashington, DC, pp. 83–100.

Martin, C.L., 2007. Ten years from the Antarctic sub-millimeter telescope and remote observatory. Highlights Astron. 14, 686–688.

Mertens, C.J., et al., 2009. Kinetic temperature and carbon dioxide from broadband infrared limb emission measurements taken from the TIMED/SABER instrument. Adv. Space Res. 43, 15–27.

Miloshevich, L.M., et al., 2004. Development and validation of a time-lag correction for Vaisala radiosonde humidity measurements. J. Atmos. Oceanic Technol. 21, 1305–1327.

Miloshevich, L.M., et al., 2006. Absolute accuracy of water vapour measurements from six operational radiosonde types launched during AWEX-G and implications for AIRS validation. J. Geophys. Res., 111. doi:10.1029/2005/JD006083.

Minier, V., et al., 2007. CAMISTIC: THz/submm astronomy at Dome C in Antarctica. HighlightsAstron. 14, 709–710.

Morrey, M.W., Harwood, R.S., 1998. Interhemispheric differences in stratospheric water vapour during late winter, in version 4 MLS measurements. Geophys. Res. Lett. 25, 147–150.

Müller, M., et al., 2003. Stratospheric water vapour as tracer for vortex filamentation in the Arctic winter. Atmos. Chem. Phys. 3, 1991–1997. doi:10.5194/acp-3-1991-2003.

Nedoluha, G.E., et al., 2002. POAM III measurements of dehydration in the Antarctic and comparisons with the Arctic. J. Geophys. Res. 107 (D20), 8290. doi:10.1029/2001JD001184.

Peter, R., 1998. Stratospheric and mesospheric latitudinal water vapour distributions obtained by an airborne millimeter-wave spectrometer. J. Geophys. Res 103, 16275–16290.

Randel, W.J., et al., 2001. Seasonal variation of water vapor in the lower stratosphere observed in Halogen Occultation Experiment data. J. Geophys. Res. 106, 14313–14325.

Randel, W.J., et al., 2009. An update of observed stratospheric temperature trends. J. Geophys. Res. 114, D02107. doi:10.1029/2008JD010421.

Rind, D., et al., 1993. Overview of the Stratospheric Aerosol and Gas Experiment II water vapor observations: method, validation, and data characteristics. J. Geophys. Res. 98, 4835–4856.

Rosen, J.M., et al., 1991. Balloon borne observations of backscatter, frost point and ozone in polar stratospheric clouds at South Pole. Geophys. Res. Lett. 18, 171–174.

Russell III, J.M., et al., 1984. Validation of water vapor results measured by the Limb Infrared Monitor of the Stratosphere Experiment on NIMBUS 7. J. Geophys. Res. 89, 5115–5124.

Tomasi, C., Vitale, V., Petkov, B., Lupi, A., Cacciari, A., 2005. Improved algorithm for calculations of Rayleigh-scattering optical depth in standard atmospheres. Appl. Opt. 44, 3320–3341.

Tomasi, C., et al., 2006. Characterization of the atmospheric temperature and moisture conditions above Dome C (Antarctica) during austral summer and fall months. J. Geophys. Res. 111, D20305. doi:10.1029/2005JD006976.

Tomasi, C., et al., 2007. Aerosols in polar regions: a historical overview based on optical depth and in situ observations. J. Geophys. Res. 112, D16205. doi:10.1029/2007JD008432.

Tomasi, C., et al., 2008. A refined calibration procedure of two-channel sun photometers to measure atmospheric precipitable water at various Antarctic sites. J. Atmos. Oceanic Technol. 25, 213–229. doi:10.1175/2007JTECHA952.1.

Tomasi, C., et al., 2010. Characterizing polar atmospheres and their effect on Rayleigh-scattering optical depth. J. Geophys. Res. 115, D02205. doi:10.1029/2009JD012852.

Tosti, G., et al., 2006. The International Robotic Antarctic Infrared Telescope (IRAIT). In: Stepp, L.M. (Ed.), Ground-based and Airborne Telescopes". SPIE Conf. Series, SPIE, Vol. 6267, 62671H, doi:10.1117/12.670302.

Town, M.S., et al., 2007. Cloud cover over the South Pole from visual observations, satellite retrievals, and surface-based infrared radiation measurements. J. Climate 20, 544–559.

Turner, D.D., et al., 2003. Dry bias and variability in Vaisala RS80-H radiosondes: the ARM experience. J. Atmos. Oceanic Technol. 20, 117–132.

Walden, V.P., et al., 1997. Infrared radiance spectra for testing radiative transfer models in cold and dry atmospheres: test cases from the Antarctic Plateau. Bull. Am. Met. Soc 78, 2246–2247.

Walden, V.P., et al., 1998. Measurements of the downward longwave radiation spectrum over the Antarctic Plateau and comparisons with a line-by-line radiative transfer model for clear skies. J. Geophys. Res. 103, 3825–3846.

Walden, V.P., et al., 2006. Radiometric validation of the Atmospheric Infrared Sounder over the Antarctic Plateau. J. Geophys. Res. 111, D09S03. doi:10.1029/2005JD006357.

Wang, J., et al., 2002. Corrections of humidity measurement errors from the Vaisala RS80 radiosonde—application to TOGA COARE data. J. Atmos. Oceanic Technol. 19, 981–1002.